APPLICATION OF STRUCTURE ACTIVITY RELATIONSHIPS OF THE *MYCOBACTERIUM TUBERCULOSIS* BETA-LACTAMASE (BlaC) AND THE NEW DELHI METALLO-BETA-LACTAMASE (NDM-1) TO COMBATING BETA-LACTAMASE MEDIATED DRUG RESISTANCE

A Dissertation

by

JOSEPH ANDREW MIRE

Submitted to the Office of Graduate Studies of
Texas A&M University
in partial fulfillment of the requirements for the degree of

DOCTOR OF PHILOSOPHY

Chair of Committee,	James C. Sacchettini
Co-Chair of Committee,	Pingwei Li
Committee Members,	David O. Peterson
	David H. Russell
Head of Department,	Gregory D. Reinhart

August 2013

Major Subject: Biochemistry

ABSTRACT

β-lactamase enzymes catalyze the irreversible hydrolysis of the four-membered cyclic amide ring characteristic of β-lactam antibiotics rendering them inactive and useless against pathogenic bacteria. Understanding structure activity relationships between β-lactam antibiotics and β-lactamases is important for designing novel β-lactams, β-lactamase inhibitors, and β-lactam-based fluorescent probes for rapid diagnosis of β-lactam antibiotic resistant infections.

The first half of this study focuses on the class A β-lactamase BlaC from *Mycobacterium tuberculosis* (*Mtb*) and addresses intermolecular interactions between BlaC and substrates, inhibitors, and biosensors that influence their kinetic parameters with BlaC and activities against *Mtb*. The substrate structure activity relationship explained the molecular basis for differential innate resistance of *Mtb* to faropenem, biapenem, and tebipenem by showing the interactions between BlaC and the lactams that govern differential acyl-intermediate stability and affinity. The inhibitor structure activity relationship revealed features of the BlaC active site that can be exploited to enhance binding and inhibition of BlaC by benzoxaboroles, and demonstrates their utility as potentiators of β-lactam antibiotic activity against *Mtb*. BlaC-specific β-lactam based fluorescent probes were designed and optimized for *Mtb* detection. Their utility was demonstrated by detecting down to 10 colony forming units of bacillus *Mycobacterium bovis* Calmette–Guérin (BCG) in human sputum.

The second half of this study focuses on the New Delhi Metallo-β-lactamase-1 (NDM-1), which is rapidly generating bacterial resistance to nearly all β-lactams. The NDM-1 gene encodes a class B1 metallo-β-lactamase enzyme. Purified recombinant NDM-1 was biochemically and biophysically characterized. The crystal structures of apo and monometalated NDM-1 provided structural insight into metal binding and the promiscuous enzymatic activity of NDM-1. Mechanistic details of the NMD-1 reaction were examined by comparing crystal structures of NDM-1 in complex with an unhydrolyzed β-lactam substrate and with hydrolyzed products. These structures were used for quantum mechanics / molecular mechanics simulations to estimate the free energy along the β-lactamase reaction coordinate. The results suggest that NDM-1 uses bulk water as the nucleophile that attacks the β-lactam ring, and a coordinated hydroxide ion or water molecule as the catalytic base depending on pH.

DEDICATION

I would like to dedicate this work to my mother and father for their unending love and support throughout my life.

ACKNOWLEDGEMENTS

I would like to thank my committee chair Dr. Sacchettini for giving me the opportunity to conduct this research, and my committee members Dr. Russell, Dr. Li and Dr. Peterson as well as my graduate advisor, Pat Swigert, for their support over the years.

I would also like to thank my collaborators: Dickon Alley with Anacor Pharmaceuticals for providing the benzoxaborole molecules, Dr. Eric Rubin and Dr. Noman Siddiqi of Harvard School of Public Health, Dr. David Russell of Texas A&M University, Dr. Jeff Cirillo of Texas A&M Health Science Center, Dr. Jainghong Rao of Stanford University School of Medicine, Dr. Andrzej Joachimiak and the Midwest Center for Structural Genomics, and Dr. Mark Cunningham of University of Texas Pan-American. It has been an honor to work with you all.

Chapter 4 is reprinted with permission from Nature Publishing Group, Copyright 2012. Joseph Mire performed the crystallization and structural studies, analyzed the data, and co-wrote the paper. Chapter 5 is reprinted with permission from the Public Library of Science, Copyright 2011. Joseph Mire performed and analyzed the biochemical data and co-wrote the paper. Chapter 6 is reprinted with permission from the Federation of American Societies for Experimental Biology, Copyright 2013. Joseph Mire performed and analyzed the biochemical data and co-wrote the paper.

I would like to thank the members of the Midwest Center for Structural Genomics and the Structural Biology Center at Argonne National Laboratory for their

support, specifically Robert Jedrzejczak for cloning the truncated NDM-1 gene. This research has been funded in part by a grant from the U.S. National Institutes of Health GM094585 (A.J.), GM094568 (J.S.), and by the U.S. Department of Energy, Office of Biological and Environmental Research, under contract DE-AC02-06CH11357. Dr. Mark Cunningham has also received support through the National Science Foundation's FaST program (HRD-0703584), administered by the Department of Educational Programs at Argonne National Laboratory. I would like to thank the Texas Advanced Computing Center (TACC; http://www.tacc.utexas.edu) at the University of Texas at Austin for providing HPC resources that have contributed to the research results reported. Additional computational resources were provided by the HiPAC cluster at the University of Texas–Pan American. Thanks to Gekleng Chhor for proofreading of the NDM-1 manuscript. The atomic coordinates and structure factors have been deposited to the Protein Data Bank (PDB IDs: 4H0D, 4HL2, 4HL1, 4HKY; http://www.pdb.org).

Last but not least, thank you to all of my friends and family members for your constant support and encouragement.

TABLE OF CONTENTS

ABSTRACT ii

DEDICATION iv

ACKNOWLEDGEMENTS v

TABLE OF CONTENTS vii

LIST OF FIGURES ix

LIST OF TABLES xi

CHAPTER I INTRODUCTION AND LITERATURE REVIEW 1

CHAPTER II STRUCTURAL AND FUNCTIONAL INSIGHTS INTO DIFFERENTIAL RESISTANCE OF *MYCOBACTERIUM TUBERCULOSIS* TO BETA-LACTAMS FAROPENEM, BIAPENEM, AND TEBIPENEM BY BlaC 21

- Overview 21
- Introduction 22
- Results 24
- Discussion 36
- Materials and Methods 43

CHAPTER III STRUCTURAL BASIS FOR POTENTIATION OF BETA-LACTAM ANTIBIOTIC ACTIVITY ON *MYCOBACTERIUM TUBERCULOSIS* BY BENZOXABOROLES: INHIBITION OF BlaC 47

- Overview 47
- Introduction 48
- Results 50
- Discussion 57
- Materials and Methods 62

CHAPTER IV RAPID POINT-OF-CARE DETECTION OF THE TUBERCULOSIS PATHOGEN USING A BlaC-SPECIFIC FLUOROGENIC PROBE 65

- Overview 65
- Introduction 66
- Results 68

Discussion 82
Materials and Methods 85

CHAPTER V STRUCTURE OF APO AND MONOMETALATED FORMS OF NDM-1, A HIGHLY POTENT CARBAPENEM-HYDROLYZING METALLO-BETA-LACTAMASE 89

Overview 89
Introduction 90
Results and Discussion 93
Materials and Methods 113

CHAPTER VI NDM-1, THE ULTIMATE PROMISCUOUS ENZYME: SUBSTRATE RECOGNITION AND CATALYTIC MECHANISM 120

Overview 120
Introduction 121
Results 124
Discussion 140
Materials and Methods 143

CHAPTER VII CONCLUSION AND FUTURE DIRECTIONS 151

REFERENCES 165

APPENDIX 191

LIST OF FIGURES

Page

Figure 2.1: Chemical structures of β-lactam scaffolds...……..27

Figure 2.2: Time course of BlaC reactions analyzed with Fourier transform ion cyclotron resonance mass spectrometry..……...29

Figure 2.3: Inhibition of BlaC by β-lactams…….31

Figure 2.4: Active site details of BlaC acyl-intermediate crystal structures...…….…32

Figure 2.5: Effect of faropenem treatment on *Mtb* infected BALB/CJ mice……...37

Figure 3.1: Competitive inhibition of BlaC by benzoxaborole AN4715…….……51

Figure 3.2: Active site details of BlaC-benzoxaborole inhibitor complexes……54

Figure 3.3: AN4715 potentiates activity of amoxicillin against *Mtb*……...58

Figure 4.1: General structures of blue fluorescent probes and their hydrolysis by BlaC…..……..69

Figure 4.2: Kinetic comparison of CDC probes with β-lactamase……...71

Figure 4.3: Comparison of BlaC and TEM-1 Bla active sites and substrate-specificity loops……..……75

Figure 4.4: Active-site details of the BlaC-CDC-OMe and BlaC–CDC-1 acyl-intermediate complexes.....……..77

Figure 4.5: β-lactamase selectivity of fluorescent probes CDG-1 and CDG-OMe…….79

Figure 4.6: Sensitivity and specificity of CDG-OMe in unprocessed human sputum.....81

Figure 5.1: NDM-1 structure and comparisons with selected carbapenemases……...97

Figure 5.2: Active site comparisons of *K. pneumoniae* NDM-1 metalated states…….100

Figure 5.3: Flexibility of the NDM-1 active site loops……..103

Figure 5.4: Active site expansion of NDM-1……105

Figure 6.1: NDM-1 in complex with hydrolyzed ampicillin……..127

Figure 6.2: NDM-1 simulation active site.....129

Figure 6.3: NDM-1 reaction mechanism.....132

Figure 6.4: Dependence of NDM-1 turnover number on divalent cation concentration.....135

Figure 6.5: pH dependence of NDM-1 turnover number.....137

Figure 6.6: Structure of NDM-1 in complex with two cadmium ions and ampicillin....138

LIST OF TABLES

Page

Table 2.1: Activity of β-lactams on *Mycobacterium tuberculosis*.....25

Table 3.1: Structure activity relationship of BlaC inhibition by benzoxaboroles.....52

Table 4.1: Kinetic parameters of fluorescent probes for BlaC and TEM-1 Bla.....73

Table 5.1: Steady state kinetic parameters of NDM-1 Δ38 with a selected set of β-lactam antibiotics.....109

CHAPTER I

INTRODUCTION AND LITERATURE REVIEW

Drug resistance presents a formidable threat to human health and modern medical practices. Pathogenic microorganisms possess many drug resistance mechanisms. Whether the genes that code for such mechanisms are innate or acquired, they have the ability to evolve and enhance the fitness of the organism by overcoming or disarming antibiotic threats to the cell.

β-lactam antibiotics are the most widely used antibiotic class in the world because of their broad spectrum activity against bacterial pathogens and relatively low toxicity to humans. They are routinely used as prophylactics during surgeries, and to treat existing infections. β-lactamase enzymes are the primary mechanism of resistance to β-lactam antibiotics. The first section of this record of study addresses ways to combat β-lactamase mediated β-lactam antibiotic resistance due to the chromosome-encoded β-lactamase of *Mycobacterium tuberculosis* (BlaC) through multidisciplinary biochemical and biophysical approaches spanning the molecular to organismal levels. The resulting structure activity relationships revealed the structural basis for differential resistance of *Mtb* to several β-lactams, structural insights into the mechanism of inhibition of BlaC by benzoxaboroles, and aided in the design of a BlaC specific probe for tuberculosis detection. The second section of this record of study identifies the biochemical,

biophysical, and mechanistic determinants for the extreme promiscuity of the recently discovered plasmid encoded New Delhi metallo-β-lactamase (NDM-1).

The serendipitous discovery of penicillin by Alexander Fleming in 1928 marked the beginning of an era where bacterial infections became routinely treatable. Fleming noticed a zone of staphylococci growth inhibition surrounding a mold that had contaminated the culture plates. The contaminant species was identified as mold from the Penicillum genus, which Fleming hypothesized released a substance that possessed the antibiotic activity. He named the active substance penicillin, and modern day β-lactam antibiotics were born[1,2].

Since the isolation, mass production, and clinical implementation of penicillin in the 1940's, several new β-lactams emerged from natural, semi-synthetic, and eventually full synthetic sources[3,4]. By the late 1990's, β-lactams were estimated to comprise greater than 65% of the world's antibiotic market[5].

Identification of the cell wall components and the penicillin-sensitive transpeptidase, carboxypeptidase and endopeptidase activities[6,7] and the mechanism of action of penicillin have been studied and reviewed extensively[8]. A variety of phenotypic effects and observations alluded to the mechanism of action of β-lactam antibiotics. Penicillin treated bacteria exhibited increases in metabolic precursors to the cell wall component murine, or peptidoglycan, and also had altered cell morphology suggesting that the target performed a cell wall biosynthetic function[9-11]. Experiments with radiolabeled penicillin were able to trace the antibiotic activity to a set of enzymes localized in the inner membrane of *Escherichia coli*[12] that were able to bind penicillin,

thus emerging the moniker penicillin binding proteins (PBP). The structural mimicry of penicillin to the D-alanyl-D-ala peptide substrate of transpeptidases suggested that penicillin and other β-lactams function through inhibition of essential cell wall biosynthetic transpeptidase enzymes[13,14]. The target of penicillin was confirmed when inhibition of the transpeptidase and carboxypeptidase enzyme activities was demonstrated *in vitro*[15]. D-D-transpeptidases function by cleaving the bond between D-Ala_4 and D-Ala_5 of the substrate pentapeptide, and subsequently cross-linking D-Ala_4 to the amino group of the third residue of the acceptor stem peptide[16]. Targeting the peptidoglycan cross-linking activity of essential transpeptidases enzymes with β-lactam antibiotics has proven to be an excellent strategy for anti-infective therapy[17].

β-lactam antibiotics exhibit extended spectrum antibiotic activity against gram-positive and gram-negative pathogens[1,18,19]. The general structure of a gram-positive cell wall is composed of an inner membrane surrounded by a thick peptidoglycan layer, where the cell wall of gram-negative organisms is composed of inner and outer membranes with a relatively thin peptidoglycan layer in the middle[20]. The mycobacterial cell wall is generally considered as gram positive, though it contains an extra layer of mycolic acids covalently linked to arabinogalactan, which is linked to the peptidoglycan layer[21]. Irreversible disruption of the peptidoglycan by inhibition of PBPs by β-lactams compromises the structural integrity of the cell wall eventually leading to cell death[8,22]. Orally available β-lactams are commonly used either alone or in combination with other antibiotics for the treatment of the following pathogenic bacterial infections: *Staphylococcus aureus,* Streptococcus species, *Haemophilus influenza, Moraxella*

catarrhalis, Listeria monocytogenes, Proteus mirabilis, Escherichia coli, Klebsiella species, Proteus vulgaris, and Enterococcus species[17]. Mycobacterial species are also susceptible to the deleterious effects of β-lactam antibiotics, but they are less sensitive due to one or more resistance mechanisms preventing clinical utility of β-lactams for these infections[23].

Stresses imposed on the bacteria by environmental conditions are the driving force for selection of mutations that increase organismal fitness. This is the basis for evolution by natural selection, and is also at the heart of bacterial resistance to antibiotics where humans have introduced selective pressure. In addition to the acquisition of compensatory mutations that decrease the efficacy of antibiotics, bacteria have innate resistance mechanisms that help evade antibiotic action. These include pumping the drug outside of the cell, modifying or swapping the target protein, or enzymatically changing the antibiotic[24]. For example, L-D-transpeptidases, a more recently discovered member of the PBP family, have been found to bypass conventional D-D-transpeptidation by forming alternative peptidoglycan crosslinks with L-Lys_3 instead of D-Ala_4[25]. Since β-lactam antibiotics target D-D transpeptidases by mimicking their polypeptide substrates D-Ala_4 D-Ala_5, not L-Lys_3 D-Ala_4, the switch from D-D transpeptidation to L-D transpeptidation is accompanied by resistance to β-lactam antibiotics[25].

Mycobacteria possess both D-D-transpeptidase as well as L-D-transpeptidase functions[26]. Experimental evidence suggests that β-lactam antibiotics target both D-D and L-D-transpeptidases[27 28], albeit with differential specificity. It was discovered that the peptidoglycan of stationary phase *Mtb* primarily contains crosslinks generated by L-

D-transpeptidation, which suggests that remodeling of the D-D peptidoglycan crosslinks may be involved in resistance to β-lactam antibiotics. The gene that encodes the L-D-transpeptidase, Ldt_{Mt1}, is upregulated in response to nutrient starvation. Notably, the enzyme Ldt_{Mt1} is inactivated by carbapenem-type β-lactams, suggesting that carbapenems, and structurally similar β-lactams, can function to target both D-D and L-D transpeptidases in actively dividing and persistent *MTB* infection[28].

The most common and often primary mechanism of resistance to β-lactam antibiotics is the expression of β-lactamase enzymes. These enzymes catalyze the irreversible hydrolysis of the active chemical moiety of β-lactams, the four membered cyclic amide or β-lactam ring. Cells expressing β-lactamase have a significant evolutionary advantage over those without β-lactamase. However, β-lactamase have very distinct substrate specificities, some narrow and some broader than others.

β-lactamases are non-essential enzymes related to the PBP family, and sequence similarity lends credence to the hypothesis that they evolved from a common ancestral enzyme[29,30]. The driving force behind selection and maintenance of β-lactamase function is likely interspecies competition[31]. It is assumed that β-lactams including penicillins, cephalosporins, and others are natural product weapons secreted by microorganisms competing for resources; therefore the evolution of β-lactamase genes was essential for co-existence[30].

In addition to chromosome-encoded β-lactamase genes, they are also maintained among bacterial populations as transmissible genes on plasmid DNA. These may be the most threatening of all types of β-lactamase because of the constantly changing

environment and selective pressure that facilitates evolution and expansion of their substrate specificities to become highly potent, promiscuous β-lactamases.

β-lactamase enzymes are historically classified based on their primary structure (classes A-D)[32] but have also been functionally classified based on their substrate specificity[33,34]. They are also further grouped into families, whose members are nearly identical to each other but may have single or multiple mutations, insertions, or deletions that change their substrate specificities, or confer resistance to inhibitors. Their diverse acronym-based nomenclature of β-lactamase families is representative of their origin, while the numeric portion distinguishes derivative mutants of each type[35].

Classes A, C, and D of β-lactamase are serine hydrolases[36], and class B enzymes are mechanistically distinct in that they require metal cofactors for function[37,38]. Though they may have evolved from a common ancestor, mechanistic studies indicate that β-lactamase classes evolved separately in response to different environmental stresses[39]. The mechanisms of serine β-lactamases have been extensively characterized by biochemical and biophysical means. Despite the fact that the first step of the reaction, acylation of the lactam at the catalytic serine, is conserved, each mechanism (class A, class C, and class D) has distinct features[30,39,40].

Class A, C, and D β-lactamase share a common reaction pathway that initiates with base catalyzed deprotonation of an active site serine that nucleophilically attacks the β-lactam carbonyl forming the acyl-enzyme intermediate complex. The reaction is terminated through hydrolysis of the acyl-intermediate complex to free the irreversibly inactivated β-lactam and regenerated enzyme. Class A and C β-lactamase differ in the

final step of the reaction, which is deacylation. For class A β-lactamase, the second half of the reaction proceeds through activation of a hydrolytic water molecule by a conserved active site base E166[41-43]. For class C β-lactamase, this conserved base is absent and it is hypothesized that the hydrolytic portion of the reaction proceeds through substrate assisted catalysis[30,39]. Class D β-lactamase rely on a conserved carbamylated lysine residue to act as the catalytic base for both serine activation and hydrolytic water activation[40,44].

Class B metallo-β-lactamase enzymes (MBLs) are less common than the other β-lactamase, and represent the most evolutionarily distant β-lactamase class evidenced by sequence alignment[30]. MBL enzymes are further divided into 3 subclasses based on their sequence similarity. Crystal structures of MBLs have played a major role in sub-classification because the modest primary structural similarity prevented facile assignment of conserved structural elements[38]. MBLs function through assisted catalysis from either one or two zinc cofactors that are coordinated within the active site. The mechanism of β-lactam hydrolysis by MBLs is hypothesized to proceed through nucleophilic attack of the lactam carbonyl carbon atom by a metal coordinated hydroxide ion and subsequent protonation of the lactam nitrogen[38]. One hypothesis suggests that an active site aspartate plays a role as a catalytic base[45]. Also, the distances between the metal ligand cofactors in MBL crystal structures and spectroscopic studies suggest potential alternative mechanisms[46-52].

In addition to the classical sequence based classification scheme of β-lactamase[32], the substrate profile-based classification scheme is especially useful to

describe drug resistant infections in clinical settings[33,53]. The β-lactamase are divided into groups named based on their ability to break down specific classes of β-lactams; some examples are penicillinases, cephalosporinases, carbapenemases, oxacillinases, and extended spectrum β-lactamase (ESBLs). The evolution of β-lactamases with highly variable activities is a reflection of the selective pressure imposed by the antibiotics used to treat infections in the past[31,54].

Clinical isolates carrying transmissible plasmids or resistance factors with penicillinase genes were reported as early as the 1960's[55,56]. The most clinically prevalent plasmid encoded β-lactamase are the TEM, SHV, CTX-M, CMY, OXA, IMP, and VIM families[57]. The fact that these β-lactamase are carried on plasmids and passed from organism to organism[58] affords them a great deal of functional diversity through independent evolution within the same family. The class A TEM family is by far the most common with 172 variants and the capacity to hydrolyze nearly all classes of β-lactams except carbapenems. The next most common is the class D OXA family composed of 158 members. These enzymes have an even more extended spectrum activity than TEM type in that they are also carbapenemases. The SHV family of class A β-lactamase has 127 members and has a similar substrate profile to the TEM family. The population of TEM, OXA and SHV families has been rapidly and steadily increasing in number since the late 1980's relative to other β-lactamase families[53]. Slightly less common are the class A CTX-M and class C CMY families with 90 and 50 members, respectively. These families have the increased ability to hydrolyze cephalosporins over penicillin. Some of the more prevalent class B enzyme families IMP (26 members) and

VIM (23 members) have extended spectrum activity against all β-lactams except aztreonam, though they are much less common relative to the class A, C, and D enzymes[53].

With β-lactamase on the rise and the continuous widespread use of β-lactam antibiotics, it is easy to imagine a future where β-lactam antibiotics no longer work. It is possible for a single organism to carry multiple plasmids that encode different β-lactamase enzymes. The combination of two extended spectrum β-lactamase could literally prevent treatment with β-lactams. Moreover, many infectious organisms are already resistant to other classes of antibiotics. This is the case for *Mycobacterium tuberculosis*, which is the causative pathogen of tuberculosis[59,60]. Essentially, we are in a perpetual antibiotic arms race with infectious microorganisms as evolution is inevitable.

Generating new antibiotics is essential to compete with the ever evolving infectious microorganisms, but we can also extend the utility of existing antibiotics by combatting the resistance mechanisms. For β-lactam resistant infections, one approach is to administer a β-lactam antibiotic that is outside the infectious organism's β-lactamase activity spectrum. An even more effective approach is to pair a β-lactam antibiotic with a β-lactamase inhibitor. Both approaches require prior knowledge of the sensitivity of the organism to β-lactam antibiotics and of the type of β-lactamase they may carry. The differences in the catalytic mechanisms and active site architecture between β-lactamase classes and families require careful selection of the appropriate combination.

There are three mechanism-based β-lactamase inhibitors that are clinically used: clavulanic acid, tazobactam, and sulbactam[61]. Clavulanic acid is a natural product that

was originally isolated from *Streptomyces clavuligerus*[62]. Sulbactam and tazobactam are sulfone derivatives of penicillin[63,64]. Clavulanic acid, tazobactam, and sulbactam are β-lactams themselves, and inhibit by forming stable acyl-intermediates with the catalytic serine residue of class A, B, and D enzymes[65-68], and are ineffective against class B MBL enzymes because they do not have a catalytic serine[30,61]. Mechanism-based inhibitors can be considered as poor β-lactamase substrates because they are eventually hydrolyzed and enzymatic activity is restored[69]. As of 2010, six inhibitor-resistant variants of the SHV family have already been clinically isolated, and dozens for the TEM family[57]. The lack of clinically approved inhibitors for MBL enzymes, and the alarming emergence of inhibitor resistant variants makes novel β-lactamase inhibitor discovery essential to maintaining the utility of existing and future β-lactam antibiotics.

Non-β-lactam β-lactamase inhibitors have yet to enter the clinic but are in development. Drawz and Bonomo provide an extensive review of β-lactamase inhibitors[61]. The classes of inhibitors that possess greater potential for clinical utility include molecules that can bind reversibly (boronic acids), irreversibly (hydroxamates), or are very slowly hydrolyzed as substrates[61,70].

The boronic acids are a unique class of inhibitors due to their ability to form reversible covalent bonds with the active site serine of proteases[71-77] and β-lactamase[78,79]. Boronic acids were originally identified as subtilisin protease inhibitors[76]. Later, the crystal structures of boronic acid covalent adducts in complex with subtilisin[73] and of alpha-lytic protease with peptide boronic acids helped to elucidate that the serine protease mechanism proceeds through a tetrahedral intermediate[77]. The tetrahedral

intermediate structure of a boronic acid inhibitor in complex with class A β-lactamase TEM-1 revealed similar mechanistic insights[80]. Extensive biochemical and biophysical characterization of boronic acids with the class C β-lactamase AmpC led to the development of low nanomolar inhibitors[81-83]. A fragment based approach to optimizing AmpC boronic acid inhibitors resulted in subnanomolar inhibitors that are active *in vivo* [84]. Recently, the benzoxaborole scaffold was identified as a new class of β-lactamase inhibitor with activity against class A β-lactamase CTX-M and TEM-1, and class C β-lactamase CMY-2 and AmpC[85]. These studies signify that boronic acids continue to show potential for pairing with β-lactam antibiotics for treatment of infectious disease.

The recent discovery that O-aryloxycarbonyl hydroxamates can inactivate class C β-lactamase P99 and AmpC, and class A enzyme TEM-1 suggests that this novel class of β-lactamase inhibitor may be useful against many infectious organisms[86]. The mechanism of inactivation is similar to the mechanism of substrate catalysis in that the molecule forms an acyl-intermediate with the catalytic serine which is subsequently hydrolyzed. Alternatively, a second aminolysis reaction occurs with catalytic lysine resulting in crosslinking of the active site with the inhibitor[87]. It is possible that these β-lactamase inhibitors may also inhibit PBPs, but studies have yet to be reported.

NXL-104, or Avibactam, is a broad spectrum non-β-lactam β-lactamase inhibitor of class A, C, and D enzymes[88]. Biochemical characterization of NXL-104 with TEM-1, KPC-2, CTX-M, demonstrate potent inhibition of β-lactamase activities and the ability to form extremely stable covalent intermediates with the enzyme due to the slow decarbamylation reaction[89-91]. Co-crystal structures with CTX-M and BlaC show that

NXL-104 forms several conserved hydrogen bonds with the active site residues that substrates contact[70,91]. NXL-104 in combination with ceftazidime has demonstrated efficacy against *Klebsiella pneumonia* and *Enterobacteriaceae species* in murine infection models[92,93].The stability of the NXL-104 adducts with β-lactamase is an improvement over classical mechanism-based inhibitors.

The distinct mechanistic difference between MBLs and serine β-lactamase precludes the use of the aforementioned β-lactamase inhibitors for MBL inhibition. MBL inhibitors primarily utilize carboxylate or thiol/mercapto functional groups to chelate the active site zinc cofactors that are required for MBL activity. Some examples include mercaptocarboxylates, pyridine carboxylates, thiomandelates, mercaptoacetic esters, and succinic acid derivatives[61]. Biochemical and biophysical characterization of thiol derivatives with MBLs demonstrate their modest micromolar affinities and function by chelating the active site zinc cofactor[61]. Unfortunately many of these inhibitors are promiscuous metal chelators, which present a challenge to designing specificity and limit their practical utility for treatment of infections. However, increasing the number of contacts that the inhibitors make with active site residues via rational design is a strategy to increase their potency and specificity.

Continuous advances to combat β-lactamase mediated β-lactam resistance through the design of β-lactamase inhibitors and more effective β-lactams is the reason that we are able to still use β-lactam antibiotics today. However, the arms race is never ending. Therefore, it is imperative that we continue to stay ahead of the drug resistance curve by developing novel inhibitors and antibiotics that evade established resistance

mechanisms.

Tuberculosis (TB) remains one of the world's most deadly infectious diseases. According to the World Health Organization (WHO) Global Tuberculosis Report 2012, 1.4 million people died from TB, and it was estimated that 8.7 million new cases emerged in 2011. While the number of new cases is slowly declining (2% from 2010 to 2011), the number of multidrug-resistant TB (MDR-TB) cases is still increasing with over 60,000 new cases reported in 2011[94].

MDR-TB is defined as being resistant to both frontline drugs isoniazid and rifampicin, at least one fluoroquinolone, and at least one second line aminoglycoside injectable. Major factors contributing to MDR-TB include genetic factors such as acquired compensatory mutations that confer resistance and poor patient compliance[59,95]. Innate resistance mechanisms also prevent the use of existing FDA approved drugs such as β-lactams.

The increase of MDR-TB demands the development of new therapeutic strategies. Mutagenesis studies revealed several essential *Mtb* genes that code for potential drug targets. Alternatively, repurposing of existing FDA approved drugs for tuberculosis treatment is of particular interest, especially in the case of β-lactams. β-lactams, the most widely used antibiotics in history, have the potential to treat one of the world's most infamous diseases. The main obstacle to using β-lactam antibiotics for TB chemotherapy is overcoming the primary mechanism of β-lactam resistance in *Mtb*.

The role of the *blaC* gene of *Mtb* in innate resistance to β-lactam antibiotics was confirmed by disc diffusion assays with the Δ*blaC* strain. No β-lactamase activity was

detected, suggesting that the *blaC* gene encoded the primary β-lactamase that conferred resistance to β-lactam antibiotics[96]. The crystal structure of the BlaC enzyme revealed a conserved class A β-lactamase architecture with a flexible active site loop[97]. Kinetic analysis of BlaC with multiple classes of β-lactams demonstrated the extended spectrum activity of BlaC, including the ability to slowly hydrolyze tight binding carbapenems, and to be inhibited by clavulanic acid[69,97]. These observations suggested that the sensitivity of *Mtb* to β-lactam antibiotics may be restored by inhibition of the BlaC enzyme.

The effectiveness of combining the β-lactamase inhibitor clavulanic acid with the β-lactam meropenem at killing extensively drug resistant *Mtb* (XDR-TB) was eventually demonstrated[98]. This observation was extremely significant because it essentially opened the door to potentially utilizing β-lactam antibiotics to combat MDR and XDR-TB. Meropenem and other carbapenems are particularly potent relative to other β-lactam classes because of their dual function of targeting essential PBPs as well as inhibiting β-lactamase[99]. Carbapenems binding tightly to BlaC (meropenem $Ki = 1.1 \pm 0.8$ μM) to form transient acyl-intermediates. However, because carbapenems are BlaC substrates, they are eventually hydrolyzed and inactivated by the enzyme[98,100]. This results in depletion of active β-lactam that could be used to target essential PBPs. Moreover, the activity of BlaC is completely restored to further degrade active β-lactams.

These preliminary investigations show marked capacity for the treatment of *Mtb* with β-lactams, but there is still room for improvement. Fighting *Mtb* with combinations of β-lactamase inhibitors and β-lactams is a two-part equation. Both the β-lactam

antibiotics and on the β-lactamase inhibitors need to be as effective and efficient as possible. The ability of β-lactams to elicit their antibiotic activity is determined by several factors including the potency against their essential PBP enzyme targets. In the case of *Mtb*, innate β-lactam resistance is due to the BlaC enzyme[96].

The main drawback to carbapenem scaffold is that they lack selectivity. An ideal target selective β-lactam would bind preferentially to its essential target PBP over BlaC. If the main hurdle to combatting *Mtb* with β-lactams is innate β-lactamase mediated resistance, it would be advantageous to use a β-lactam that is potent against *Mtb* cells and evades BlaC mediated resistance. A structure activity relationship (SAR) focused on identification and characterization of *Mtb* active β-lactams that evade β-lactamase mediated resistance would be a step toward designing new target selective β-lactams that resist binding to BlaC.

Chapter 2 of this investigation addresses the structural relationship between β-lactams and the BlaC active site to understand how specific intermolecular interactions influence β-lactamase activity and ultimately resistance of *Mtb* cells to these β-lactams. In order to identify target selective β-lactams, the contribution of BlaC to resistance to individual β-lactams was determined using whole cells of *Mtb*. The results showed variation in the magnitude of resistance due to BlaC. Biochemical and biophysical characterization of the β-lactams with BlaC lead to the identification of the structural basis for the observed differential magnitudes of resistance of *Mtb* to the β-lactams, and specifically shed light on how faropenem evades BlaC mediated resistance more than all other β-lactams investigated. The results demonstrate the biological repercussions of a

hydrophobic interaction between BlaC and β-lactams that increases resistance on the organismal level.

Previous studies with existing clavulanic acid demonstrated the ability to inactivate BlaC and to potentiate the activity of β-lactams antibiotics against *Mtb in vitro* and *in vivo*[69,98,101]. Clavulanic acid inhibits BlaC (K_i = 12.1 μM) by forming a covalent acyl-enzyme adduct, but because it is a β-lactam it is eventually hydrolyzed by the enzyme and β-lactamase activity is restored[69,70,102]. More recently, a non-β-lactam mechanism-based inhibitor of BlaC was reported to form a more stable inhibitor complex than clavulanate, but the authors report the poor affinity of NXL-104 for BlaC prevents practical implementation until derivatives are designed[70]. The continuous advancement of inhibitors of *Mtb* BlaC holds promise for future treatment of *Mtb* with β-lactams.

Chapter 3 of this investigation illustrates a biochemical and biophysical inhibitor SAR with BlaC that identifies the structural features of the active site that are important for potent inhibition by boronic-acids, and demonstrates their utility as potentiators of β-lactam antibiotic activity against *Mtb*. Boronic acids have recently proven to be extremely potent β-lactamase inhibitors with demonstrated activity *in vivo*[84], and remain an untapped class of inhibitors for BlaC and combination with β-lactams to combat *Mtb*[85]. Boronic acids are also not degraded by β-lactamase.

To identify boronic acid inhibitor scaffold for rational design of BlaC inhibitors, a boronic acid library was enzymatically screened with BlaC. The results from the screen identified benzoxaborole as an inhibitor scaffold, and several benzoxaborole

derivative molecules were synthesized for SAR generation. The derivative inhibitor molecules were enzymatically characterized with BlaC which enabled identification of the structural features of the benzoxaborole inhibitors that drive potent inhibition of BlaC. The co-crystal structures of BlaC with three benzoxaborole inhibitors revealed how the functional moieties of the derivative inhibitors interact with the BlaC active site, and how those interactions influence affinity for the enzyme inhibitory activity. The most potent benzoxaborole competitively inhibited BlaC (K_i = 0.7 μM), and the SAR offered insights to further improve affinity. Moreover, preliminary experiments demonstrate the ability of the benzoxaboroles to potentiate the antibiotic activity of amoxicillin on *Mtb* cells. Cumulatively, the results demonstrate the utility of benzoxaboroles as BlaC inhibitors and potential to be paired with a β-lactam antibiotic for combating *Mtb*.

Chapter 4 of this study addresses the challenge of early tuberculosis diagnosis through the design and optimization of BlaC-specific molecular probes[103]. The WHO estimated that nearly 9 million new cases of tuberculosis appeared in 2011, and more frightening is that the number of MDR-TB cases is increasing[94]. Without diagnosis, infected persons may remain unknowingly contagious and exponentially transmit disease. Early detection and diagnosis of tuberculosis would reduce dissemination and mortality rates. Diagnostics must be specific enough to discriminate between pathogens, and sensitive enough to prevent false negatives. Many of the commonly used diagnostics including smear tests, skin tests, and chest X-rays are not sensitive or specific enough to rule in or rule out tuberculosis alone[104-106]. Several probes were synthesized and

enzymatically characterized to identify characteristics that enhance probe specificity and selectivity for BlaC over TEM-1[103]. Crystal structures of BlaC and the fluorescent probes illustrate the structural determinants for the observed selectivity. The efficacy of a BlaC specific β-lactam-based fluorogenic probes was demonstrated by detecting down to 10 colony forming units of bacillus *Mycobacterium bovis* Calmette–Guérin (BCG) in human sputum[103].

The New Delhi Metallo-β-lactamase-1 (NDM-1) gene is rapidly spreading to pathogenic microorganisms all over the world[107]. NDM-1 is a potent, broad spectrum class B1 metallo-β-lactamase that confers bacterial resistance to all classes of β-lactams, except for monobactams[108]. Since the first reported isolation of NDM-1 producing *Klebsiella pneumoniae* in Sweden in[109], NDM-1 has surfaced in several countries around the globe in multiple pathogenic microorganisms[110-125]. Many of the infectious organisms are already resistant to several frontline therapeutics, which suggests the possibility of a future with many untreatable infectious diseases.

Chapter 5 of this investigation describes the biochemical and biophysical characterization of the class B β-lactamase NDM-1 that identified the structural and molecular basis for the promiscuous activity of NDM-1[48]. The results show the flexible nature of the NDM-1 active site, which is comprised of 5 loops that donate residues that form the catalytic triads that coordinate the zinc cofactors. The flexible NDM-1 active site loops and the enlarged active site relative to other MBL's contribute to the observed promiscuous extended spectrum substrate specificity of NDM-1.

The diverse sequences of MBLs and inconsistency with the number of zinc cofactors required for activity make the mechanism of MBLs a controversial subject[126,127]. Crystal structural data from multiple MBLs suggests that a zinc coordinated solvent molecule, likely a hydroxide serves as the nucleophile that attacks the β-lactam carbonyl for ring opening[45,127]. Spectroscopic data suggest three reaction species including substrate, ring-opened intermediate, and product[51]. Reaction completion requires protonation of the lactam amide nitrogen, and the origin of the proton has not been elucidated. The catalytic base is also subject of debate. One hypothesis suggests that a conserved aspartic acid residue participates in the reaction mechanism as the general base, but mutation of the conserved aspartate to alanine in CphA decreased but did not abolish β-lactamase activity[128,129], excluding the conserved aspartate as the catalytic base.

Chapter 6 of this investigation reveals the mechanism of NDM-1 β-lactamase activity and identifies additional factors that give NDM-1 the capacity to hydrolyze substrates without discrimination[52]. The biochemical activity of NDM-1 and the distance between the zinc cofactors in crystal structures were determined to be pH dependent. As the pH increased, the distance between the zinc cofactors in crystal structures decreased, and the catalytic activity of NDM-1 increased. The distances between the zinc cofactors were consistent with coordination of a catalytic water molecule at lower pH and a hydroxide ion at higher pH, emphasizing the role of pH in the NDM-1 reaction mechanism[52]. Crystal structures of NDM-1 were solved in complex with an unhydrolyzed β-lactam substrate and with hydrolyzed products. These structures were

used for quantum mechanics / molecular mechanics (QM/MM) simulations to estimate the free energy along the β-lactamase reaction coordinate using several mechanistic models. The results suggest that the most energetically favorable reaction mechanism uses bulk water as the nucleophile that attacks the β-lactam for ring opening by NDM-1[52]. The proposed mechanism is in accordance with biochemical and biophysical pH dependence data in that the reaction is energetically favorable using either zinc coordinated water molecule or hydroxide ion as the base. Taken together, the flexibility of the active site loops, the lack of specific interactions between the substrates and NDM-1 active site, the ability to utilize multiple divalent cations to recognize substrates, catalyze hydrolysis of β-lactams over a wide pH range, and use a coordinated water molecule or hydroxide ion as the catalytic base all contribute to NDM-1's extreme promiscuity[52,108].

CHAPTER II

STRUCTURAL AND FUNCTIONAL INSIGHTS INTO DIFFERENTIAL RESISTANCE OF *Mycobacterium tuberculosis* TO BETA-LACTAMS FAROPENEM, BIAPENEM, AND TEBIPENEM BY BlaC

OVERVIEW

Mycobacterium tuberculosis (*Mtb*) is innately resistant to β-lactam antibiotics because the bacilli express the broad spectrum class A β-lactamase, BlaC. β-lactamase inhibitors like clavulanate potentiate the activity of β-lactams that are susceptible to inactivation by BlaC. We show that the MIC of faropenem on *Mtb* does not change with the addition of the β-lactamase inhibitor clavulanate. Inhibition of BlaC by clavulanate did not potentiate the activity of faropenem like other β-lactams, suggesting that the structure activity relationship of BlaC with faropenem is distinct. Faropenem, biapenem, and tebipenem form covalent adducts that inhibit BlaC; their stabilities were monitored with mass spectrometry. BlaC acyl-intermediate (AI) crystal structures with β-lactams show specific active site interactions that explain the difference in the affinity of BlaC for the lactams and the difference in the stability of the AI complexes. The results provide structural and functional insight into the differential resistance of *Mtb* to these antibiotics by BlaC. To test faropenem's activity *in vivo,* the bacterial burden in the lung of *Mtb* infected mice was assessed. Faropenem treatment reduced lung cfus by 0.7 logs

within 6 days, demonstrating faropenem's potential utility as a therapeutic, possibly alone or in combination with other antibiotics.

INTRODUCTION

The β-lactam antibiotics are the most widely used antibiotics in history[5] because their essential microbial targets are not present in humans[4]. β-lactams elicit their antibiotic activity by binding to and inactivating essential cell wall biosynthetic enzymes, penicillin binding proteins (PBPs)[6-8]. Resistance mechanisms include upregulation of PBP that are less susceptible to β-lactams[130], and upregulation of PBPs that change the peptidoglycan structure of the cell wall[131]. The primary mechanism of resistance can be attributed to the dissemination of plasmid encoded β-lactamase genes among infectious microorganisms[36,37,53]. β-lactamase mediated drug resistance has been the subject of detailed investigation for decades; however, research is increasingly important due to the emergence of totally drug resistant infections[132], and the evolution of β-lactamase that can inactivate nearly all β-lactam antibiotics[133]. β-lactams are not used to treat *Mtb* infection because the bacilli express a chromosome-encoded broad spectrum class A β-lactamase, BlaC. Investigation of the anti-mycobacterial properties of β-lactams goes back several decades[134,135], but still no orally available or FDA approved β-lactams exist for tuberculosis treatment.

The role of the blaC gene of *Mtb* in innate resistance to β-lactam antibiotics was confirmed by disc diffusion assays with the ΔblaC strain. No β-lactamase activity was

detected, suggesting that the blaC gene encoded the primary β-lactamase that conferred resistance to β-lactam antibiotics[96]. The crystal structure of the BlaC enzyme revealed a conserved class A β-lactamase architecture with a flexible substrate specificity loop[97]. Thorough kinetic analysis of BlaC with multiple classes of β-lactams demonstrated the extended spectrum activity of BlaC, including the ability to slowly hydrolyze tight binding carbapenems, and the ability to become inactivated by the mechanism based inhibitor clavulanate[69]. More recently, a non-β-lactam mechanism-based inhibitor of BlaC was reported to form a more stable inhibitor complex than clavulanate[70].

Carbapenems are effective β-lactam antibiotics that inhibit essential PBP targets. They also potentiate their activity by transiently inhibiting class A β-lactamase. The combination of meropenem with the β-lactamase inhibitor clavulanate has activity on *Mtb in vitro*, and even has modest activity against a chronic infection model of murine tuberculosis[101]. Combining carbapenems with β-lactamase inhibitors is effective because carbapenems only transiently inhibit β-lactamase, and eventually become hydrolyzed and inactivated[69,99].

Ideally, a more efficient β-lactam would selectively bind to essential PBP targets over β-lactamase, which would reduce resistance and eliminate the requirement for a combination with a β-lactamase inhibitor. Carbapenems do not fit this description because they characteristically bind very tightly to class A β-lactamase like BlaC[69,98-100]. The structural similarity that provides PBPs, transpeptidases, and β-lactamase the ability to bind to and hydrolyze the same β-lactams, makes designing a selective molecule

challenging[29,30]. A recently reported β-lactam probe demonstrated selectivity for BlaC over the very similar β-lactamase, TEM-1[103].

Screening for a target-selective β-lactam antibiotic for tuberculosis can be done by comparing the minimum inhibitory concentrations (MIC) of β-lactams on *Mtb* cells in presence and absence of active BlaC enzyme. β-lactams with no change in MIC would theoretically be less affected by innate resistance due to β-lactamase. We found that *Mtb* is less resistant to faropenem than all β-lactams tested. Biochemical and biophysical characterization of the β-lactams with BlaC elucidated the molecular basis of decreased resistance that distinguishes faropenem from structurally similar β-lactams biapenem and tebipenem.

RESULTS

Whole cell assays

The potency of β-lactam antibiotics against *Mtb* may be severely decreased by the presence of active BlaC enzyme. Clavulanate, potentiates the whole cell activities of β-lactams against *Mtb* by inhibiting BlaC and preventing the depletion of active β-lactam available to target essential PBP's. Except for faropenem, the potency of each β-lactam was enhanced when clavulanate was added (Table 2.1). We interpreted the magnitude of change between the MIC in the presence and absence of clavulanate to reflect the amount of degradation of each β-lactam by BlaC. For example, the MIC of β-lactams reported to be rapidly turned over by BlaC, e.g., amoxicillin (k_{cat} = 600 ± 20

β-lactam	MIC (μg mL^{-1})	[a]MIC (μg mL^{-1})
Amoxicillin	>10.0	1.3
Biapenem	2.5	0.6
Cefotaxime	1.3	0.6
Faropenem	0.6	0.6
Imipenem	5.0	0.6
Meropenem	2.5	0.6
Tebipenem	0.6	< 0.3

Table 2.1. Activity of β-lactams on *Mycobacterium tuberculosis.* Minimum inhibitory concentration (MIC) of β-lactam antibiotics to inhibit growth of *Mtb*. [a]MIC assayed in presence of 2.5μg mL^{-1} clavulanate.

min-1), were expected to decrease with the addition of clavulanate more than β-lactams that are not rapidly turned over by BlaC, e.g., imipenem (k_{cat} = 10 ± 1 min-1) and meropenem (k_{cat} = 0.08 ± 0.01 min-1)[69]. When clavulanate was added, amoxicillin's MIC decreased from >10 µg mL-1 to 1.3 µg mL-1, imipenem's MIC decreased 8-fold from 5 µg mL-1 to 0.6 µgmL-1, and meropenem's MIC decreased 4-fold from 2.5 µg mL-1 to 0.6 µg mL-1.

Fourier transform ionization cyclotron resonance mass spectrometry

The class A β-lactamase reaction proceeds to form a covalent acyl-intermediate (AI), which is hydrolyzed by a nucleophilic hydroxyl radical generated by deprotonation of the hydrolytic water coordinated by catalytic base Glu166[61]. If the reaction doesn't complete, the covalently bound AI stalls the enzyme in a catalytically incompetent state. The characteristic R1 hydroxyethyl group of carbapenems is responsible for the formation of stable AIs that inhibit β-lactamase[98,100,136,137].

Faropenem, a penem, is structurally distinguished from carbapenems by the presence of a sulfur atom at the 4 position of the dihydrothiazole ring, but shares the AI stabilizing R1 hydroxyethyl group (Figure 2.1). The MIC of faropenem on *Mtb* did not change when clavulanate was added, which may partially be due to inhibition of BlaC by formation of a stable AI analogous to carbapenems. To test this, the stabilities of the BlaC AI complexes with faropenem, biapenem, and tebipenem were monitored using Fourier transform ion cyclotron resonance mass spectrometry (FTICR-MS). The raw mass spectra showed two reaction species for each AI complex in the early time

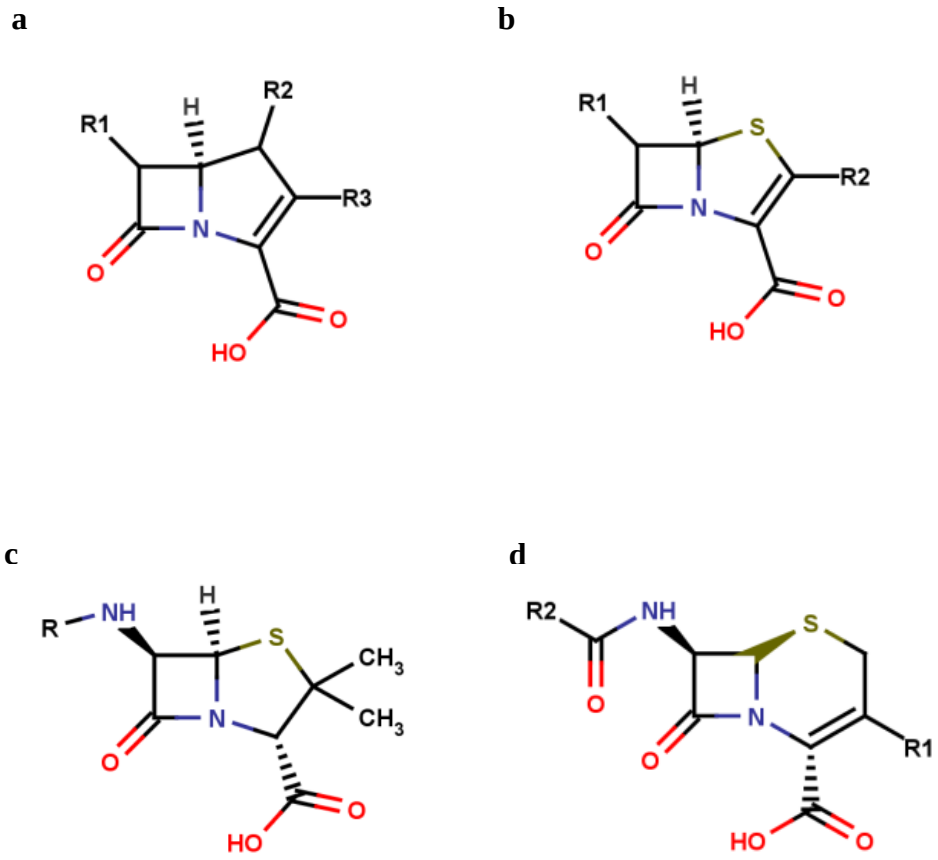

Figure 2.1. Chemical structures of β-lactam scaffolds. (a) carbapenem, (b) penem, (c) penam, and (d) cephalosporin β-lactams.

points, which corresponded to the masses of AI complexes with BlaC (Appendix Figure A1). The masses of the first AIs corresponded to the BlaC-biapenem complex (30886 Da), BlaC-faropenem complex (30820 Da), and BlaC-tebipenem complex (30918 Da). The masses of the second AIs corresponded to the BlaC-biapenem complex – 44 Da (30842 Da), BlaC-faropenem complex – 44 Da (30776 Da) and BlaC-tebipenem complex – 44 Da (30874 Da). The masses of the second AI reaction species (– 44 Da) were consistent with the proposed model of deacetylation[98].

As the reactions reached completion, the AI reaction species decreased concomitantly with the appearance of regenerated BlaC (30535 Da). To reduce the data sets for comparison, regenerated BlaC enzyme was plotted as a function of time for each reaction (Figure 2.2). Regeneration of the free BlaC enzyme is dependent upon the stability of the AI complex. The more stable the AI complex, the longer it takes to regenerate the free BlaC enzyme. The graph shows that BlaC's reaction with tebipenem took the longest time to regenerate free BlaC enzyme, followed by biapenem and faropenem.

Inhibition kinetics

Inhibiting BlaC by forming stable AIs results in decreased β-lactam hydrolysis and inactivation. β-lactams that are poor substrates for β-lactamase behave as classical competitive inhibitors[99]. Inhibition of BlaC by faropenem, biapenem, and tebipenem was measured by monitoring the linear initial velocities of nitrocefin hydrolysis in presence of varying concentrations of the β-lactams. Inhibition curves and chemical structures are

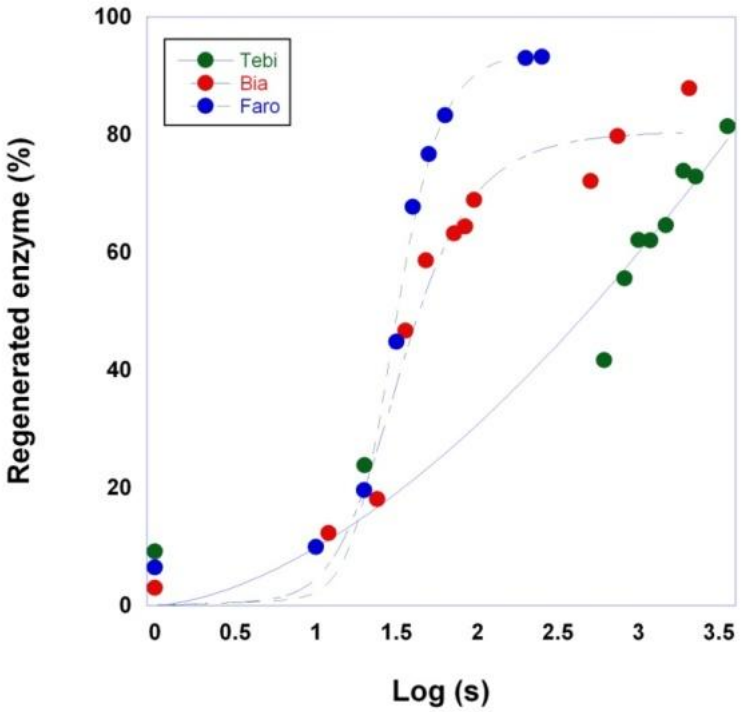

Figure 2.2. Time course of BlaC reactions analyzed with Fourier transform ion cyclotron resonance mass spectrometry. The population of regenerated enzyme for BlaC reactions with tebipenem (green), biapenem (red), and faropenem (blue) are plotted as a function of time (s).

displayed for each β-lactam (Figure 2.3). Faropenem (K_i = 14.2 ± 2.5 μM) inhibits BlaC with an affinity that is 5-fold less than tebipenem (K_i = 3.0 ± 0.2 μM) and 4 fold less affinity than biapenem (K_i = 3.7 ± 0.3 μM).

BlaC-β-lactam acyl-intermediate crystal structures

BlaC AI complex crystal structures were solved to examine the structural features that influence the affinity for the BlaC active site and stability AI complexes. Crystallographic data collection and refinement statistics are reported in Appendix Table A1. Catalytically incompetent BlaC Glu166Ala mutant crystals were used to trap amoxicillin, cefotaxime, cefoperazone, and faropenem AIs in the BlaC active site. Each structure had four crystallographically independent molecules in the asymmetric unit, two of which had adequate solvent accessibility to allow ligand binding.

Each lactam was covalently linked to BlaC by the catalytic Ser70, which positioned the carbonyl oxygen in the acyl-linkages to hydrogen bond with the backbone amide nitrogen of Thr237 (Figure 2.4). The amoxicillin AI (Figure 2.4 a) 2'-carboxylate hydrogen bonded to side chain hydroxyls of Ser130 (2.8 Å), and Thr235 (2.8 Å). The Thr237 backbone carbonyl oxygen hydrogen bonded to amoxicillin's side chain amide nitrogen (3.0 Å). The side chain carbonyl oxygen of Asn170 of the substrate specificity loop formed a 2.2 Å hydrogen bond with the amino group of amoxicillin in chain B, with a distance of 3.5 Å in chain C of the asymmetric unit. The difference underscores the flexibility of the loop and weak electron density in this region.

Cephalosporins, cefotaxime and cefoperazone, were designed with bulky R2

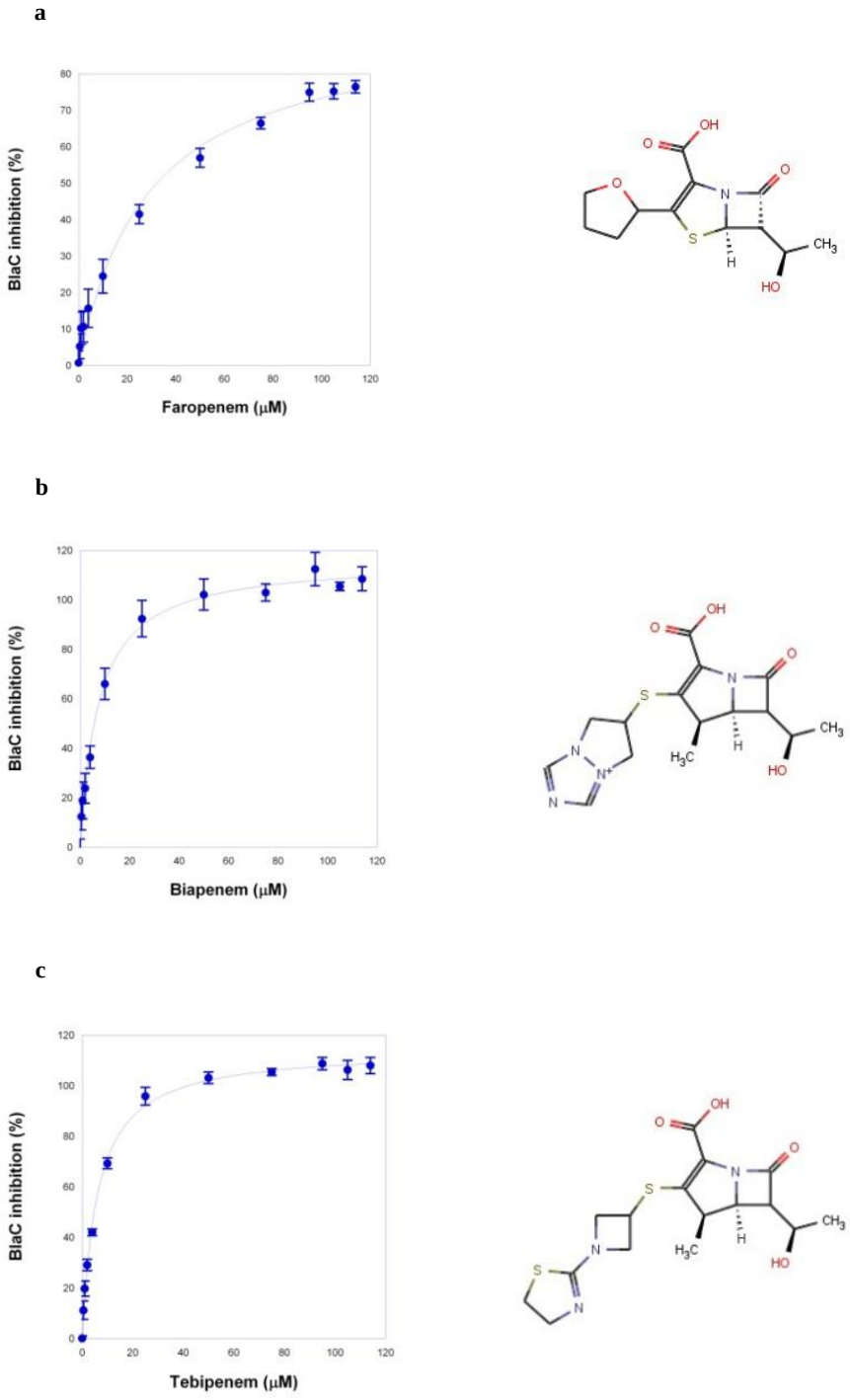

Figure 2.3. Inhibition of BlaC by β-lactams. Faropenem (a), Biapenem (b), and Tebipenem (c).

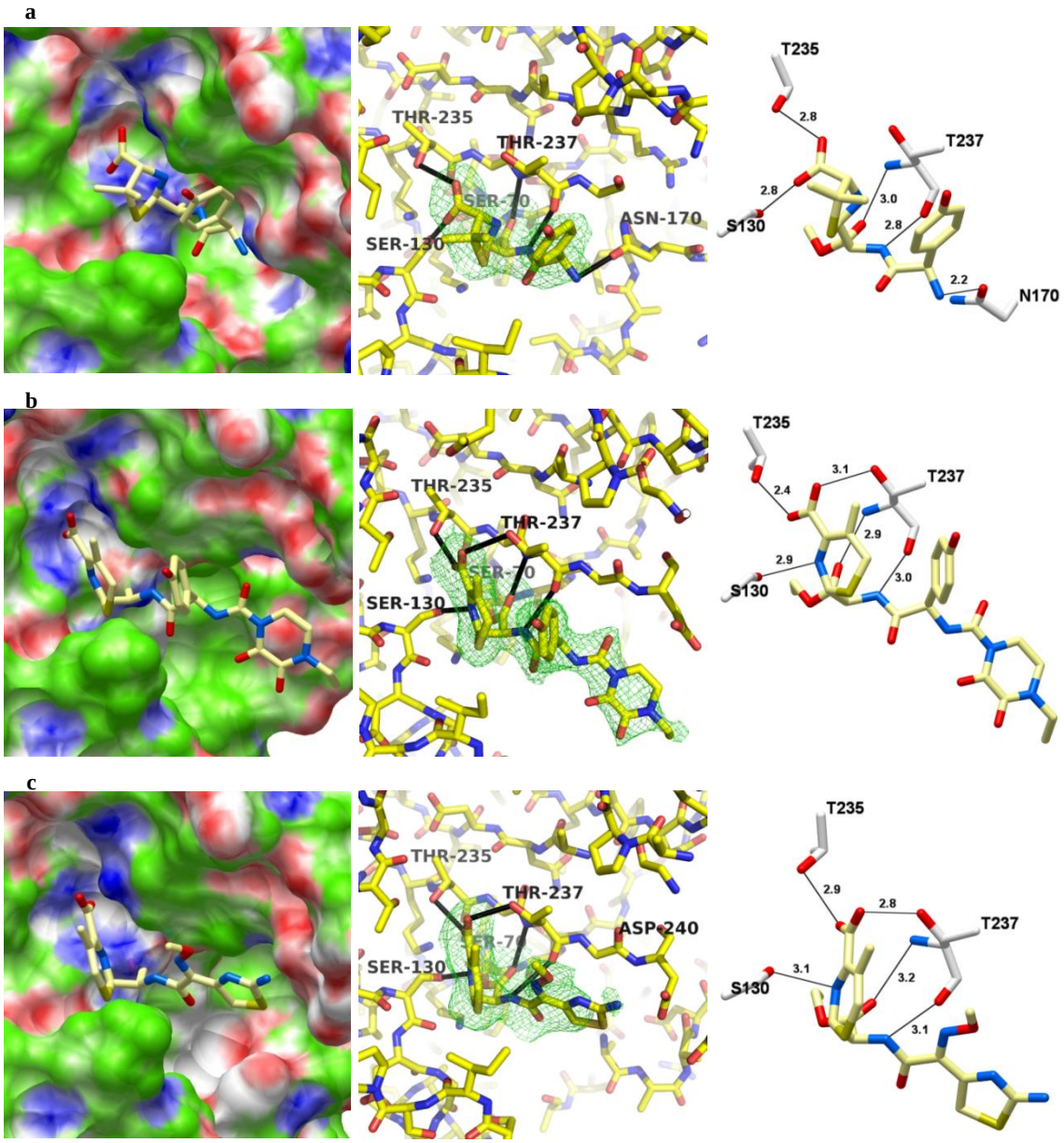

Figure 2.4. Active site details of BlaC acyl-intermediate crystal structures. (Left) Ligand binding pocket surface colored by binding property. white = neutral surface, green = hydrophobic surface, red = hydrogen bonding acceptor potential, and blue = hydrogen bond donor potential. (Middle) F_O-F_C omit map electron density surrounding acyl-intermediates contoured at 2σ (green) and hydrogen bonds as displayed as black lines. (Right) Active site interactions of BlaC acyl-intermediates represented as black lines. (a) amoxicillin, (b) cefoperazone, (c) cefotaxime.

groups that confer stability to β-lactamase mediated hydrolysis[138,139]. The structures showed that the BlaC active site was large enough to contain cefoperazone and cefotaxime AIs. Stabilizing salt bridges between Asp172 - Arg178 and Asp176 - Arg178 present in the BlaC apo structure[97] were broken to increase the flexibility of the loop for Michaelis complex and AI formation.

The BlaC cefoperazone AI structure is the first crystal structure of cefoperazone in complex with β-lactamase (Figure 2.4 b). The structure depicts conserved hydrogen bonds between the side chain hydroxyl of Ser130 and the lactam amide nitrogen (2.9 Å), the 2'- carboxylate oxygen atoms and the side chain hydroxyls of Thr235 (2.4 Å) and Thr237 (3.1 Å), and the backbone amide nitrogen (2.9 Å) and carbonyl oxygen atoms (3.0 Å) of Thr237 with cefoperazone. Displacement of the substrate specificity loop (residues 164 - 172) enlarged the BlaC active site to accommodate the cefoperazone AI.

The BlaC cefotaxime AI (Figure 2.4 c) formed the same hydrogen bonds with Ser130 (3.1 Å), Thr235 (2.9 Å), and Thr237 (2.8 Å) side chain hydroxyls and to the backbone amide nitrogen (3.2 Å) and carbonyl oxygen atoms of Thr237 (3.1 Å). In both liganded molecules of the asymmetric unit, freedom of rotation of cefotaxime's 2-amino-4-thiazolyl prevents precise placement of atomic coordinates. The cefotaxime AI was bound in the same orientation as other class A β-lactamase structures in complex with cefotaxime, with the aminothiazole in proximity of the side chain carboxylate of Asp240[140,141]. The Asp240Gly mutation in class A β-lactamase CTX-M-27 reduced cefotaxime turnover, demonstrating the importance of this residue in cefotaxime binding[142]. Sparse electron density for the substrate specificity loop prevented the

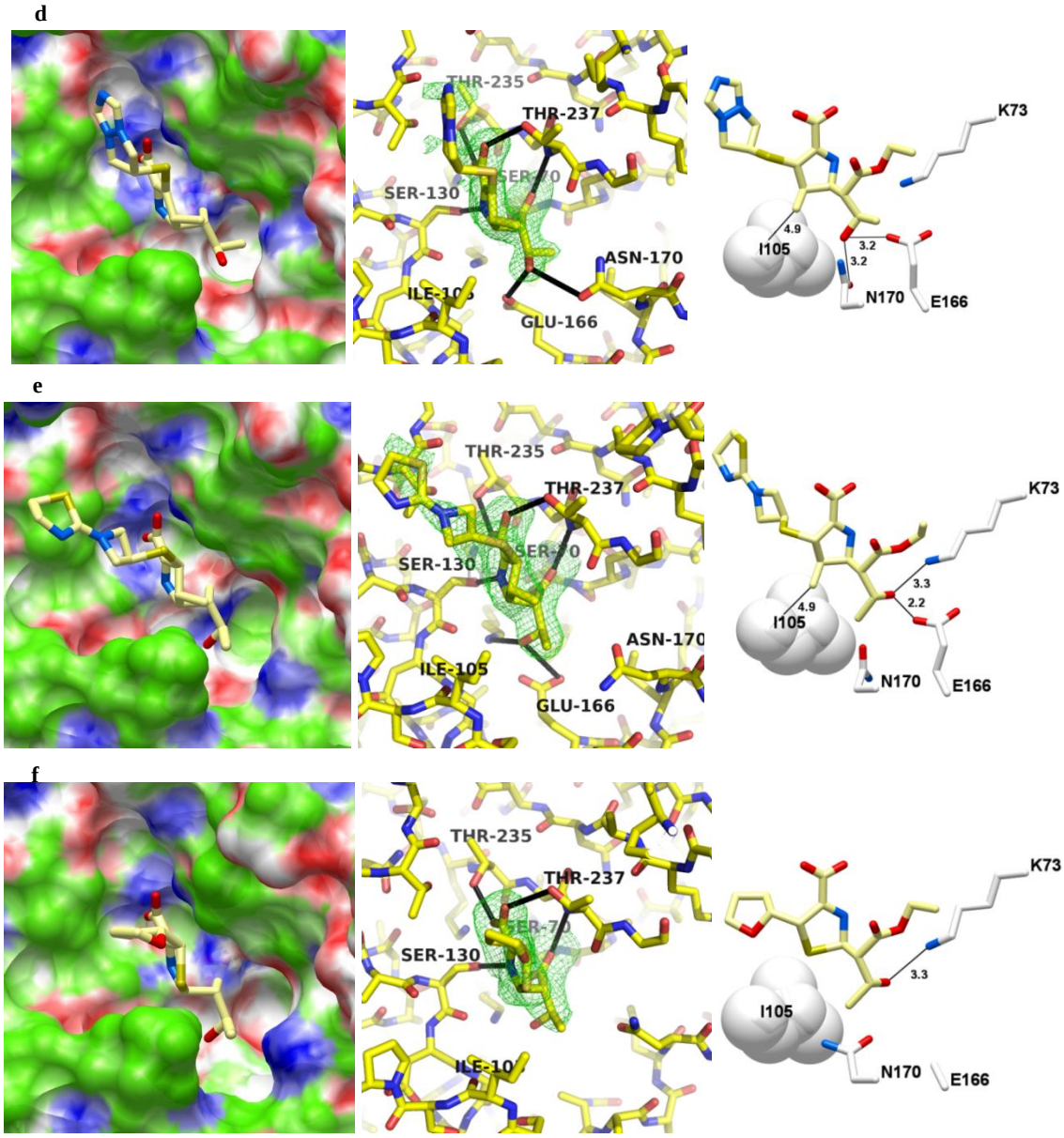

Figure 2.4 continued. Active site details for BlaC acyl-intermediates (d) biapenem, (e) tebipenem, and (f) faropenem.

placement of the side chains and backbone atoms for residues 164-169.

AI crystal structures of BlaC with biapenem, tebipenem, and faropenem showed conserved hydrogen bonds with the substrate recognition residues (Ser130, Thr235, Thr237) and delicate variations in the interactions with the substrate specificity loop and Ile105 that influence binding and stability (Figure 2.4 d-f). The BlaC biapenem AI hydroxyethyl group is positioned to share hydrogen bonds with the side chain carboxylate oxygen of Glu166 (3.2 Å) and the neighboring side chain oxygen of Asn170 (3.2 Å) of the substrate specificity loop, similar to the pre-isomerized ertapenem and doripenem AIs with BlaC[100]. In contrast, the BlaC tebipenem AI tautomerized to the Δ1-pyrroline isomeric state, evidenced by the sp3 hybridized C3 atom. Instead, the tebipenem hydroxyethyl formed a 2.4 Å hydrogen bond with Glu166 side chain carboxylate oxygen atoms and a 3.2 Å hydrogen bond with Lys73 side chain amino nitrogen. This conformation is consistent with the post-isomerized ertapenem, doripenem, and meropenem BlaC AI complexes[98,100]. The R2 methyl group of biapenem and tebipenem faced the hydrophobic side chain of Ile105 side chain that encloses the BlaC active site. The BlaC faropenem AI did not tautomerize to the Δ1-pyrolline isomer. The absence of stabilizing interactions between faropenem's hydroxyethyl group, Glu166, Asn170, and Lys73 were attributed to the Glu166Ala mutation. Since faropenem lacks the R2 methyl group that is present in biapenem and tebipenem, no hydrophobic interaction occurred between the side chain of Ile105 and faropenem.

Therapeutic efficacy of faropenem against M. tuberculosis *infected mouse model*

The lack of innate resistance of *Mtb* to faropenem in whole cell assays prompted us to examine if faropenem has activity on *Mtb in vivo*. Balb/CJ mice were infected with 50-100 cfus/lung *Mtb* Erdmann strain by aerosol inhalation. The experiment included a not treated control, isoniazid treated control, and faropenem treated groups (n=5). After 6 days of once daily treatment, faropenem reduced the bacterial burden in the lung by 0.7 log cfu relative to the no treatment control group (Figure 2.5). Isoniazid decreased the bacterial burden by 2.3 log cfu. The preliminary data demonstrated faropenem's activity *in vivo* and potential utility as a therapeutic in combination with other antibiotics.

DISCUSSION

Since the unveiling of the *Mtb* H37Rv genomic sequence[143], numerous investigators have made significant contributions to understanding the TB pathogen, and develop new cost effective therapeutic regimens. These advancements realize the possibility of eradication of one of the most infamous global diseases. There are many drug targets and lead molecules in development that have potential to become therapeutics. β-lactams have endured the test of time and remain a safe, highly effective, and untapped resource for tuberculosis chemotherapy. Historically, innate resistance of *Mtb* to β-lactams has prevented clinical implementation.

A plausible approach to circumvent innate resistance of *Mtb* to β-lactams

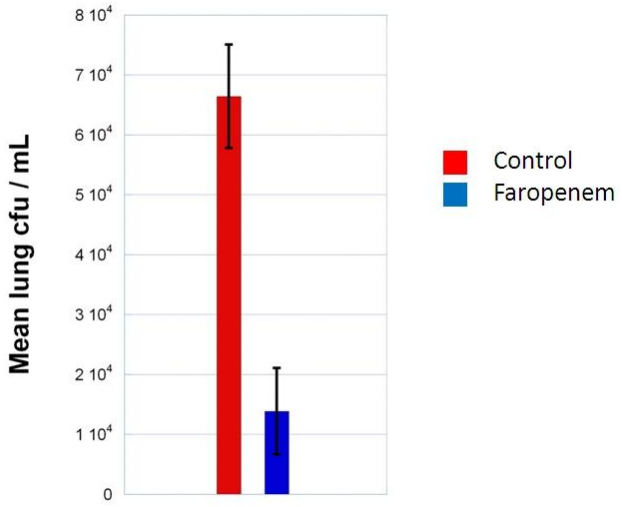

Figure 2.5: Effect of faropenem treatment on *Mtb* infected BALB/CJ mice. Lung colony forming units (cfu/mL) are displayed for faropenem treated and not treated control groups. Error bars represent the standard deviation for each group (n=5).

includes combining a β-lactamase inhibitor with a β-lactam. Meropenem-clavulanate combination has proven to be effective against *Mtb in vitro*[98], and even has activity in vivo[101]. An alternative approach involves treating *Mtb* with a "magic bullet" β-lactam that does not require an inhibitor of β-lactamase to prevent innate resistance. To identify β-lactams that are less susceptible to BlaC mediated innate resistance in *Mtb*, we compared the MIC of β-lactams alone and in combination with the BlaC inhibitor clavulanate. BlaC AI crystal structures were solved to understand the intermolecular interactions that explain the differential innate resistance of *Mtb* to these β-lactams by BlaC. We also compared the difference in stability of the BlaC-AI complexes and ability to inhibit BlaC. The structure activity relationship depicted structural features of amoxicillin, cefoperazone, cefotaxime, biapenem, tebipenem, and faropenem AIs that distinguish their susceptibility to inactivation by BlaC and whole cell activities against *Mtb*.

Each class of β-lactam antibiotics has a characteristic structure that determines susceptibility to β-lactamase enzymes (Figure 2.1). The BlaC amoxicillin AI structure finally depicted amoxicillin's size, shape, and electrostatic complementarity to the active site that facilitates rapid turnover of penams[69]. Penams, like amoxicillin (MIC >10 μgmL-1), are more effective against *Mtb* when combined with clavulanate ([a]MIC = 1.3 μgmL-1) because they are specific class A β-lactamase substrates that don't form stable AI complexes or behave as inhibitors[53]

Cephalosporin AI crystal structures showed that the bulky cephalosporin R2 groups sterically hinder binding to BlaC by forcing displacement of the substrate

specificity loop. This observation is consistent with the reported K_m of cefotaxime (5570 ± 1360 μM)[69]. Cefotaxime (MIC = 1.3 μg mL^{-1}), or newer fourth generation cephalosporins that evade innate resistance by resisting binding and turnover by BlaC may be useful scaffolds for rational design of target selective β-lactam for *Mtb*.

Carbapenems and penems possess a characteristic R1 hydroxethyl group that interrupts the completion of the class A β-lactamase reaction by binding to and stabilizing the enzyme in a catalytically incompetent conformation[98,136,137,144]. We measured the stability of faropenem, biapenem, and tebipenem BlaC-AIs with mass spectrometry. The spectra showed that tebipenem formed a more stable AI complex with BlaC than faropenem or biapenem, evidenced by the duration of detectable AI and the time required to regenerate the free BlaC enzyme. These results suggest that tebipenem should be less susceptible to BlaC mediated resistance by inhibiting further turnover.

Faropenem, biapenem, and tebipenem differ primarily by the structure of their R3 side chains, but the crystal structures did not show any specific interactions between the R3 side chains and the active site, indicating that the differences in the stability of their AI complexes and susceptibility to inactivation by BlaC are due to other interactions (Figure 2.4 d-f). The tebipenem AI isomerized within the BlaC active site and formed hydrogen bonds with Glu166 (2.4 Å) and Lys73 (3.2 Å), where the less stable biapenem AI formed interactions with Glu166 (3.2 Å) and Asn170 (3.2 Å). Previous characterization of ertapenem and doripenem AIs with BlaC revealed that these conformations and interactions were time dependent, and suggested that the isomerized conformation was the most thermodynamically preferred orientation[144]. It is plausible

that biapenem and faropenem could also isomerize and adopt a more stable AI conformation, but no evidence suggests that isomerization is necessary for reaction completion. The structures showed that the stability of the faropenem, biapenem, and tebipenem AI complexes are partly dependent on subtle differences in the orientation of the R1 hydroxyethyl group relative to residues in the BlaC active site.

Certainly, the affinity of BlaC for the β-lactams has an effect on the level of innate resistance observed. If the β-lactams do not bind to the β-lactamase enzyme, they will not be turned over. Inhibition constants determined for tebipenem (*Ki* = 3.0 ± 0.2 μM) and biapenem (*Ki* = 3.7 ± 0.3 μM) were similar to the previously determined inhibition constant for meropenem (K_i = 1.1 ± 0.8 μM). The previously reported steady state Michaelis constant for faropenem (K_m =55 ± 11 μM) was approximately 4 times greater than the inhibition constant determined for faropenem (K_i = 14.2 ± 2.5 μM) in this study. Whether assayed as an inhibitor or a substrate, faropenem does not bind as tightly to BlaC as carbapenems.

The main feature that reduces the affinity of BlaC for faropenem relative carbapenems is the likely the lack of the R2 methyl group on faropenem (Figure 2.2). The active site of BlaC is partially bordered by a loop containing Ile105, which forms a hydrophobic environment that encloses substrates. BlaC AI with biapenem and tebipenem both have an R2 methyl group that can form hydrophobic interactions with the side chain of Ile105 upon binding to the active site (Figure 2.4 d-e). This interaction likely contributes to the affinity of BlaC for biapenem and tebipenem. Faropenem lacks

the R2 methyl group and hydrophobic interaction with Ile105, which is consistent with the decreased affinity of faropenem for BlaC relative to biapenem and tebipenem.

Despite their structural similarity, the results showed that *Mtb* is more resistant to biapenem and tebipenem than faropenem; when clavulanate was added, biapenem's MIC decreased from 2.5 μg mL^{-1} to 0.6 μg mL^{-1}, tebipenem's MIC decreased from 0.6 μg mL-1 to < 0.3 μg mL^{-1}, and faropenem's MIC remained at 0.6 μg mL^{-1}. However, tebipenem binds more tightly to BlaC than biapenem and faropenem, and forms the most stable AI complex, suggesting that tebipenem would be less susceptible to inactivation. Therefore, it seems that binding is the limiting factor to evading inactivation by BlaC because the formed AI is committed to hydrolysis. For example, tebipenem (K_i = 3.0 ± 0.2 μM) binds 4 fold tighter to BlaC than faropenem (K_i = 14.2 ± 2.5 μM), which results in increased inactivation of tebipenem relative to faropenem at their MIC (0.6 μg mL^{-1} or 1.9 μM).

A recent study involving chronically *Mtb*-infected mice reported a modest reduction in lung cfu's after 6 days of meropenem-clavulanate treatment, demonstrating the efficacy of carbapenems in murine tuberculosis models[101]. Faropenem by itself seems to have as much activity *in vivo* as the combination of meropenem-clavulanate. Further experiments will be required to determine optimal dosing as well as investigate the *in vivo* efficacy of faropenem in combination with frontline and second-line drugs. While the activity of β-lactams is only modest against *Mtb*, experience in other organisms suggests that β-lactams synergize with a broad range of other antimicrobials, possibly by increasing the permeability of the cell wall and allowing other drugs to

penetrate better aminoglycosides[24,56]. Thus, this class of compounds could prove to be useful clinically in combination even if they are not highly potent themselves.

Faropenem is already on the market in Japan[145], and has demonstrated clinical efficacy against acute bacterial sinusitis, acute exacerbations of chronic bronchitis, and community acquired pneumonia from phase III clinical trials in the US, demonstrating faropenem's bioavailability in the respiratory tract[145]. Faropenem and tebipenem are intravenously, as well as orally, available in prodrug form as faropenem medoxomil[146] and tebipenem pivoxil[147], which potentially extends the treatment radius to locations without available intravenous therapy.

The structure activity relationship explains the molecular basis for differential innate resistance of *Mtb* to faropenem, biapenem, and tebipenem by showing the specific interactions between BlaC and the lactams that govern AI complex stability and affinity for the BlaC active site. These results are important for the rational design and dual optimization of β-lactams, like faropenem, that circumvent innate resistance by reduced binding to BlaC as well as transient inhibition of the enzyme once bound. With structural and mechanistic information available for the *Mtb* persistent state targets of β-lactams[148-150], selectivity of β-lactams that bind more tightly to essential PBP targets than BlaC can be rationally designed.

MATERIALS AND METHODS

Cloning, expression, and purification

Wild-type BlaC was cloned from *M. tuberculosis* H37Rv genomic DNA as described[97]. The deacylation deficient Glu166Ala mutant was generated using the Quickchange™ site directed mutagenesis kit (Stratagene no. 200519). Mutant and wild-type protein expression and purification were performed as described[97].

Crystallization

Crystals of wild-type and Glu166Ala BlaC were grown using the hanging drop vapor diffusion method[151]. BlaC was concentrated to 10 mg/ml and equilibrated overnight at 4º C with mother liquor (2.0 M $NH_4H_2PO_4$, .1M Tris pH 8.0) at a 1:1 ratio (protein-:-mother liquor). The solution was centrifuged for 10 min at 13 krpm to remove insoluble precipitate. Hanging drops were set up and equilibrated against 1ml of mother liquor. Microseeding with horsehair was sufficient to produce larger diffraction quality crystals. Crystals were transferred to a stabilization solution containing 30% glycerol in mother liquor and were subsequently soaked with β-lactam antibiotics for 2-4 hours. The concentration of substrate was slowly increased by transferring the crystals to successive drops to prevent cracking. Derivatized crystals were flash frozen in liquid nitrogen. Data Collection and Processing. X-ray diffraction data was collected on beamlines 19ID and 23ID at The Advanced Photon Source, Argonne National Laboratory, Argonne, IL. Data sets were reduced using HKL3000[152]. Data was collected at a temperature of 120 K.

Structure determination

Initial phases were obtained by molecular replacement using Phaser Crystallographic Software[153] in the CCP4 suite[154] and 2GDN as a search model[97]. Each data set was refined against the resulting model, and iterative cycles of model building and refinement were performed with Coot 0.6.1[155] and PHENIX[156]. PDB ID's are as follows for the following BlaC-acyl intermediates: amoxicillin (4EBN), cefoperazone (4EBO), cefotaxime (4EBP), faropenem (4EBL), biapenem (4EBM), and tebipenem (4EBI).

Inhibition kinetics

Apparent inhibition constants (*Ki*) for BlaC were determined by monitoring the linear burst of reporter substrate, nitrocefin (60 μM), hydrolysis as a function of β-lactam concentration as described[99]. The resulting IC50's were used to calculate apparent inhibition constants (*Ki*)[157]. Error bars represent the standard deviation of at least 6 data sets.

$K_i = (IC_{50}) / (1 + ([S] / K_m))$

Fourier transform ion cyclotron resonance mass spectrometry

Purified BlaC (100 μM) in 10 mM ammonium acetate was saturated with 1 mM β-lactam substrates to achieve 100% conversion to the acyl intermediate. The reactions were aliquoted and flash frozen in liquid nitrogen to trap the reaction at different time points. Quenched reactions were diluted to 2 μM as the working concentration with an

electrospray ionization (ESI) solution of 50% acetonitrile containing 0.1% formic acid. All MS experiments were performed on a SolariX 9.4 T: hybrid quadrupole-FTICR mass spectrometer (Burker Daltonik GmbH, Bremen, Germany) equipped with a nano-ESI source and acquired in positive ion mode (m/z 300-3000) using electrospray voltage of +1800 V. All MS spectra were obtained by quadrupole mass selection of m/z 950 to 1050 and accumulation of 50 spectra. The mass accuracy and resolution were approximately 5 ppm and 85,000, respectively, for m/z 1018.8, the 30+ charge state of BlaC. The molecular weight of each protein sample was calculated based on the mass-to-charge (m/z) ratio of the +30 charge state of each reaction species using the equation of m = (m/z x 30) – 30 on the centroid of the isotopic cluster. Reaction species including AIs and regenerated BlaC were detected by monitoring the change in relative abundance of representative peaks over time. The raw data was displayed as a function of time. Relative abundances of the AI and regenerated enzyme species were plotted as a percent of the BlaC population as a function of time. Data for the regenerated enzyme were fit to a four parameter non-linear regression.

F(x) = ((A-D)/(1+((x/C)^B))) + D

Whole-cell assays

Cultures of M. tuberculosis $Mc^2$7000 were grown as previously described[158]. Cultures were grown with serial dilutions of β-lactams in the presence and absence of 2.5 μg ml-1 clavulanate. MIC was determined as described[159].

Animal experiments

BALB/CJ mice, 6-8 weeks old, were obtained from Jackson laboratory, Maine, USA. The mice were infected with M. tuberculosis Erdmann strain. 50-100 cfus/lung were deposited via an aerosol infection method. 6 days post infection (PI), the bacterial colony forming units (cfu) in lung for 5 mice was determined. The mice were treated with drugs starting Day 7 PI. The drugs faropenem (160mg/kg body weight) and Isoniazid (25mg/kg body weight) were administered (intraperitoneally) every day for six days. A no drug control group received buffered saline. The efficacy of the drugs was assessed after three and six doses. The homogenates of lungs and spleens from 5 mice (from each drug group) were collected, plated on Middlebrook 7H10 agar plates and incubated at 37°C. The bacterial colonies were counted three weeks later and cfu determined. All protocols, animal purchases, and personnel were approved by the Institutional Animal Care and Use Committee (IACUC).

CHAPTER III

STRUCTURAL BASIS FOR POTENTIATION OF BETA-LACTAM ANTIBIOTIC ACTIVITY ON *Mycobacterium tuberculosis* BY BENZOXABOROLES: INHIBITION OF BlaC

OVERVIEW

Multidrug resistant strains of *Mycobacterium tuberculosis* (*Mtb*) are on the rise which increases the need for alternative antibiotic therapeutic strategies for treatment of infection. β-lactams are an unexploited class of antibiotics for tuberculosis (TB) treatment because of the innate resistance of *Mtb* to β-lactams conferred by the β-lactamase BlaC. Potentiation of β-lactam antibiotic activity by inhibiting BlaC activity is a strategy to resensitize *Mtb* to this class of drugs. To develop new BlaC inhibitors, a boronic acid inhibitor library was enzymatically screened with BlaC which revealed benzoxaborole as a potential inhibitor scaffold. Biochemical characterization of several benzoxaborole inhibitor derivatives with BlaC revealed chemical moieties that increased potency of BlaC inhibition. Co-crystal structures of the inhibitors with BlaC reveal structural insights into the binding and inhibition of BlaC by benzoxaboroles. Lead molecule AN4715 competitively inhibited BlaC (K_i = 0.79 ± 0.02 μM) and potentiated the antibiotic activity of amoxicillin against *Mtb*.

INTRODUCTION

The World Health Organization (WHO) estimated that tuberculosis claimed 1.4 million lives in 2011 [94]. The *Mtb* genome has been acquiring mutations over the last several decades that confer resistance to the classical chemotherapy cocktail of Isoniazid, Rifampicin, Ethambutol, Pyrazinamide and other second-line drugs[95]. Multidrug resistant tuberculosis (MDR-TB) strains are additionally resistant to a fluoroquinolone and an aminoglycoside limiting treatment options[59,160-162]. The need for new anti-tubercular drugs is paramount.

The *blaC* gene in *Mtb* encodes a broad spectrum class A β-lactamase (BlaC) that is responsible for the innate resistant of *Mtb* to β-lactam antibiotics[96]. Effective inhibition of BlaC restores sensitivity of *Mtb* to β-lactams[98]. FDA approved β-lactamase inhibitors like clavulanic acid, tazobactam, and sulbactam[61] mimic β-lactam antibiotic substrates and inhibit BlaC by forming transient covalent acyl-intermediate complexes with a catalytic serine residue. Once the inhibitor acyl-intermediate becomes hydrolyzed by the enzyme, the inhibitor is no longer active. These inhibitors are actually poor BlaC substrates because they are turned over and eventually enzymatic activity is restored within minutes for sulbactam and tazobactam, and hours for clavulanic acid[69,70]. NXL104 is a mechanism-based β-lactamase inhibitor, which also forms a covalent linkage with the catalytic serine residue of serine β-lactamase. It was recently characterized with BlaC and found to form incredibly more stable adducts with the

enzyme than clavulanic acid. However, the authors described modest affinity of BlaC for NXL104 prevents practical application[70].

Boronic acids have long been studied as serine protease inhibitors because their electron deficient boron atom acts as an electrophile by forming covalent bonds with the deprotonated active site serines[71-75]. They have also been extensively characterized as inhibitors of serine β-lactamases because they share a similar mechanism. Boronic acid based-inhibitors of class C β-lactamase AmpC have been optimized for the last decade and have reached subnanomolar binding constants and activity *in vivo*[81-84].

Benzoxaborole are derivatives of phenylboronic acids that have received recent attention for their biological activity as antifungals, anti-inflammatory, and sugar sensing molecules[163]. Benzoxaboroles were also recently reported to inhibit both class A and class C β-lactamases with low micromolar to nanomolar affinities[85]. To develop tight-binding BlaC inhibitors, we enzymatically screened a library of boronic acids and confirmed that the benzoxaborole scaffold also inhibited BlaC. Several derivatives were enzymatically characterized to generate a structure activity relationship. The most potent benzoxaborole, AN4715, competitively inhibited purified BlaC enzyme as well as potentiated the activity of β-lactams against whole cells of *Mtb*. The co-crystal structures of BlaC with three benzoxaboroles were solved to reveal structural insights into the binding and the mechanism of inhibition of BlaC. The results suggest additional modifications to the benzoxaborole scaffold that may increase potency for BlaC, and support the belief that tight binding benzoxaboroles can be used to restore sensitivity of *Mtb* to β-lactam antibiotics by competitively inhibiting BlaC.

RESULTS

Inhibition of BlaC by benzoxaboroles

Screening of a boronic acid based library led to the identification of the lead benzoxaborole molecule AN4715 (Appendix Figure A2). The mode of inhibition of AN4715 was determined to be competitive by inspection of the Lineweaver-Burke plot (Figure 3.1 b). Fitting the data to a competitive inhibition model with a global non-linear regression revealed the inhibition constant (K_i = 0.79 ± 0.02 μM).

To investigate the functional groups on the benzoxaborole scaffold that contribute to the inhibitory activity against the BlaC enzyme, IC_{50}'s were determined for benzoxaboroles with different modifications at the 3', 4', and 6' positions. The results are summarized in Table 3.1. Inhibitory activity of the benzoxaborole scaffold diminished when the 3' carboxymethyl was substituted with sulfonyl methyl, phosphonomethyl, or ethyl ester groups, confirming the importance of the 3' carboxymethyl in BlaC binding and inhibition. The 4'position tolerated a variety of hydrophobic substitutions without drastically effecting the $IC_{50's}$ (4.1 ± 0.2 - 6.6 ± 0.4 μM). When more hydrophilic substitutions were made, the IC_{50} increased up to 3-fold (19.6 ± 0.7 μM), suggesting that the 4' position contributes to binding and inhibition through hydrophobic interaction with BlaC. Heterocyclic substitutions made at the 6' position increased the IC_{50} by > 100-fold (122 ± 15 μM). Compounds with one aryl group were more potent than the bulkier compounds with heterocycles, indicating that the 6' position is subject to steric constraints in the BlaC active site (Table 3.1).

a

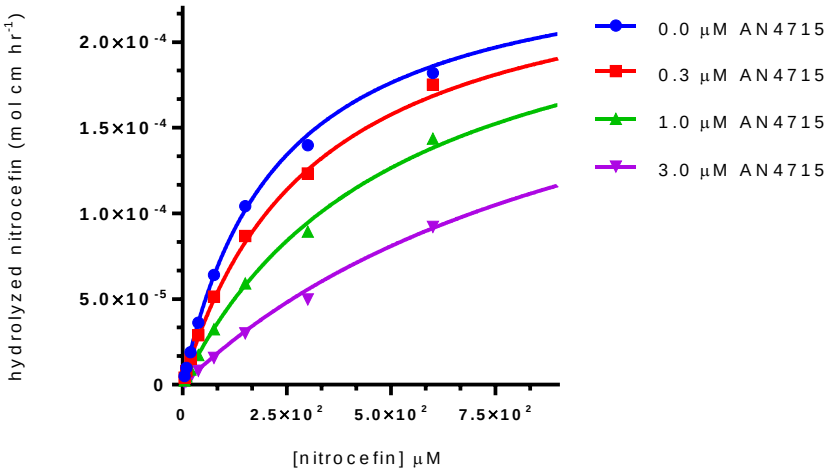

b

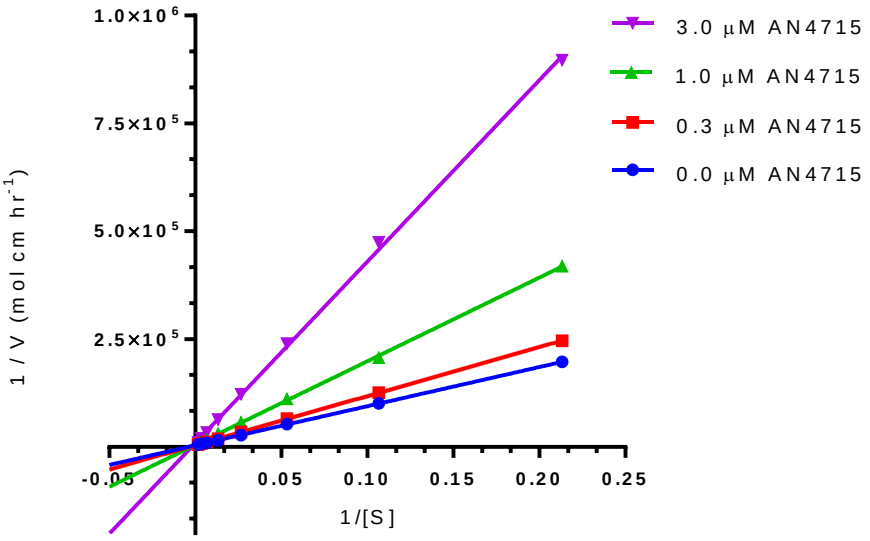

Figure 3.1. Competitive inhibition of BlaC by benzoxaborole AN4715. (a) Nitrocefin hydrolysis by BlaC in presence of varying concentrations of AN4715. (b) Double reciprocal plot of BlaC reaction with nitrocefin in presence of varying concentrations of AN4715.

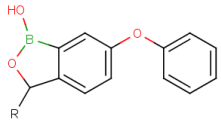
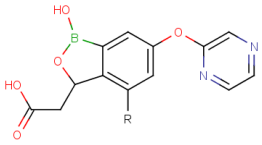
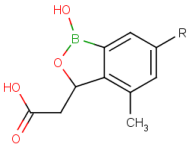

ID	3'R	IC_{50} (µM)		ID	4'R	IC_{50} (µM)		ID	6'R	IC_{50} (µM)
AN3447		29 ± 3		AN4845	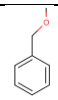	4.1 ± 0.2		AN4715	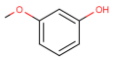	0.99 ± 0.05
AN3668		76 ± 11		AN4482		4.2 ± 0.1		AN4967	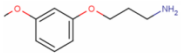	3.3 ± 0.5
AN3737		> 250		AN4449		4.4 ± 0.2		AN3740		8.0 ± 1
AN3446		> 250		AN4497		6.6 ± 0.4		AN5620	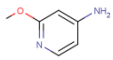	19.6 ± 0.7
				AN3973		5.4 ± 0.2		AN3915	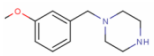	25.7 ± 0.5
				AN4474		6.1 ± 0.2		AN3893	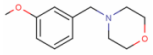	122 ± 15
				AN4496		15.8 ± 0.3				
				AN4892		19.6 ± 0.7				

Table 3.1. Structure activity relationship of BlaC inhibition by benzoxaboroles. Modifications were made at the 3'R group (left), 4'R group (middle), and 6'R group (right) derivatives. *IC_{50}*s (µM) are listed for each compound.

Co-crystal structures of BlaC-benzoxaborole complexes

To further understand the structure activity relationship between benzoxaboroles and inhibition of the BlaC enzyme, co-crystal structures of 3 benzoxaborole inhibitors were solved in complex with BlaC, each bearing at least one different R group from the others. The data collection and refinement statistics are summarized Appendix Table A2. Two of the four BlaC molecules in the asymmetric unit had adequate solvent accessibility to the active site to allow inhibitor binding, and the other two active sites were relatively buried.

The benzoxaborole inhibitors shared many of the same interactions with the BlaC active site, many of which mimic substrate binding. Each inhibitor made contacts with substrate recognition resides Ser70, Ser130, Thr235 and Thr237 (Figure 3.2 a-c). The benzoxaboroles formed covalent bonds between the boron atom of the oxaborole ring and the side chain oxygen of the catalytic Ser70 of BlaC. Adjacent to the boron atom, the 1' hydroxyl group hydrogen bonded to the backbone carbonyl oxygen of Thr237 (2.7 - 3.1 Å), similar to how β-lactam acyl-intermediates are stabilized. Also, the 2' oxygen accepted hydrogen bonds from the side chain hydroxyl of either Ser130 or the backbone amide nitrogen of Thr237. The negatively charged 3' carboxymethyl of the benzoxaborole was electrostatically attracted to the positively charged pocket of the BlaC active site adjacent to the oxyanion hole. The carboxylate fit directly between the side chain hydroxyl groups of Thr235 and Thr237 forming stabilizing hydrogen bonds (2.2 - 3.1 Å) with the enzyme in a manner analogous to how the conserved carboxylate group of β-lactams binds to BlaC.

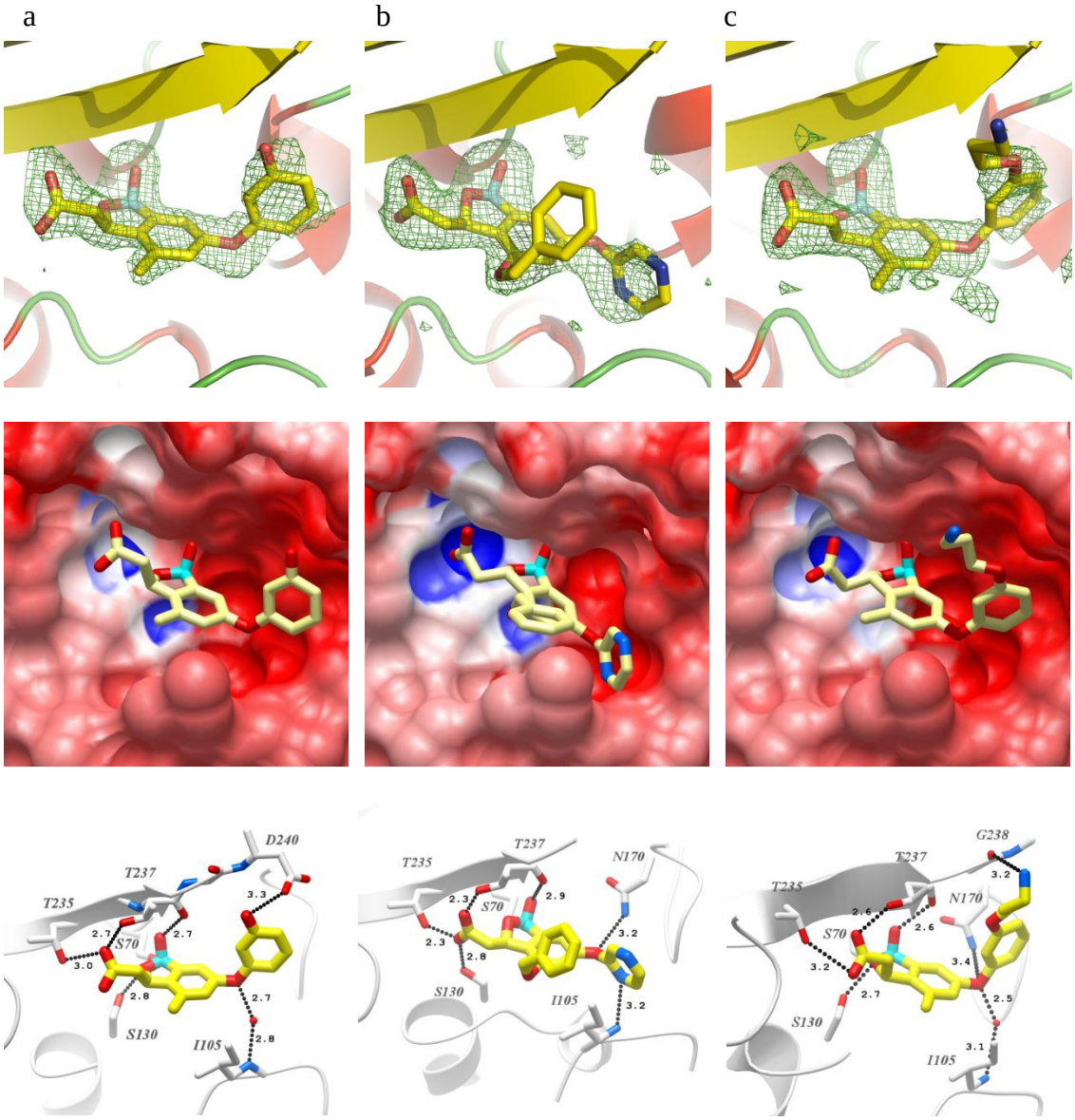

Figure 3.2. Active site details of BlaC-benzoxaborole inhibitor complexes. AN4715 (a), AN4845 (b), AN4967 (c). F_O-F_C omit map electron density surrounding benzoxaboroles contoured at 1.5σ (top). Ligand binding pocket surface colored by electrostatic potential red = negative, blue = positive (middle). Active site hydrogen bonds between BlaC and benzoxaboroles represented as black dotted lines (bottom).

The 4’ position of the benzoxaborole was occupied by either a methyl group (Figure 3.2 a,c) or a bulky methoxyphenyl group (Figure 3.2 b). The methyl groups formed long range hydrophobic interactions with the aliphatic side chain of Ile105 at distances ranging from 4.4 - 4.5 Å similar to how the methyl group of biapenem and tebipenem (Chapter 2) interacts with Ile105. The larger flexible methoxyphenyl group reached out of the active site and into open solvent; its freedom of rotation and the lack of specific interaction with the enzyme surface resulted in decreased electron density for the 4’ methoxyphenyl group (Figure 3.2 b, top). Therefore, it is assumed that the methoxyphenyl group adopts multiple conformations that are capable of forming transient hydrophobic interactions with the side chain of Ile105 once bound to the enzyme.

Each of the inhibitors selected for co-crystal structure determination with BlaC differed primarily by the substitutions at the 6’ position because the inhibition profile at this position resulted in a wide range of BlaC inhibition (0.99 ± 0.05 - 122 ± 15 μM). Each 6’ substitution of the benzoxaborole formed hydrogen bonds with the backbone amide nitrogen of Ile105. Interestingly, two of the inhibitors, AN4715 and AN4976 (Figure 3.2 a, c, bottom), formed this interaction indirectly through a bridging water molecule and the 6’ oxygen atom linking the cyclic substituent. The 6’ pyrazine of AN4845 (Figure 3.2 b, bottom) directly hydrogen bonded to the backbone amide nitrogen of Ile105 at 2.46 Å.

In contrast to AN4845, both, AN4715 and AN4967 6’ substitutions rotated approximately 90 ° about the oxygen linker toward the roof of the BlaC active site

(Figure 3.2 a - c). The propyl amine of AN4967 reached up into the acidic pocket at the top of the active site, and donated a hydrogen bond to the side chain carboxylate oxygen atom of Asp240 (3.37 Å) in molecule C of the asymmetric unit. However, this did not happen in molecule B, which underscores the flexibility of the propylamine group. The unbiased Fo-Fc electron density for the 6' phenol ring of AN4715, was consistent with two possible orientations, where one had less occupancy than the other. In the dominant orientation (Figure 3.2 a), the hydroxyl group of AN4715 donates a hydrogen bond to the side chain carboxylate oxygen atom Asp240 at 3.18 and 3.27 Å in molecules C and B, respectively. If rotated approximately 180°, the phenol hydroxyl group of AN4715 is poised to form a cation-pi interaction with the guanidinium of Arg171. Once bound to the enzyme, the small size of the 6' substitution of AN4715 relative to AN4967 affords rotation within the active site, and facilitates an additional interaction with Arg171.

AN4715 potentiates β-lactam activity against Mycobacterium tuberculosis

The BlaC enzyme is constitutively expressed by *Mtb*[164,165], and is the major determinant for resistance to β-lactam antibiotics [96]. A common strategy for overcoming resistance due to β-lactamase is combining a β-lactam with a β-lactamase inhibitor. The most potent benzoxaborole inhibitor of BlaC in this investigation, AN4715, was selected to test for potentiation of β-lactam activity against *Mtb.* Amoxicillin was chosen as a model β-lactam because of its specificity for BlaC. Cultures of *Mtb* were treated with amoxicillin in presence and absence of 10 μM AN4715, and cell viability was assayed as described[159]. The cell viability averaged from 4 experiments was plotted as a logarithmic

function of amoxicillin concentration, and the dose response curves were fit to a four parameter non-linear regression (Figure 3.3). Combining AN4715 with amoxicillin potentiates the activity of β-lactam antibiotics against whole cells of *Mtb*, decreasing the MIC by approximately two-fold.

DISCUSSION

The prevalence of drug-resistant *Mycobacterium tuberculosis* infections drastically reduces treatment options and extends already exhaustive treatment regimens. Development of new TB diagnostics and drugs, as wells as repurposing existing drugs as TB therapeutics, are effective strategies for reducing disease transmission and decreasing morbidity rates.

β-lactam antibiotics are attractive candidates for TB chemotherapy because they effectively bind to and inhibit target penicillin-binding proteins (PBP) hypothesized to remodel the *Mtb* cell wall during the persistent state of infection[28,166]. The chromosome-encoded β-lactamase enzyme BlaC is the primary mechanism of resistance to these antibiotics[96]. The combination of β-lactam antibiotics with mechanism-based β-lactamase inhibitors has proven to be effective against *Mtb in vitro*[98], and has modest activity against murine tuberculosis models[101]. Increasing the effectiveness of β-lactams against *Mtb* can be achieved by improving bioavailability, increasing the affinity of β-lactams for their target PBPs, and importantly decreasing BlaC-mediated resistance with β-lactamase inhibitors.

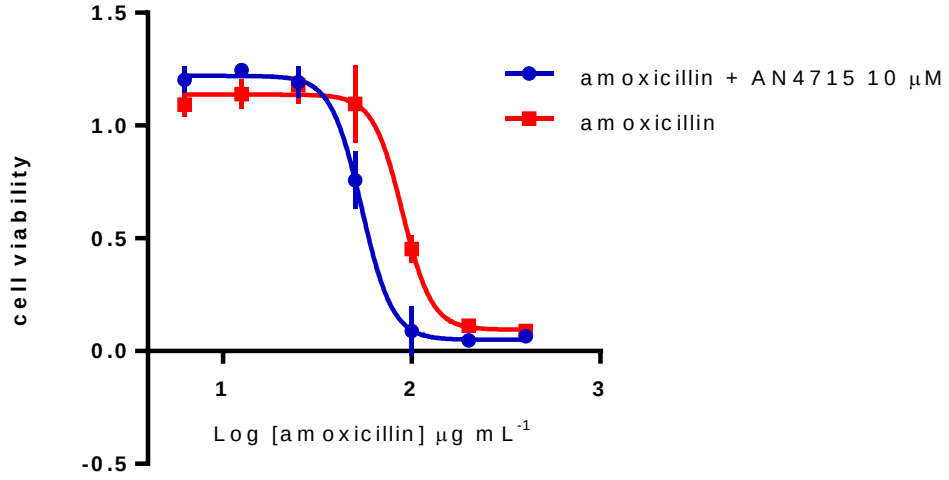

Figure 3.3. AN4715 potentiates activity of amoxicillin against *Mtb*.

Inhibition of class A β-lactamases by clavulanic acid proceeds through formation of a covalent acyl adduct with the enzyme's catalytic serine residue[61]. For BlaC, enzymatic activity is restored within a matter of hours due to hydrolysis of the enzyme-inhibitor complex, which leaves the inhibitor inactive and unable to rebind[70]. This suggests that it would have to be administered continuously for maximum effectiveness use as a therapeutic in combination with effective β-lactams like meropenem. The slow decarbamylation reaction of NXL-104 with BlaC holds promise for future potent and stable derivatives as useful BlaC inhibitors[70].

Benzoxaboroles have demonstrated inhibitory activity against class A and C serine β-lactamase CMY-10, TEM-1, CTX-M, and AMP-C**,** suggesting that they would also inhibit BlaC[85]. To develop potent inhibitors that can potentially be used in combination with β-lactam antibiotics, we enzymatically screened BlaC against a boronic acid library and identified the benzoxaborole inhibitor AN4715 (K_i = 0.79 ± 0.02 μM). Kinetic characterization confirmed the competitive mode of inhibition of BlaC by benzoxaboroles (Figure 3.1 a, b). A structure activity relationship was constructed by substitution of the benzoxaborole 3', 4', and 6' positions and subsequent IC_{50} determination with BlaC (Table 3.1), which led to identification of modifications that increased the potency of the inhibitors for BlaC. Crystal structures of BlaC in complex with the inhibitors demonstrated that benzoxaboroles are β-lactam substrate mimics that form many of the same interactions observed the BlaC acyl-intermediate structures (Chapter 2).

The 4’ position seemed to tolerate the most diverse modifications with the least consequential loss of BlaC enzymatic inhibitory activity with IC_{50} values ranging from 4.1 ± 0.2 to 19.6 ± 0.7 μM. This is likely because the 4’ groups mostly face away from the BlaC active site cavity and into open solvent, but still within proximity of the Ile105. Crystal structures elucidated that even distant hydrophobic interactions (4.2 - 4.5 Å) between the 4’ substituents and the side chain of Ile105 played a role in binding and inhibition of BlaC, as these hydrophobic substitutions were the most potent 4’ modifications. This observation is supported by the ~4-fold increase in IC_{50} (5.4 ± 0.2 - 19.6 ± 0.7) resulting from exchanging a methyl with a hydroxyl at position 4’.

The acidic groups at the benzoxaborole 3’ position were indispensable for BlaC inhibition. Substitution with sulfonyl methyl was sufficient to maintain binding and inhibition, but resulted in a 3-fold decrease in potency relative to carboxymethyl. Phosphonomethyl substitution at this position abolished inhibitory activity. Despite similar structure and the electronegative character of the 3’ modifications, their inhibitory activities deviated drastically. The inhibitor co-crystal structures with BlaC illustrated the delicate fit of the carboxymethyl group required for maintaining optimal potency and hydrogen bonding geometry with side chains of substrate recognition residues Thr235 and Thr237 (Figure 3.2 a - c). The sulfonate group of NXL-104 mediates similar hydrogen bonds with Thr235 and Thr237[70], suggesting that substitution of the sulfonate with a carboxylate group may improve binding affinity of NXL-104 for BlaC.

The 6’ position of the benzoxaborole seems to offer the most opportunity for improvement of the affinity for BlaC. Initial development and optimization of the benzoxaborole as β-lactamase inhibitor scaffold revealed that a bridging oxygen atom is the best linker for aryl modifications at the 6’ position[85]. The crystal structures of BlaC with such benzoxaboroles demonstrate the involvement of the bridging oxygen atom in hydrogen bonding to the backbone amide nitrogen of Ile105 indirectly through ordered solvent mediated contacts. The distal region of the BlaC active site is wide and can expand through movement of the substrate specificity loop (residues 160-180). Smaller monoaryl 6’ substituents fit within this pocket without requiring active site expansion, and can potentially form hydrogen bonds with any of the surrounding residues including Asn170, Glu166, Arg171, and Asp240. The inhibitors characterized in this investigation show that a single hydrogen bond formed between the 6’ hydroxyl group on AN4715 and the side chain carboxylate of Asp240 increases the potency 8 fold relative to the same compound without the hydroxyl group (AN3740). Since the inhibition constant of AN4715 is sub-micromolar, it is easy to envisage designing a sub-nanomolar BlaC inhibitor by picking up a few more hydrogen bonds in this region, which is a feat that has recently been surmounted using fragment based design to optimize boronic acids for AmpC inhibition[84]. The 5’ and 7’ positions of the benzoxaborole scaffold have yet to be explored in chemical space, which offer two additional places for modifications that may enhance specificity and potency for BlaC. Furthermore, the dual conformations and interactions of the 6’ phenol of AN4715 with BlaC suggest that additional hydrogen

bond donor or acceptor modifications to the phenol ring will improve potency by hydrogen bonding with backbone or side chain atoms in the substrate specificity loop.

The results of this investigation reveal the molecular basis for inhibition of class A β-lactamases by benzoxaboroles, and provided structural and functional insights into the binding and inhibition of BlaC by benzoxaboroles. The structure activity relationship presents a useful framework to enable future optimization and structure based design of benzoxaboroles with increased potency and specificity for BlaC. Moreover, the prospective utility of these inhibitor molecules as potentiators of β-lactam antibiotic activity against *Mtb* has been demonstrated. Combination of an appropriately selected β-lactam antibiotic that either evades BlaC inactivation by reduced binding or slow turnover with a potent benzoxaborole could prove to be clinically useful to resensitize the TB pathogen to the most widely used antibiotic class in history.

MATERIALS AND METHODS

Cloning, expression, and purification

Wild-type BlaC was cloned from *M. tuberculosis* H37Rv genomic DNA as described[97]. The deacylation deficient Glu166Ala mutant was generated using the Quickchange™ site directed mutagenesis kit (Stratagene no. 200519). Protein expression and purification were performed as described[97].

Inhibition kinetics

Inhibition of BlaC by benzoxaboroles was measured by monitoring the initial velocities of reporter substrate hydrolysis (CENTA, λ = 404 nm) in presence of varying concentrations of inhibitors (.122 - 250 μM). Reactions were performed in 50 mM potassium phosphate buffer (pH = 7.0) with 0.1 % Triton-X 100 and 10 nM enzyme. Percent inhibition of BlaC activity was plotted versus inhibitor concentration and the concentration of inhibitors required to decrease the reaction velocity by 50% (IC_{50}) were determined by fitting the mean values from 3 data sets to a nonlinear regression model in Prism 6.0. BlaC inhibition constant (*Ki*) of AN4715 was measured by monitoring the initial velocities of reporter substrate hydrolysis (nitrocefin, λ = 486 nm, ε =20,500) in presence of 0.0, 0.3, 1.0, and 3.0 μM of AN4715. Reactions were performed in 50 mM potassium phosphate buffer (pH = 7.0) with 0.1 % Triton-X 100 and 1 nM enzyme. The mean values from 3 data sets data were fit to a global nonlinear regression model of competitive inhibition using Prism 6.0.

Crystallization

Crystals of wild-type and Glu166Ala BlaC were grown using the hanging drop vapor diffusion method[151]. BlaC was concentrated to 10 mg/ml and equilibrated overnight at 4º C with mother liquor (2.0 M NH4H2PO4, .1M Tris pH 8.0) at a 1:1 ratio (protein-:-mother liquor). The solution was centrifuged for 10 min at 13 Krpm to remove insoluble precipitate. Hanging drops were set up and equilibrated against 1ml of mother liquor. Microseeding with horsehair was sufficient to produce larger diffraction quality

crystals. Crystals were transferred to a stabilization solution containing 30% glycerol in mother liquor and were subsequently soaked with β-lactam antibiotics for 2-4 hours. The concentration of inhibitor was slowly increased by transferring the crystals to successive drops to prevent cracking. Derivatized crystals were flash frozen in liquid nitrogen.

Data collection and processing

X-ray diffraction data was collected on beamlines 19ID and 23ID at The Advanced Photon Source, Argonne National Laboratory, Argonne, IL. Data sets were reduced using HKL3000[152]. Data was collected at a temperature of 120 K. For data quality, crystallographic, and refinement statistics, see Table 2.

Structure determination

Initial phases were obtained by molecular replacement using Phaser Crystallographic Software[153] in the CCP4 suite[154] and 2GDN as a search model[97]. Each data set was refined against the resulting model, and iterative cycles of model building and refinement were performed with Coot 0.6.1[155] and PHENIX[156].

CHAPTER IV

RAPID POINT-OF-CARE DETECTION OF THE TUBERCULOSIS PATHOGEN USING A BlaC-SPECIFIC FLUOROGENIC PROBE*

OVERVIEW

Early diagnosis of tuberculosis can dramatically reduce both its transmission and the associated death rate. The extremely slow growth rate of the causative pathogen, *Mycobacterium tuberculosis* (*Mtb*), however, makes this challenging at the point of care, particularly in resource-limited settings. Here we report the use of BlaC (an enzyme naturally expressed/secreted by tubercle bacilli) as a marker and the design of BlaC-specific fluorogenic substrates as probes for *Mtb* detection. These probes showed an enhancement by 100–200 times in fluorescence emission on BlaC activation and a greater than 1,000-fold selectivity for BlaC over TEM-1 β-lactamase, an important factor in reducing false-positive diagnoses. Insight into the BlaC specificity was revealed by successful co-crystallization of the probe/enzyme mutant complex. A refined green fluorescent probe (CDG-OMe) enabled the successful detection of live pathogen in less than ten minutes, even in unprocessed human sputum.

---

*Reprinted with permission from Rapid point-of-care detection of the tuberculosis pathogen using a BlaC-specific fluorogenic probe. Xie, H., Mire, J., Kong, Y., Chang, M., Hassounah, H., Thornton, C. N., Sacchettini, J. C., Cirillo, J. D., and Rao, J., (2012). *Nature Chemistry, 4*, 802-809, Copyright 2012 by Nature Publishing Group.

This system offers the opportunity for the rapid, accurate detection of very low numbers of *Mtb* for the clinical diagnosis of tuberculosis in sputum and other specimens.

INTRODUCTION

Tuberculosis is one of the most deadly diseases that kills over one million people each year and infects one-third of the world's population[167]. The disease is spread by infection with *Mycobacterium tuberculosis* (*Mtb*). Owing to its airborne transmission, early diagnosis is critical to the prevention and control of TB. Standard diagnostic methods, acid-fast smear from sputum, often do not become positive until after transmission occurs, which allows the spread of the disease. Culture-based techniques are more sensitive, but take weeks to obtain results because of the extremely slow growth rate of *Mtb*. Recently, nucleic acid-based diagnostic strategies were shown to have a higher sensitivity than that of sputum smear microscopy[168-170]. With a semi-automated DNA amplification system (Cepheid GeneXpert), it is thought that TB can be diagnosed with 98% reliability[171]. However, its high cost[172] and requirement for a high technical competence to carry out the test prevent it from being widely available in resource-limited settings. In addition, the sensitivity of this test has not reached that of the gold standard culture, and it cannot evaluate bacterial viability, a critical aspect of evaluating therapeutic outcome. TB eradication efforts would be facilitated greatly by methods that can detect tubercle bacilli in a sensitive, rapid, specific and quantitative

manner *in vitro* at a low cost, particularly in resource limited settings where TB is the most prevalent.

Tubercle bacilli naturally express BlaC, an enzyme that belongs to the class A β-lactamase family[96,98]. Extended spectrum class A β-lactamase are capable of hydrolyzing all classes of β-lactam substrates, including cephalosporins. The mechanism of cephalosporin hydrolysis by β-lactamase yields hydrolyzed β-lactam and, more importantly, may be concomitant with the loss of a 3′ leaving group[139,173-175]. Based on this mechanism, a number of fluorogenic and bioluminogenic probes were developed for the detection of β-lactamase activity *in vitro*, in living cells and even in whole animals[176-180]. We developed cephalosphorin-based fluorogenic substrates that enable the sensitive detection of *Mtb* and bacillus Calmette– Guérin (BCG) *in vitro* and in living mice[181]. Previous probes lack specificity for BlaC in *Mtb*; the common TEM-1 β-lactamase (TEM-1 Bla) in gram-negative bacteria can also generate fluorescence, which reduces its utility for TB diagnosis. Earlier probes are generally large and display slow hydrolytic kinetics for BlaC. Here we report a rational design of a series of fluorescent probes based on chemically modified cephalosporins by taking advantage of the unique flexibility of the BlaC substrate-specificity loop. Enzymatic kinetic, structural analyses and whole-cell assays confirmed their high specificity and sensitivity for BlaC over its close class A homologue TEM-1 Bla as well as over β-lactamase produced by Pseudomonas, Staphylococcus and the environmental *Mycobacterium smegmatis*. Successful detection and imaging of BCG directly in unprocessed patient sputum at levels of less than 100 bacilli are demonstrated, even with a simple, inexpensive imaging

system of a cellular phone. This new BlaC-specific probe has potential for the clinical diagnosis of *Mtb* in patient sputum and other diagnostic specimens. Structural insights obtained from the BlaC acyl intermediates in this work should facilitate the development of more BlaC-specific probes for *Mtb* detection and imaging, and of BlaC-specific inhibitors to be used in anti-*Mtb* therapeutic regimens.

RESULTS

Design of BlaC-specific fluorogenic probes

The substrate specificity of class A β-lactamase is conferred by Ambler residues (163–178) that comprise the omega loop, or substrate-specificity loop, and is partially dependent on the ability of the catalytic base, E166, to assume the optimal conformation for hydrolytic water coordination and deacylation[182,183]. To design a cephalosporin substrate specific for BlaC to achieve the specific detection of *Mtb*, we exploited the unique flexibility of the BlaC substrate-specificity loop by introducing bulky substitutions on the lactam. Such a cephalosporin may be accommodated by the BlaC substrate-specificity loop with the coordination of E166 still optimal for efficient deacylation.

We designed a series of fluorescent probes with substitutions on the side chain (R1) of the 7-amino group or the 7-position of the lactam ring (R2) (Figure 4.1). Each probe contains the alkylated umbelliferone at the 3′-position and initially fluoresces little when excited at 400 nm. We hypothesized that these substituted substrates could be

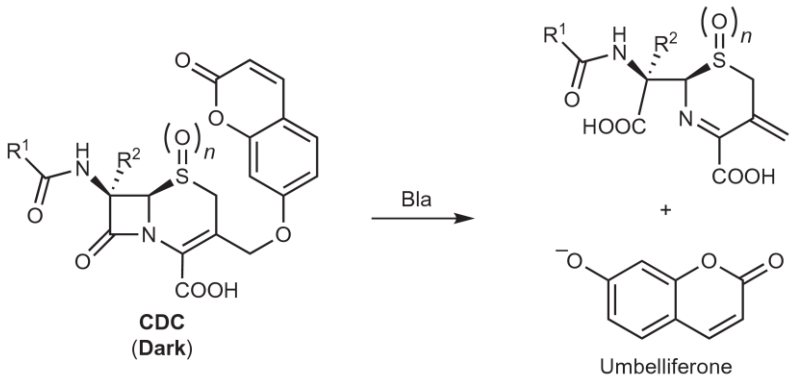

CDC-1: R^1 = Bn, R^2 = H, n = 0
CDC-2: R^1 = Bn, R^2 = H, n = 1
CDC-3: R^1 = 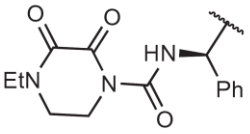 , R^2 = H, n = 0

CDC-4: R^1 = Me, R^2 = H, n = 0
CDC-5: R^1 = Me, R^2 = OMe, n = 0
CDC-OMe: R^1 = Bn, R^2 = OMe, n = 0
CDC-OEt: R^1 = Bn, R^2 = OEt, n = 0

Figure 4.1. General structures of blue fluorescent probes and their hydrolysis by BlaC. Hydrolysis triggers the release of umbelliferone and turns on fluorescence.

hydrolyzed readily by BlaC and release free fluorophore to turn on the fluorescence, but their hydrolysis by other β-lactamase, such as TEM-1 Bla, would proceed with much slower kinetics. These blue fluorescent probes were synthesized[184,185] and unambiguously characterized.

Enzymatic kinetics for BlaC and TEM-1 Bla

We first recorded the fluorescent spectra of CDC-1, CDC-3, CDC-OMe and CDC-OEt before and after BlaC treatment to examine their responses to BlaC. With excitation at 400 nm, all the probes exhibited over a 100-fold increase in the fluorescence intensity at 455 nm after incubation with BlaC (Figure 4.2 a), but their reaction rates varied significantly (Figure 4.2 b). Under the same conditions, the hydrolytic rate by BlaC decreased in the order CDC-1.CDC-OMe.CDC-OEt, which appears to correlate with the size of the R2 group. CDC-OMe showed more than a 30-fold enhancement of fluorescence intensity in less than 30 minutes. The larger substitution (ethoxy versus methoxy) provided CDC-OEt with only a slight fluorescence enhancement within 30 minutes. In comparison, the same concentration of TEM-1 Bla (50 nM) gave no change in the fluorescence intensity within 30 minutes with CDC-OMe, but produced rapid fluorescence with CDC-1 and CDC-3. These results demonstrate that CDC-OMe can preferentially detect BlaC over TEM-1 Bla.

We next examined the response of CDC-OMe to varying concentrations of BlaC and TEM-1 Bla (in the range 1 pM to 100 nM) to investigate its specificity (Figure 4.2 c). BlaC (1 nM,100 ml) induced a 130% increase in the fluorescence intensity within

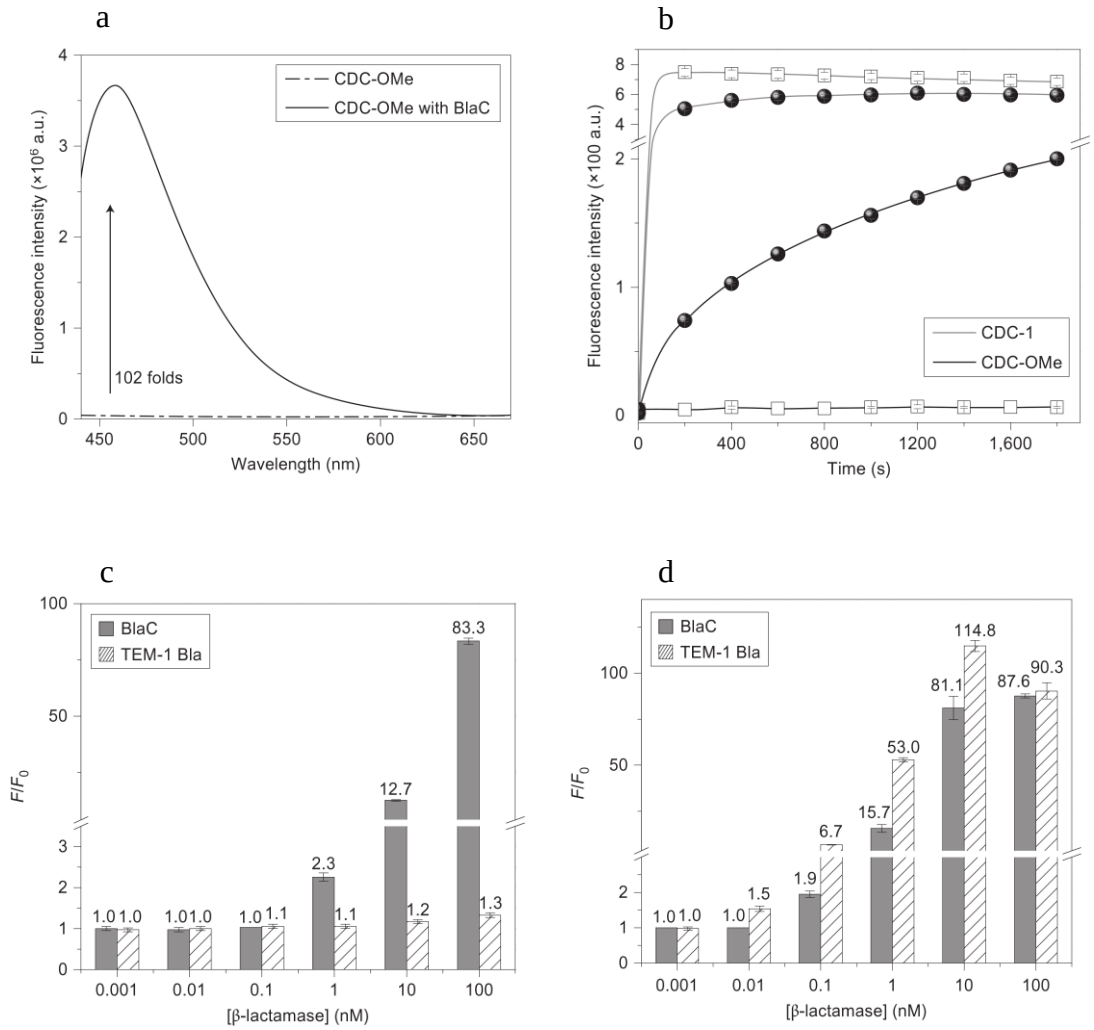

Figure 4.2. Kinetic comparison of CDC probes with β-lactamase. (a) Fluorescent emission spectrum of CDC-OMe (1 mM in PBS) before and after treatment with BlaC (1 mM) (excitation, 400 nm). (b) Time courses of fluorescent activation of CDC-1 and CDC-OMe with BlaC (filled circles) or TEM-1 Bla (open squares). (c,d) Enhanced fluorescent intensity of CDC-OMe (c) and CDC-1 (d) (5mM in PBS) by BlaC or TEM-1 Bla at the indicated concentrations for one hour. F/F_0 represents the turn-on ratio of fluorescence intensity by β-lactamase. Error bars are ± standard deviation (s.d.). a.u.= arbitrary units.

one hour (F/F0 = 2.3), but a 100-fold higher TEM-1 Bla concentration (100 nM) produced only a 30% fluorescence enhancement ($F/F_0 = 1.3$). In contrast, TEM-1 Bla generated a stronger signal with CDC-1 than with BlaC (Figure 4.2 d).

The kinetic parameters of fluorescent probes for both BlaC and TEM-1 Bla, including the catalytic constant *kcat* and the Michaelis constant K_m, were obtained from Lineweaver–Burk plots and are summarized in Table 4.1. Consistent with the above observations, the kinetic efficiency ($kcat/K_m$) of CDC-OMe for BlaC is 2.1×10^4 s^{-1} M^{-1}, over 1,000 times higher than that for TEM-1 Bla (16 s^{-1} M^{-1}). When an ethoxy group is introduced at the 7-position (CDC-OEt), no hydrolysis by TEM-1 Bla was detected, and the value of *kcat*/Km by BlaC decreased substantially to 1.9×10^2 s^{-1} M^{-1}.

Additional structural modifications were explored for their effects on the enzymatic kinetics of BlaC and TEM-1 Bla. Probes with a large substitution group on the 7-amine position (R^1), such as CDC-3, displayed less catalytic efficiency for BlaC (8.7×10^4 s^{-1} M^{-1}) than for TEM-1 Bla (1.3×10^6 s^{-1} M^{-1}). However, substitution by phenylacetyl or acetyl groups (for example, CDC-1 and CDC-4) at this position resulted in only a slight difference in the catalytic efficiency between BlaC and TEM-1 Bla (CDC-1, 2.1×10^5 versus 3.6×10^5 s^{-1} M^{-1}; CDC-4, 6.8×10^4 versus 7.5×10^4 s^{-1} M^{-1}, respectively). Oxidation of the sulfur into sulfoxide (CDC-2) caused a decrease in the kinetic efficiency for both BlaC and TEM-1 Bla. These kinetic analyses confirm CDC-OMe as a BlaC-specific fluorogenic probe with more than a 1,000-fold higher catalytic efficiency for BlaC than for TEM-1 Bla.

	Name	BlaC			TEM-1 Bla			Spontaneous hydrolysis rate ($\times 10^{-7}$ s^{-1})
		K_m (μM)	k_{cat} (s^{-1})	k_{cat}/K_m (s^{-1} M^{-1})	K_m (μM)	k_{cat} (s^{-1})	k_{cat}/K_m (s^{-1} M^{-1})	
1	**CDC-1**	63±6	13±0.5	2.1×10^5	135±16	48±3.8	3.6×10^5	2.4±0.3
2	**CDC-2**	136±44	0.5±0.1	3.7×10^3	454±37	7±0.7	1.5×10^4	1.1±0.1
3	**CDC-3**	69±7	6±0.2	8.7×10^4	59±10	77±6.6	1.3×10^6	1.8±0.2
4	**CDC-OMe**	47±9.4	1±0.1	2.1×10^4	50±2	8±0.3 × 10^{-4}	16	2.8±0.1
5	**CDC-OEt**	131±40	0.026±0.005	1.9×10^2	ND	ND	ND	2.3±0.2
6	**CDC-4**	148±50	10±1.9	6.8×10^4	133±18	10±1	7.5×10^4	1.9±0.1
7	**CDC-5**	139±22	0.52±0.05	3.6×10^3	ND	ND	ND	2.6±0.3
8	**CDG-1***	2.1±0.3 (2±0.4)	4±0.2 (1.0±0.1)	1.9 × 106 (5×10^5)	1.0±0.1 (2±0.2)	9±0.4 (5±0.1)	9×10^6 (2.5×10^6)	3.3±0.1 (6.0±0.1)
9	**CDG-OMe***	3±0.3 (5±0.3)	0.7±0.04 (0.8±0.01)	2.3×10^5 (1.6×10^5)	30±8 (40±4)	1±0.2 × 10^{-3} (7±0.6 × 10^{-4})	33 (18)	2.5±0.1 (1.9±0.1)

Table 4.1. Kinetic parameters of fluorescent probes for BlaC and TEM-1 Bla. Kinetic data were measured in PBS buffer (×1, pH = 7.4) at room temperature (22 °C) unless otherwise noted. All data indicate averages of three replicate experiments. *Data in parentheses were measured in MES buffer (0.1 M, pH 6.6) at 22 8C. ND = not determined due to extremely slow kinetics.

Analysis of the crystal structure

X-ray crystallographic structures of the acyl intermediate complex structures of CDC-OMe and CDC-1 with BlaC were obtained to probe the structural origin of the observed specificity of CDC-OMe for BlaC (Table 4.1). The substrate-specificity loops of TEM-1 Bla and BlaC share a 67% sequence identity over 20 residues (160–180). Conserved saltbridges in both enzymes formed by D172–R178 (E171–R178 in TEM-1 Bla) and D176–R178 stabilize the loop conformers of the unoccupied active sites (Figure 4.3 a)[97,186].

The largest phenotypic difference between the two enzymes results from residue 164, which is an arginine in TEM-1 Bla and an alanine in BlaC. R164 plays a central role in the molecular dynamics of the substrate-specificity loop in TEM-1 Bla. The R164 guanidinium side-chain nitrogens (Nε, NH and NH2) stabilize a triad of carboxylates from the D176, D179 and E171 side chains with electrostatic interaction distances of 3.99 Å, 2.75Å and 2.87 Å, respectively[186], by forming three additional salt bridges (Figure 4.3 b)[97,186].

A164 mutation results in the loss of these stabilizing salt bridges in BlaC, which ultimately increases the flexibility of the BlaC substrate-specificity loop relative to that of TEM-1 Bla. The increased flexibility is underscored by B-factors for residues that surround E166 (164–168), which are 108% of the mean B-factor in BlaC and 87% of the mean B-factor in TEM-1 Bla[97,186]. The structural plasticity of these residues allows the catalytic base E166 to sample multiple conformations and increases the capability of BlaC to hydrolyze substrates in the acyl-intermediate state. The acyl-

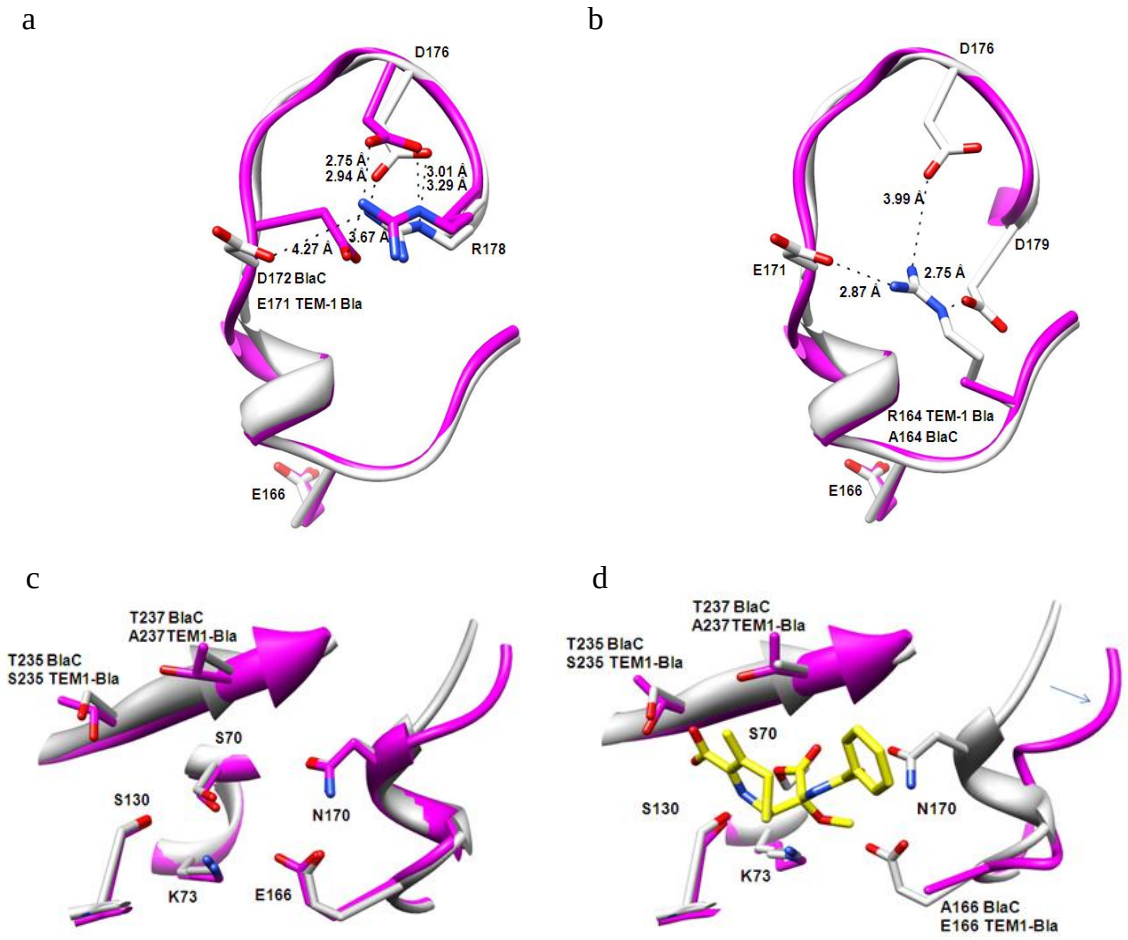

Figure 4.3. Comparison of BlaC and TEM-1 Bla active sites and substrate-specificity loops. a, Conserved salt bridges in both enzymes formed by D172–R178 and D176–R178 stabilize the loop conformers of the unoccupied active sites. b, TEM-1 Bla (1M40, white) R164 forms salt bridges with E171 (2.87 Å), D176 (3.99 Å) and D179 (2.75 Å). BlaC (2GDN, purple) A164 prevents these stabilizing interactions, which results in an increased flexibility of the loop and catalytic base E166. c, Superimposition of unoccupied TEM-1 Bla and BlaC active sites. d, Superimposition of unoccupied TEM-1 Bla (white) and the BlaC–CDC-OMe acyl intermediate complex (purple). The arrow indicates the expansion of the substrate loop in BlaC on binding CDC-OMe.

intermediate complex structures of BlaC–CDC-1 and BlaC–CDC-OMe exist in similar orientations, and share conserved electrostatic interactions with substrate-recognition residues T235, T237, S130 and S70 (Figure 4.4). The phenyl groups in both CDC-1 and CDC-OMe are disordered as a result of the lack of active-site contacts and facing open to the solvent. In contrast, CDC-1 makes a unique hydrogen bond (2.76 Å) with the backbone carbonyl oxygen of T237. The methoxy group of CDC-OMe forms an electrostatic interaction with the side-chain amino group of K73 (3.29 Å). The orientation of the CDC-OMe 7′-phenylacetylamino substituent is rotated approximately 90° relative to the CDC-1 acyl intermediate (Figure 4.4 c). The CDC-OMe–K73 interaction positions the methoxy group directly in the path between the acyl bond and catalytic residue E166, which may interfere with the hydrolytic water coordination for deacylation and lead to a decreased turnover number for CDC-OMe (Table 4.1). Replacement of the methoxy group with a bulkier ethoxy group (CDC-OEt) causes a more serious occlusion, which leads to a further 40-fold reduction in turnover number (Table 4.1). However, these unique interactions in the CDC-OMe acyl intermediate accommodated by the BlaC flexible substrate-specificity loop confer the specificity of CDC-OMe for BlaC (Figure 4.3 c,d).

Detection and imaging of live mycobacteria

We first sought to evaluate the feasibility of CDC-OMe for the detection of BlaC expressed by *Escherichia coli*. CDC-OMe was incubated with the same number of *E. coli* that expressed no β-lactamase, TEM-1 Bla or BlaC for two hours and a strong

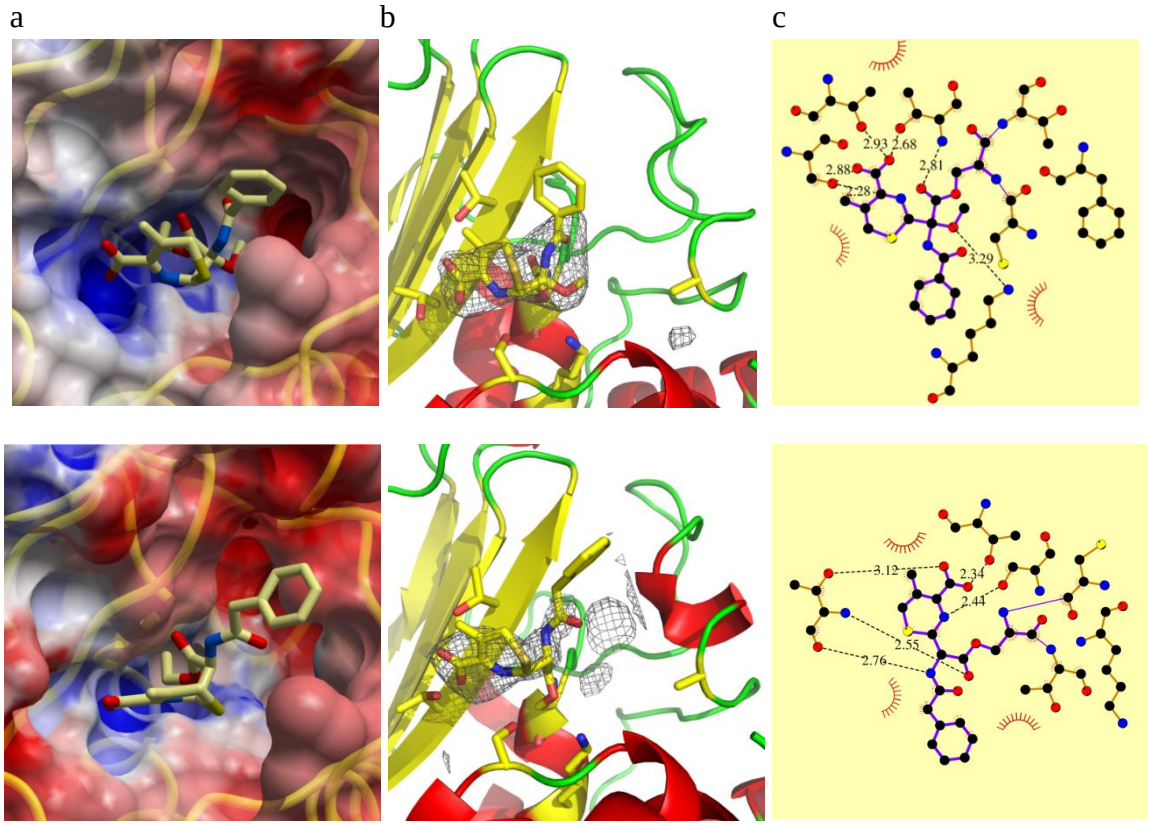

Figure 4.4. Active-site details of the BlaC-CDC-OMe (top) and BlaC–CDC-1 (bottom) acyl intermediate complexes. (a,b) Electrostatic surface potential (a) and cartoon diagrams (b) of acyl intermediates with F_O - F_C electron-density maps displayed in grey for CDC-OMe (2.0s) and CDC-1 (1.5s) prior to fitting each ligand for refinement protocols. Active-site residues are displayed as sticks. (c) Ligplot analysis of active-site interactions.

fluorescence was observed only with *E. coli* that expressed BlaC. As a control, the fluorescence for CDC-1 was present in *E. coli* that expressed either TEM-1 Bla or BlaC. This result demonstrates that CDC-OMe can detect BlaC specifically in intact *E. coli*. However, the sensitivity for detecting BlaC expressed by the *Mtb* var. bovis strain BCG is low because of the high background of BCG at the excitation and emission wavelengths of umbelliferone. Therefore, we replaced umbelliferone with the green fluorescent dye Tokyo Green (Figure 4.5 a). Tokyo Green allows a stable single-site attachment at its phenolic position[187], but the direct coupling product with cephalosporin at the 3′-position, similar to that in CDC probes, displayed a 21-fold less stability (with a spontaneous hydrolysis rate of 7×10^{-6} s^{-1} in PBS) than that of CDC-OMe. A benzyl ether linker was thus introduced between the 3′-position of the lactam and Tokyo Green to increase its stability (Figure 4.5 a).

On treatment with BlaC, the fluorescence emission of CDG-OMe at 520 nm increased by up to 218-fold (Figure 4.5 b). In addition to the gain in the stability of the probe obtained from the additional linker, the specificity of CDG-OMe for BlaC improved, with an 11-fold increase in *kcat*/Km to 2.3×10^{5} s^{-1} M^{-1} in PBS (Table 4.1). Even at a more than 1,000-fold higher concentration, the fluorescence signal of CDG-OMe generated by TEM-1 Bla (400 nM) was just 30% of that generated by BlaC (400 pM) in 300 minutes, which confirms its high selectivity for BlaC (Figure 4.5 c). Less than 1 fmol of BlaC was readily detectable with CDG-OMe after eight hours of incubation (Figure 4.5 d). When TEM-1 Bla- and BlaC-expressing *E. coli* were

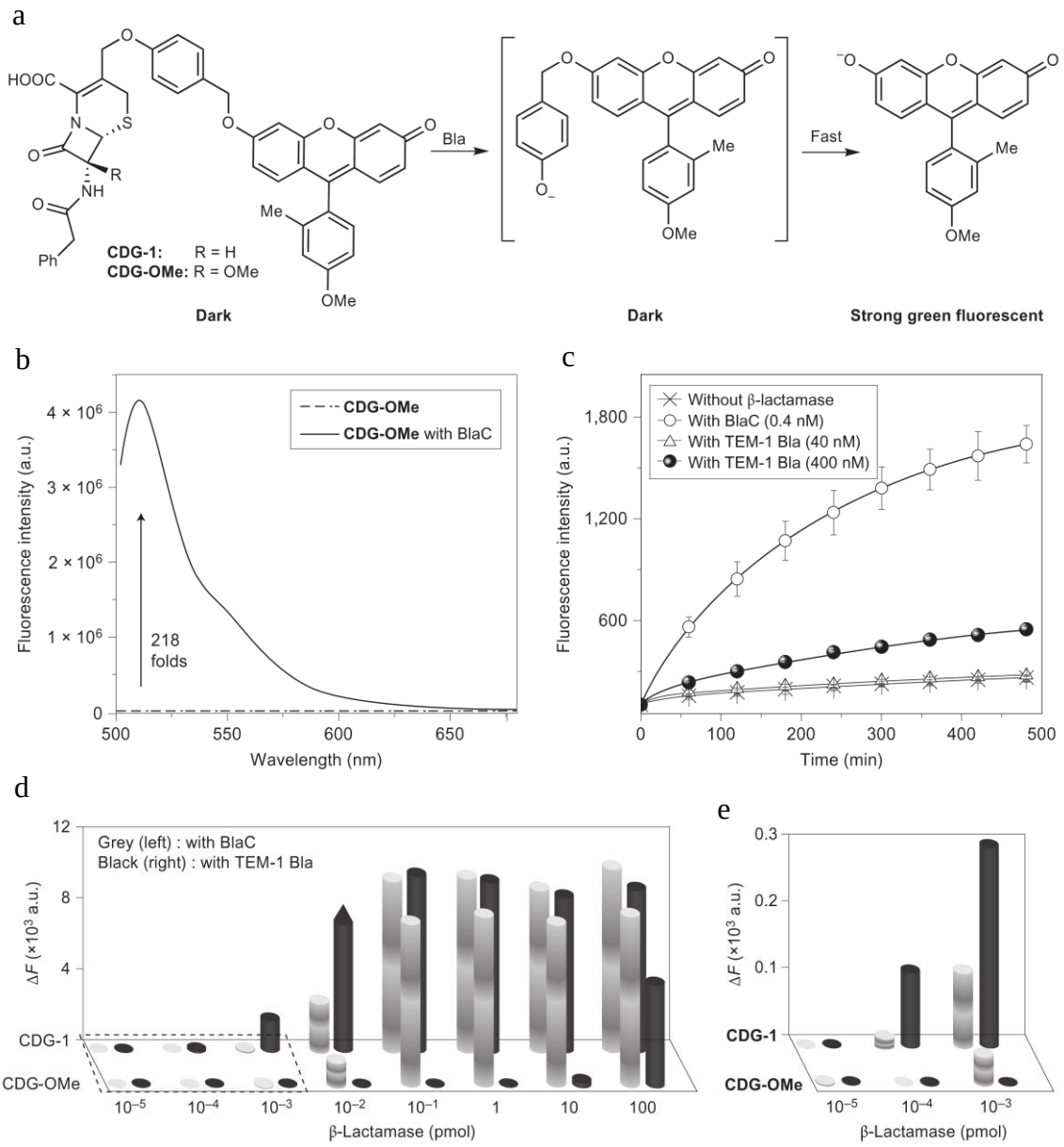

Figure 4.5. β-lactamase selectivity of fluorescent probes CDG-1 and CDG-OMe. a, BlaC hydrolyses green probes and turns on the fluorescence signal. b, Fluorescent emission spectrum of CDG-OMe (20 nM in MES) before and after treatment of BlaC (0.2 μM) (excitation, 490 nm). c, Time courses of fluorescence enhancement with CDG-OMe (8 μM in MES buffer) and various concentrations of β-lactamase. d, Enhanced fluorescence intensity of CDG-OMe (8 μM in MES, front) and CDG-1 (8 μM in MES, back) by serially diluted solutions of BlaC or TEM-1 Bla for eight hours. Data were collected in 384-well plates with a total volume of 25 μl in each well. e, Magnified view of the rectangular region in (d). ΔF represents the difference in fluorescence intensity with and without β-lactamase incubation. Data in (d) and (e) are the average of three replicate experiments. Error bars are ± s.d.

incubated with CDG-1 and CDG- OMe, CG-1 displayed no selectivity, but CDG-OMe showed excellent selectivity for BlaC over TEM-1 Bla.

We further tested the sensitivity and specificity of CDG-OMe for detecting bacteria present in raw unprocessed sputum samples obtained from cystic fibrosis patients. BCG or other bacteria that expressed β-lactamase, including *E. coli*, methicillin-resistant *S. aureus* (MRSA), *P. aeruginosa* strain PA01 and *M. smegmatis* were incubated with CDG-OMe in human sputum. We could detect *Mtb* readily in sputum down to ten colony-forming units (c.f.u.) ($P < 0.05$), which demonstrates the high sensitivity of this system for evaluating clinical samples (Figure 4.6 a). Fluorescence emission generated by 10 c.f.u. of BCG in sputum is significantly ($P < 0.05$) higher than fluorescence from the negative control and 10^5 c.f.u. of *E. coli*, MRSA, PA01 and *M. smegmatis* (Figure 4.6 b).

To investigate the applicability of this system in low-resource settings, we built a handmade box equipped with a simple LED light source, excitation filter and emission filter, and took a picture with a cell phone through a hole in the box. As shown in Figure 4.6 c, 10 c.f.u. of BCG in 200 µl of human sputum was detected readily within ten minutes of incubation with the probe, and the use of luminance mapping allowed facile optimization of image visualization. In summary, CDG-OMe demonstrates excellent sensitivity and specificity for detecting *Mtb* var. bovis strain BCG in clinical specimens, even using low-cost detection systems.

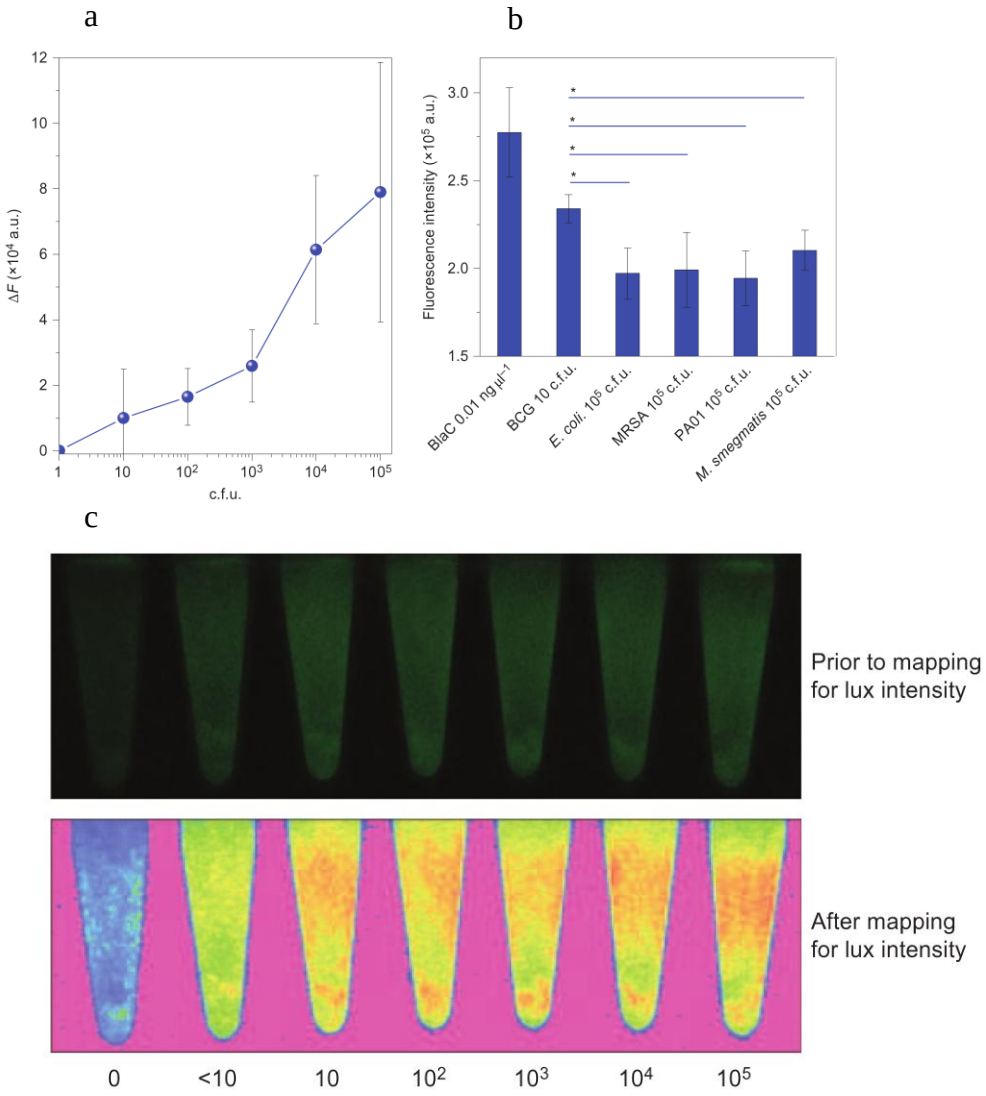

Figure 4.6. Sensitivity and specificity of CDG-OMe in unprocessed human sputum. a, Detection of BCG in sputum with CDG-OMe. b, Specificity of CDG-OMe for detecting BCG in sputum. 10 c.f.u. of BCG or 10^5 c.f.u. of the indicated β-lactamase-expressing bacteria were added to human sputum samples obtained from cystic fibrosis patients and incubated with CDG-OMe (2.5 µM) at room temperature for 160 minutes. Fluorescence was measured with excitation at 490 nm and emission at 535 nm. *P < 0.05 as compared to 10 c.f.u. of BCG. c, Imaging of BCG in sputum with CDG-OMe using a cellular phone. BCG-spiked sputum samples were incubated with CDG-OMe (5 µM) at room temperature for ten minutes before they were imaged in a simple handmade light box: light from an off-the-shelf LED assembly (<US$10.00) passed through a 490 nm excitation filter (bandpass 20 nm) was reflected through a 530 nm emission filter (bandpass 43 nm) and photographed with an iPhone 4S. The photograph was analyzed with iPhotoLux v. 1.0. Error bars are ± s.d.

DISCUSSION

One of the critical needs for improving the diagnosis of TB is to identify accurate biomarkers for active *Mtb*[188]. Recently, the trehalose mycolyltransferase enzymes were utilized to incorporate unnatural trehalose analogues into *Mtb* for TB detection[189]. As it requires cell culturing for the probe incorporation, the process can take a long time because of the slow growth rate of *Mtb*. BlaC has the potential to serve here and has many advantages as a diagnostic marker. All TB complex bacteria examined displayed a strong signal dependent on β-lactamase, including BCG, TB laboratory strains and TB clinical isolates, with a total of more than 20 different strains. In addition, complete genome sequencing of more than 54 *Mtb* strains from numerous geographical regions, multidrug resistant and extensively drug-resistant strains demonstrates that BlaC is highly conserved in all *Mtb* clinical isolates, with only two non-synonymous single-nucleotide changes, but they still produce an active enzyme[95]. These observations are consistent with reports in the literature that indicate 100% (18 examined for *Mtb*, nine for *M. bovis*, five for *M. africanum*) of the strains within the TB complex and *M. kansasii* (17 examined) produce β-lactamase and are positive for enzymatic activity[190]. As BlaC is an enzyme, its activity promises great sensitivity for the detection of tubercle bacilli, as we have shown with fluorogenic substrates. However, previously available probes lack specificity for BlaC[181], which allows activation by other β-lactamase, such as TEM-1 Bla, commonly found in gram-negative bacteria[54,191], which reduces their accuracy for TB diagnosis.

Extensive research is devoted to β-lactamase because of their role in rendering bacteria resistant to lactam antibiotics. However, most previous studies focused on designing molecules that are poor β-lactamase substrates[69,100], in contrast to the goal of this study, to design substrate probes that have rapid kinetics and are selective for BlaC. We took advantage of the unique substrate specificity loop of BlaC and explored its chemistry to design BlaC-specific fluorogenic substrates. The replacement of R164 in TEM-1 Bla by Ala results in the loss of stabilizing salt bridges in BlaC and thus an increase in the flexibility of the BlaC substrate specificity loop. Therefore, it is more probable that the active site of BlaC accommodates chemical modifications on the lactam structure. Based on this structural insight, we explored substitutions at the 7-C position of the lactam ring. The introduced methoxy group is accommodated well in the pocket of BlaC, as revealed by the acyl intermediate structural complex. In this study, we examined the effect of modifications only on the 7-C position of the lactam ring, and it remains possible that other positions on the lactam structure may be modified to generate specificity for BlaC.

CDC-OMe showed excellent selectivity for BlaC over TEM-1 Bla, but low catalytic efficiency for BlaC ($kcat/K_m$ = 2.1 ×10^4 s^{-1} M^{-1}), which requires long co-incubation times for a positive result. CDG-OMe has a much improved kinetic efficiency (an 11-fold increase of $kcat/K_m$, 2.3 × 10^5 s^{-1} M^{-1}) and still maintains high stability and selectivity for BlaC over TEM-1 Bla. The use of green fluorophore further enhanced its sensitivity for detecting live mycobacteria in solution.

Using a simple handmade device and a cell phone, we detected as low as 10 c.f.u. of BCG in human sputum, which not only demonstrates excellent sensitivity, but also suggests high specificity, because the cystic fibrosis patients from whom these samples were obtained commonly have chronic infection of S. aureus, *Haemophilus influenza* and *P. aeruginosa*[192], which can express β-lactamase activity. Indeed, we found high levels of ampicillin resistant bacteria in our sputum samples but their presence did not impact selectivity or sensitivity.

In summary, we have developed a series of fluorogenic probes specific for *Mtb* by taking advantage of the uniquely flexible substrate-specificity loop of the BlaC enzyme expressed by tubercle bacilli. These probes are chemically modified cephalosporin lactams with a 7a-methoxy substitution. The acyl intermediate complexes of the E166A BlaC mutant and the probes were co-crystallized successfully for X-ray structure determination to reveal structural insights into the observed specificity of the probes for BlaC. A green fluorescent probe, CDG-OMe, enabled the successful detection and imaging, with high specificity, of live pathogen present at very low levels in patient sputum. With such a good sensitivity and specificity, it is highly promising that CDG-OMe could be developed easily into a rapid, low-cost TB diagnostic tool to meet the needs of people who live in remote, resource-limited areas. The success of this strategy may greatly contribute to decreasing *Mtb*-associated death rates and transmission.

MATERIALS AND METHODS

Cloning, expression, and purification of BlaC

Wild-type BlaC was cloned from *Mtb* H37Rv genomic DNA as described previously[97]. The deacylation deficient E166A mutant was generated using the Quickchange site-directed mutagenesis kit (Stratagene no. 200519). Mutant and wild-type protein expression and purification were performed as described previously[97].

Enzymatic kinetics

To a series of different concentrations of the probe (20, 40, 60, 80, 100, 120 and 150 μM) in 1× PBS (pH 7.4) in a 96-well plate (black and flat bottomed) was added TEM-1 Bla or BlaC. PBS was added to adjust the total volume to 100 μl. The fluorescence intensity at 454 nm was measured immediately in a microplate reader (excitation wavelength of 400 nm) over a period of 20-minutes at 22 °C. The values of the kinetic parameters (K_m and *kcat*) were determined from the double reciprocal plot of the hydrolysis rate versus the substrate concentration (Lineweaver–Burk plot). To determine the spontaneous hydrolysis rate of the probes, the fluorescence intensity was monitored over five days without the addition of enzyme. The rate was calculated from the plot of $\ln([S]_0/([S]_0 - [P]))$ versus time. Fluorescence spectra were collected on a Fluoromax-3 spectrafluorometer (Jobin Yvon). Kinetic experiments were conducted in a M1000 microplate reader (TECAN, Research Triangle Park, North Carolina).

Crystallization

Crystals of wild-type and E166A BlaC were grown using the hanging-drop vapour-diffusion method[151]. BlaC was concentrated to 10 mg ml^{-1} and equilibrated overnight at 4° C with the mother liquor (2.0 M NH4H2PO4, 0.1 M Tris buffer, pH 8.0) in a 1:1 ratio (protein:mother liquor). The solution was centrifuged for ten minutes at 13,000 revolutions per minute to remove insoluble precipitate. Hanging drops were set up and equilibrated against 1 ml of mother liquor. Microseeding with horsehair was sufficient to produce large diffraction-quality crystals. Crystals were transferred to a stabilization solution that contained 30% glycerol in the mother liquor and subsequently soaked with substrates for 2–4 hours. The concentration of substrate was increased slowly by transferring the crystals to successive drops to prevent cracking. Derivatized crystals were flash frozen in liquid nitrogen.

Data collection and processing

X-ray diffraction data were collected on beam lines 19ID and 23ID at the Advanced Photon Source, Argonne National Laboratory, Argonne, Illinois. Data sets were reduced using HKL3000[193]. Data were collected at a wavelength of 0.97 Å and a temperature of 120K. Data collection and refinement statistics reported in Appendix Table A3.

Structure determination

Initial phases were obtained by molecular replacement[153] using the CCP4 suite[154]

and 2GDN as a search model[97]. Each data set was refined against the resulting model, and iterative cycles of model building and refinement were performed with Coot 0.6.1[155] and PHENIX[156]. Protein Data Bank codes for BlaC–CDC-1 and BlaC–CDC-OMe acyl intermediate crystal structures are 3VFH and 3VFF, respectively.

Detection of mycobacteria in sputum

Mtb var. *bovis* strain BCG was cultured in 7H9 medium with a 10% oleic acid albumin dextrose complex (OADC) and 0.25% Tween-80 until it reached the log phase (optical density at 600 nm (OD600) of 0.5–1). *E. coli*, MRSA, *P. aeruginosa* strain PA01 and *M. smegmatis* were cultured in Luria–Bertani medium until OD_{600} = 0.5–1. After measuring the bacterial OD_{600}, 10^7 c.f.u. of each bacterial strain was added into Eppendorf tubes. Bacteria were centrifuged, the supernatant removed and resuspended into the same medium (7H9 medium with 10% OADC) to normalize the autofluorescence from different media. A series of tenfold dilutions of BCG were made. Bacteria were then incubated at 37 °C to allow β-lactamase production for 0.3–0.5 bacterial generations, using a 20 hour calculated generation time for BCG, a two hour calculated generation time for *M. smegmatis* and a 20 minute calculated generation time for Pseudomonas, Staphylococcus and *E. coli*. Then 10 µl of bacteria, 40 µl of sputum and 50 µl of CDG-OMe (5 µM) were mixed in a 96-well plate, incubated at room temperature for 160 minutes and the fluorescence read with a spectrometer (Mithras LB 940, Berthold Technologies, Oakridge, Tennessee) at 490 nm excitation and 535 nm

emission. For cellular phone imaging, the handmade imaging box consisted of a light-tight box, true cyan color light-emitting diode (LED) with a peak emission at 505–510 nm, an excitation filter (490 ± 10 nm) between the LED and sample, and an emission filter (530 nm, bandpass 43 nm) between the sample and an imaging hole in the box. BCG (10 µl), sputum (90 µl) and CDG-OMe (10 µM, 100 µl) were mixed, and after ten minutes samples were photographed with an Apple iPhone 4S through a hole in the box. The photograph was then analyzed for luminance (cd m^{-2}) using iPhotoLux v.1.0 (Maxime Bombrun, ISIMA, France), a free iPhone application.

CHAPTER V

STRUCTURE OF APO AND MONOMETALATED FORMS OF NDM-1, A HIGHLY POTENT CARBAPENEM-HYDROLYZING METALLO-BETA-LACTAMASE*

OVERVIEW

The New Delhi Metallo-β-lactamase (NDM-1) gene makes multiple pathogenic microorganisms resistant to all known β-lactam antibiotics. The rapid emergence of NDM-1 has been linked to mobile plasmids that move between different strains resulting in world-wide dissemination. Biochemical studies revealed that NDM-1 is capable of efficiently hydrolyzing a wide range of β-lactams, including many carbapenems considered as ‘‘last resort’’ antibiotics. The crystal structures of metal-free apo- and monozinc forms of NDM-1 presented here revealed an enlarged and flexible active site of class B1 metallo-β-lactamase. This site is capable of accommodating many β-lactam substrates by having many of the catalytic residues on flexible loops, which explains the observed extended spectrum activity of this zinc dependent β-lactamase. Indeed, five loops contribute residues in the active site including side chains involved in metal binding. Loop 1 in particular, shows conformational flexibility, apparently related to the

*Reprinted with permission from Structure of Apo- and Monometalated Forms of NDM-1—A Highly Potent Carbapenem-Hydrolyzing Metallo-β-Lactamase. Kim, Y., Tesar, C., Mire, J., Jedrzejczak, R., Binkowski, A., Sacchettini, J., Joachimiak, A., (2011). *PLoS ONE, 6*, e24621, Copyright 2011 by the Public Library of Science.

acceptance and positioning of substrates for cleavage by a zinc-activated water molecule.

INTRODUCTION

The imminent threat posed by the recent discovery and dissemination of the plasmid encoded New Delhi Metallo-β-lactamase (NDM-1) gene (blaNDM-1) harbored by multiple pathogenic microorganisms has prompted the formation of a global scientific corps d'armée[194]. Biochemical and structural elucidation of NDM-1 facilitates the thorough mechanistic understanding required for a rational design of small molecule inhibitors specific to NDM-1 for co-administration with β-lactam antibiotics. The crystal structures of NDM-1 presented here reveal an open, enlarged and flexible active site that explains the observed extended spectrum activity of this zinc dependent β-lactamase.

One of the last lines of defense against multiple and extensively drug resistant infections is the carbapenem class of β-lactam antibiotics, which was developed to evade β-lactamase mediated resistance posed by aerobic as well as anaerobic pathogens. Unfortunately, the integrity of the ''big guns'' (meropenem, imipenem, doripenem, ertapenem) has become compromised by a number of β-lactamase with extended spectrum activity, that is, the ability to inactivate all classes of β-lactam antibiotics, including carbapenems[195].

β-lactams are the most broadly used antibacterials world-wide due to their effectiveness at irreversibly inhibiting cell wall biosynthetic enzymes required for

peptidoglycan recycling, and minimal toxicity in humans[61,196]. The first β-lactam discovered, penicillin, inhibits the function of the D-Ala-D-Ala transpeptidase that links the peptidoglycan molecules in bacteria[1,8,13,14,22,61]. Simultaneously, cell wall hydrolases and autolysins continue to break down peptidoglycan crosslinks, resulting in cellular lysis and death. Since the discovery of penicillin, several classes of naturally occurring and semi-synthetic β-lactams have entered the clinic. Concomitantly, broad use of β-lactams as antibacterials applies a selective pressure that increases the reproductive success of pathogenic strains carrying evolved β-lactamase genes capable of combating our arsenal of β-lactam antibiotics.

The vast structural diversity designed into the semi-synthetic β-lactams evades β-lactamase mediated resistance by either preventing initial Michaelis complex formation, or by stabilizing transient intermediates that inhibit further β-lactam turnover. Carbapenems have proven to be the most effective broad-spectrum β-lactams, and their utility is generally reserved as a last line of defense against the toughest drug-resistant infections including MRSA[197], XDR-TB[198], and bacterial meningitis[199].

However, it appears that the ‘‘target’’ met the challenge. In the past several years, new pathogenic strains carrying carbapenemase genes have been documented in patients from India, Pakistan, Bangladesh and other countries[200-206]. Carbapenemases are members of class A (KPC, IMI/NMC, SME), class B (IMP, VIM, SPM) and D (OXA) β-lactamase, for review see references[57,126,207]. Class B β-lactamase depend on divalent cation metal cofactors for their activity, and are described as metallo-β-lactamase (MBLs)[126,207-209] Unlike serine β-lactamases, MBLs are not inhibited by the classic

irreversible β-lactamase inhibitors such as clavulanic acid, sulbactam and tazobactam, but instead are inhibited by metal chelators such as EDTA and o-phenanthroline[57,126,209]. Thiol compounds such as 2-omega-phenylalkyl-3-mercaptopropionic acid[210] and N-(2-mercaptoethyl)-2-phenylacetamide[211]are also competitive inhibitors. However, thus far the therapeutic potential of these inhibitors has not been demonstrated.

MBLs have been found in widely distributed bacteria such as Escherichia coli, *Klebsiella pneumoniae* and *Acinetobacter baumannii*[206,212,213]. VIM and IMP are the most frequently acquired subclasses of B enzymes[57]. MBLs show significant diversity of the active site, catalytic properties, and metal ion requirements and have been divided into three subclasses: B1, B2, and B3[57,126,195]. Subclass B1 includes several chromosomally encoded enzymes BcII, Bacillus cereus [214], CcrA, *Bacteroides fragilis*[215],BlaB, *Chryseobacterium meningosepticum*[216], and transferable VIM, IMP, SPM, and GIM type enzymes[126,217,218]. Subclass B2 includes CphA[219] and ImiS[220] lactamases from the *Aeromonas spe*cies and Sfh-I from *Serratia fonticola*[221]. Subclass B3 is represented by L1 from *Stenotrophomonas maltophilia*[222,223], FEZ-1 from *Fluoribacter gormanii*[216,224], GOB from *E. meningoseptica*[225,226], CAU-1 from *Caulobacter crescentus*[227], and THIN-B from *Janthinobacterium lividum*[228].

A new mobile subgroup B of MBLs was recently discovered and named New Delhi Metallo-β-lactamase (blaNDM-1). This multidrug resistance gene was characterized initially in an isolate from Sweden that originated from New Delhi, India. Since then, Enterobacteriaceae isolates harboring the NDM-1 gene have been found in multiple areas of India, Pakistan, Bangladesh but also in the USA, Canada, China, Japan,

and United Kingdom[200-206]. The emergence of blaNDM-1 in India and China has been linked to its spread on the IncL/M incompatibility plasmid group types[229]. A current survey of the New Delhi vicinity identified NDM-1 carrying isolates from drinking water and seepage[212]. NDM-1 has been reported to be a highly potent carbapenem-hydrolyzing, zinc-dependent MBL. When expressed in bacteria, it makes these bacteria resistant to a broad range of β-lactams. Currently, no inhibitor of NDM-1 approved for medical treatment is available. NDM-1 positive bacterial infections can only be treated with a few antibacterials, including colistin, tigecycline, fluoroquinolones, D-captopril, and polymyxin B[109]. In view of the emerging multidrug-resistant strains carrying NDM-1, the discovery of effective inhibitors is critical and urgent. Here we report hydrolytic activity of NDM-1 against selected β-lactams and carbapenems, the three high-resolution crystal structures of apo- and the first structure of monometalated form of NDM-1 derived from *K. pneumoniae*. Our results show that NDM-1 is unique among other MBLs due to its enlarged and flexible active site, and explain the observed extended spectrum β-lactamase activity.

RESULTS AND DISCUSSION

Expression, purification and structure determination of NDM-1

The NCBI database lists a number of identical sequences to NDM-1 from *K. pneumoniae* [CAZ39946)] from a number of other organisms [BAJ76899 [*Stenotrophomonas maltophilia*], ADY00041 and ADP20459 [*E. coli*], AEA41876

[*Acinetobacter baumannii*], ADU02194 [*A. junii*], and ADP37377 [*Enterococcus faecium*]]. Identical sequence entries are found in other records where the N-terminal region is missing. The N-terminal region of the NDM-1 protein contains a signal peptide [1–28] according to the Phobius transmembrane topology and signal peptide prediction server[230] consistent with the possible cleavage site after residue 28. Several other MBLs (VIM-1-Ec, VIM-2-Pa, IMP-1-Ab and IMP-4-Kp) contain signal peptides. In contrast, the PSORTb subcellular localization tool predicts no signal peptide and no predictive localization of the enzyme[231]. The sequence alignment of several selected MBLs reinforces the presence of a signal with possible localization to the periplasm.

We expressed in *E. coli* full-length recombinant *K. pneumoniae* NDM-1 β-lactamase, but because it expressed poorly and showed low solubility, we designed several constructs. These constructs were based on the NDM-1 homology models obtained using tools developed as part of the Protein Structure Initiative[232] and low sequence similarity MBLs with structures available in Protein Data Bank (PDB) IMP-1, PDB id 1DD6 [233], VIM-2, PDB id 2YZ3[234] and VIM-4, PDB id 2WHG[235]. Three recombinant NDM-1 β-lactamase: full-length NDM-1, and two constructs NDM-1 Δ38 and NDM-1 Δ36NY, which showed improved solubility, were expressed and purified to homogeneity. Purified enzymes exhibited a single band on SDS-PAGE, indicating Mr= 28.5 and 24.5 and 24.8 kDa for NDM-1, NDM-1 Δ38, and NDM-1 Δ36NY, respectively.

NDM-1 structure

The three apoNDM-1 structures include two pairs of monomers A and B and one monomer A, and the structure of monometalated NDM-1 (mZnNDM-1 Δ36NY) includes four monomers (A, B, C, D), respectively in the asymmetric unit, providing nine crystallographically independent views of the molecule for NDM-1 Δ38, NDM-1 Δ36NY (monoclinic), NDM-1 Δ36NY (orthorhombic), mZn-NDM-1 Δ36NY (tetragonal) (Appendix Table A4). Full length NDM-1 and NDM-1 Δ36NY are monomers in solution as shown by size exclusion chromatography. The model for NDM-1 Δ38 contains 226 residues (45–270) out of a possible 232 residues and 131 water molecules. The electron density maps obtained for the NDM-1 Δ38 structure allowed modeling of 226 residues of both A and B chains, except the 10 N-terminal residues including the three residues Ser-Asn-Ala left over from cloning, which are disordered and not included in the final model. The NDM-1 Δ38 models were refined against 2.0 Å data with a final Rwork of 19.5% and Rfree of 24.3% (Appendix Table A4). The structure of NDM-1 Δ36NY, which includes two chains each containing residues of 45–270 (A) and 44–270 (B), is very similar to that of NDM-1 Δ38 (rmsd between Cα atoms of comparing 452 residues of both chains is 0.21 Å), except for a few loop regions and an acetate molecule found in the active site in chain A. The two structures of NDM-1 Δ36NY obtained under different crystallization conditions and in different crystal packing are virtually identical (rmsd between Cα atoms of comparing 436 residues of both chains is 0.45 Å). Our NDM-1 Δ38 and two NDM-1 Δ36NY structures are also very similar to the recently published high-resolution structure of

dizinc NDM-1 Δ29[236], except for the N-terminal region (missing or disordered in our structures and some loop regions). The structure of mZnNDM-1 Δ36NY was obtained in the presence of 10 mM zinc chloride. The structure contains one zinc atom bound in the active site to the metal site 1 (Zn1). The metal bound structure is very similar to apo structures (for example, rmsd between Cα atoms of apoNDM-1 Δ38 comparing 218 residues of chain B of mZnNDM-1 Δ36NY is 0.46 Å).

NDM-1 resembles the common β-lactamase fold, although it shows low sequence similarity to β-lactamase deposited in PDB (20–33% sequence identity). The protein is made up of four layers α/β/β/α and forms a sandwich. The core of NDM-1 consists of two β-sheets, one (N-terminal) is composed of seven antiparallel strands (β1–β7) and the other (C-terminal) is composed of five antiparallel strands (β8–β12). The N-terminal β-sheet is highly twisted (>100 degrees). The interaction between β-sheets is mainly hydrophobic. The seven connecting helices are located below (α1–α4 and 3_{10} helix 5) and above (α6–α7) the plane of the β-sandwich (Figure 5.1 a). The interactions between helices and β-sheets are hydrophobic but also involve several hydrogen bonds (Q96 with carbonyl of Y64, T98 with carbonyl of A92, Y229 with carbonyl of Leu209 and S232 with carbonyl of P187). Strands and helices are connected through flexible loops with the most prominent loop (residues 206–228) located above an >600 $Å^3$ active site cavity containing a sulfate ion in monomer A and two sulfate ions in monomer B. The two β-sheets and four associated helices show a previously reported two-fold symmetry of the ‘‘ββββαβαβ’’ topological motif[214]. The symmetry is not ideal with one unit showing a ‘‘βββαβαβ’’ motif and the second unit ‘‘ββββαβαβαβ’’ is enlarged. The

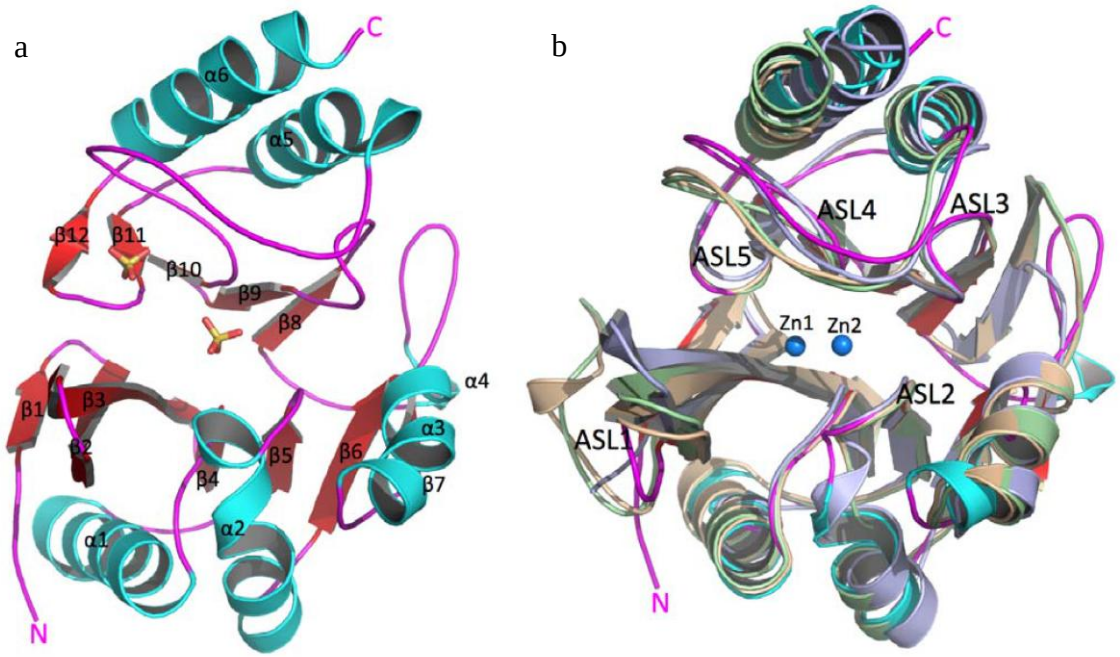

Figure 5.1. NDM-1 structure and comparisons with selected carbapenemases. a. Aerial view of active site (represented by two phosphate ions), the protein is made up of four layers, α/β/β/α, and forms a sandwich. Secondary structure elements and N- and C-termini are labeled. b. Comparison of *K. pneumoniae* NDM-1 (PDB id 3RKJ – magenta, N and C-termini are labeled) with three MBLs with carbapenemase activity *P. aeruginosa* VIM-2 (PDB id 2YZ3 - wheat), *P. aeruginosa* IMP-1 (PDB id 1DD6 - light blue) and *P. aeruginosa* VIM-4 (PDB id 2WHG - pale green). Loops contributing to the active site are labeled ASL1–5. Zn1 and Zn2 (blue spheres) are from the structure of VIM-2.

NDM-1 secondary structure is shown in Figure 5.1 a.

The search for structural homologs of NDM-1 using the DALI server[237] identified a number of closely related homologs. More than 400 entries were identified with a Z-score higher than 4. The closest structural homologs are MBLs (class B), followed by class A, C, and D β-lactamase. Over 1,200 β-lactamase superfamily members were also identified in 340 species showing highly diverse sequences. The top 250 structural homologs (Z-score>10) were clustered using CD-HIT[238] with a 90% sequence identity cut-off value resulting in 40 structure classes. Similar clustering was observed using 80% and 70% cut-off values. Representative structures from the 40 structure clusters were aligned based on the secondary structure. The alignment reveals that the NDM-1 structure (and its MBL homologs) displays expansions in some loop regions, for example ASL1, ASL4. The proteins belonging to the 40 structure clusters show several different catalytic activities (lactamase, oxidoreductase, hydroxyacylglutathione hydrolase, glyoxalase, nitric oxide reductase, parathion hydrolase, teichoic acid phosphorylcholine esterase). These enzymes utilize a broad range of substrates (β-lactams, hydroxyacylglutathione, nitric oxide, parathion, phosphorylcholine) suggesting that the lactamase fold seems highly adaptable and has evolved to support multiple functions and accept a wide range of substrates[126].

Active site expansion in NDM-1 and implications for ligand binding

Active site template searches using ProFunc[239] identified the *B. fragilis* MBL (PDB id 1BMI)[240] as an active site match with a similarity score of 422.6 and E-value of

$1.09x10^{-10}$. Seven active site residues in the *B. fragilis* MBL structure (His82, His84, Asp86, His145, Cys164, Asn176, His206) matched the corresponding residues in NDM-1 (His120, His122, Asp124, His189, Cys208, Asn220, His250) with an rmsd of 1.87 Å (over 13 atoms). Overall, the template identified 19 identical residues and 8 similar residues in the NDM-1/*B. fragilis* MBL active sites with local sequence identity of 52.8%. These residues form a solvent accessible surface that extends along the middle of the molecule between two β-sheets (Figures 5.1, 5.2). This well-defined hydrophobic and partly positively charged cavity is shaped by five active site loops (ASL1–5). From the bottom (as viewed in Figures 5.1 a, 5.2 and 5.3), two loops between strands β2 and β3 (residues 65–73, ASL1) and β5 and α2 (residues 118–124, ASL2) are contributing to form the base of the active site. At the top of the pocket, loops between β8 and β9 (residues 184–194, ASL3), β10 and α5 (residues 206–228, ASL4), and β11 and β12 (residues 248–255, ASL5) form the roof and walls of the active site (Figure 5.1). In MBLs, these loops provide key conserved side chains for coordinating metal ions as well as proposed catalytic general acid/base. As evident from the NDM-1structures, these residues appear to have well-defined conformations in the absence and presence of metal ions and this part of the active site is structurally well conserved (Figure 5.2). Additional residues from these loops, in particular ASL1, seem to also participate in the positioning of ligands in the active site in an orientation suitable for hydrolysis of the β-lactam ring. This is evident from several crystal structures of MBLs obtained with ligands[216,233,241-244]. MBLs, including NDM-1, show the longest ASL1 as compared with other β-lactamase superfamily members. The alignment of the NDM-1 structure with the closest

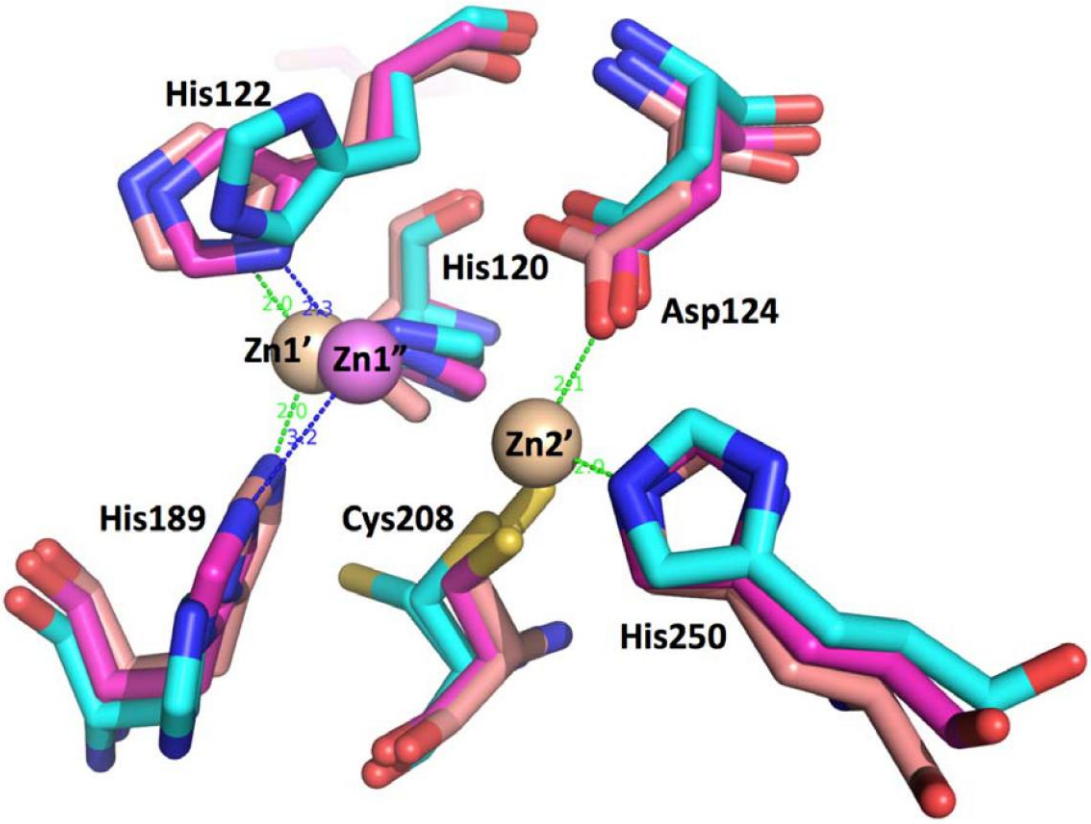

Figure 5.2. Active site comparisons of *K. pneumoniae* NDM-1 metalated states. Apo (PDB id 3RKJ) (aqua) vs monozinc NDM-1 (PDB id 3SFP) (violet) vs dizinc NDM-1 PDB id 3Q6X (wheat). Zn1' and Zn2' (wheat) are from the structure of di-zinc NDM-1 and Zn1" is from the structure of monozinc NDM-1. Conformations of residues coordinating Zn1 (His120, His122 and His189) and Zn2 (Asp124, Cys208 and His250) are shown for all three structures.

MBL structural homologs, di-zinc VIM-4 (PDB id 2WHG, Z-score 31.9, rmsd 1.9 Å), VIM-2 (PDB id 2YZ3, Z-score 11.2, rmsd 1.45 Å, between chain A of 3RKJ and chain A of 2YZ3), and IMP-1 (PDB id 1DD6, Z-score 11.7, rmsd 1.52 Å , between chain A of 3RKJ and chain A of 1DD6) reveals several unique features of the NDM-1 structure (Figure 5.1). Region 162–176 shows a very different conformation with a short 3_{10} helix (α4) formed in the middle of the loop region (Figure 5.1 b). This region forms a β-strand in VIM-2, VIM-4 and IMP-1. NDM-1 and IMP-1 show the longest ASL1 loop (Figure 5.1) but NDM-1 has a Phe insertion instead of Trp in this loop. This smaller side chain may provide more flexibility to accommodate bulky substrates. In NDM-1, ASL4 shows a more open conformation and the C-terminal helix is quite shifted in comparison to VIM-2, VIN-4 and IMP-1. However, the most important difference between these MBLs structures is a significantly larger active site cavity. This region in NDM-1 provides the opportunity to accommodate large substrates. In VIM-2, VIM-4 and IMP-1, side chains from the ASL1 and ASL4 loops bridge over the active site, dividing it into sub-cavities[233-235,240]. In contrast, the NDM-1 ASL1 and ASL4 loops are shifted outward considerably (Figures. 5.1 b and 5.3) and do not close over the active site but instead leave the site much more open and accessible to potential ligands (Figures 5.1 b and 5.3).

There is a reduction in the volume of residues contributing to the active site (Ala121 in NDM-1, typically Phe or Trp in other MBLs; Tyr229 in NDM-1, typically Trp in other MBLs; sequence Ala72Val73 in NDM-1 in ASL1, which is typically Val or Phe in other MBLs; Phe70 in NDM-1 in ASL1 which is Trp in IMP-1 and related

MBLs). There is also a reduction in the volume of residues contributing to the hydrophobic core. One indication of this volume reduction is an increase (15.2%) in alanine occurrence in NDM-1, which is nearly double the average alanine occurrence typically found in other proteins. These changes can contribute to the opening of the groove to solvent and can also increase the flexibility of structural elements. A larger active site would be more accessible to a broader range of antibiotics (or inhibitors) and thus provide an evolutionary advantage to bacteria. This can explain the observed enzyme promiscuity in accepting and hydrolyzing a broad range of β-lactams and carbapenems. A more open active site would allow for many substrates to bind in an extended conformation along the elongated-shaped groove with the β-lactam ring positioned over the active site metal ions while the rest of the substrate could be further stabilized by the interaction with side chains projecting from flexible loops ASL3, ASL4, and ASL5 (Figures 5.3, 5.4).

To investigate the structural implications of residue substitutions near the active site cavity, we performed a surface analysis on IMP-1 (PDB id 1DD6), VIM-2 (PDB id 2YZ3), VIM-4 (PDB id2WHG), and NDM-1. For each protein, solvent accessible cavities were identified[245]. NDM-1 has the largest cavity (surface area = 412.4 $Å^2$; volume = 591.3 $Å^3$) followed by IMP-1 (surface area = 339.5 $Å^2$; volume = 303.1 $Å^3$), VIM-2 (surface area = 223.9 $Å^2$; volume = 140.1 $Å^3$), and VIM-4 (surface area = 112.4 $Å^2$; volume = 45.3 $Å^3$). The active site cavity for each protein is shown in Figure 5.4 (green). It should be noted that the VIM-2 structure has a bound ligand in the cavity, which may affect the apo cavity structure and volume. However, even in a bound state

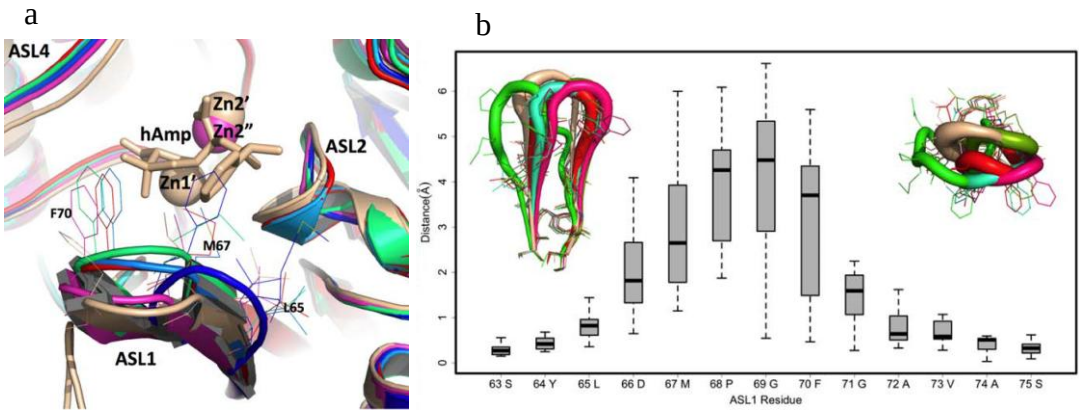

Figure 5.3. Flexibility of the NDM-1 active site loops. a. Structures of six NDM-1 molecules (identified using PDB ids) were aligned (PDB id 3RKJ (this work) molecule A - blue, PDB id 3RKJ (this work) molecule B - light blue, PDB id 3SBL (this work) molecule A - green, PDB id 3RKK (this work) molecule B – red, PDB id 3SFP (this work) molecule B – violet and PDB id 3Q6X[236] molecule B – wheat), hAmp is a hydrolyzed ampicillin and Zn1' and Zn2' are zinc atoms from the structure of NDM-1 (PDB id 3Q6X molecule B) and Zn1" is from the structure of monozinc NDM-1. b. The structural variability at each residue position in the ASL1 loop is evaluated across six structurally unique loops shown in A. After a structural alignment of the entire molecules, the Euclidean distance between the residues' center-of-mass was measured between all pair combinations at each position. The results are summarized as a boxplot showing the median, quartiles, maximum and minimum distances for each residue. The aligned loops are shown in cartoon putty representation, with the loop radius proportional to residue B-factors (view facing active site, left; top-down view, right).

the volume is considerably less than the NDM-1 cavity. To highlight the differences between the cavities, the molecules were superimposed onto the NDM-1 molecule. It is VIM-2 (surface area = 223.9 $Å^2$; volume = 140.1 $Å^3$), and VIM-4 (surface area = 112.4 $Å^2$; volume = 45.3 $Å^3$). The active site cavity for each protein is shown in Figure 5.4 (green). It should be noted that the VIM-2 structure has a bound ligand in the cavity, which may affect the apo cavity structure and volume. However, even in a bound state the volume is considerably less than the NDM-1 cavity. To highlight the differences between the cavities, the molecules were superimposed onto the NDM-1 molecule. It is evident that the expanded cavity volume in NDM-1 is due to residue substitutions occurring in the surrounding loops. Figure 5.4 shows the protruding residues in both stick and surface rendered forms.

In our three apo and one monozinc structures, there are nine independent representations of NDM-1 molecules with different crystallization conditions and packing environments. In these structures, most active site loops show very small conformational changes with the exception of ASL1 (Figures 5.1 b and 5.3) and to some extent ASL4. These are key loops contributing to the expansion of active site accessibility. Zhang and Hao, based on the comparison of their NDM-1 structure with other MBLs, hypothesized that the ASL1 loop may be flexible[236]. Our data clearly demonstrate that this is indeed true. As shown in Figure 5.3 b, ASL1 shows the ability of assuming several alternative conformations that may be important for binding ligands.

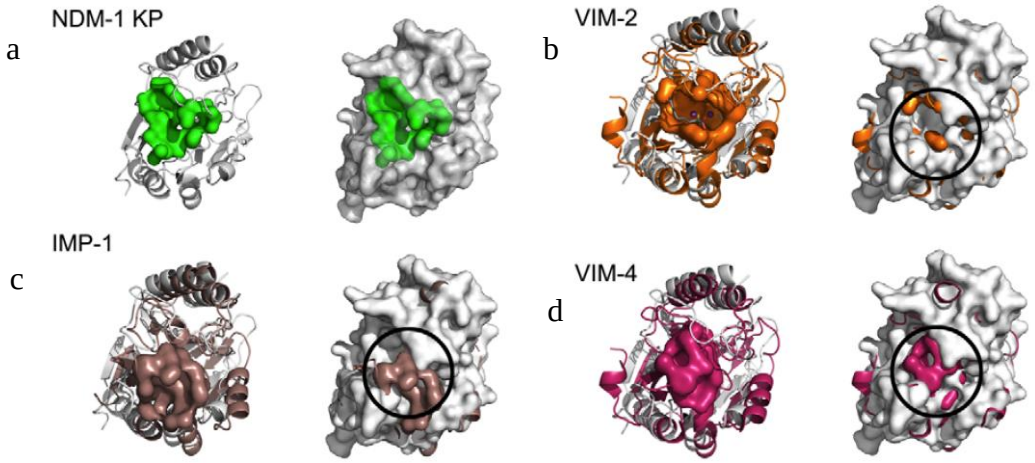

Figure 5.4. Active site expansion of NDM-1. The active site cavity comparisons of *K. pneumoniae* NDM-1 (gray) and three MBLs: IMP-1 (light brown), VIM-2 (orange) and VIM-4 (magenta). Superposition of the IMP-1, VIM-2 and VIM-4 molecules with NDM-1 reveal highly conserved structural arrangements. The most prominent variations occur between the catalytic sites (shown as surface representations), in which the side chains of IMP-1, VIM-2 and VIM-4 restrict the access to the active site by decreasing the volume of the cavity. (a) depicts NDM-1 and its active site surface (green) in secondary structure cartoon (left) and surface representation (right). (b-d) NDM-1 structural alignments with IMP-1, VIM-2 and VIM-4. Each highlights the IMP-1, VIM-2 and VIM-4 molecules' respective active sites, shown as colored surfaces. To highlight the greater accessibility to the NDM-1 active site, the aligned NDM-1 molecule is shown in surface representation (right). The obstructing interactions between ASLs restricting access to active site in IMP-1, VIM-2 and VIM-4 are observed as colored protrusions through the NDM-1 molecule and are highlighted for IMP-1, VIM-2 and VIM-4 with black circles.

Metal binding

NDM-1 has both β-lactamase and carbapenemase activities that are zinc-dependent[212,236,246,247], this work. Three of our apoNDM-1 structures are zinc-free and are the first structures of a wild-type apo-enzyme in subclass B1. Interestingly, the second crystal form (PDB id 3RKK) was obtained in the presence of 5 mM zinc acetate. No zinc is found in the structure and only an acetate ion can be modeled in the active site interacting with His250. Because of the location, the architecture and sequence conservation of the active site in NDM-1 are very similar to the metal binding sites of other β-lactamase. The active site similarity (presence of principal zinc-binding motif (HaHqD)) allows us to unambiguously identify all residues involved in zinc coordination. The active site template search identified all residues that are involved in metal binding in other MBLs of B1 subclass. It is predicted that NDM-1 would bind two zinc ions. Zinc 1 would be coordinated by His120, His122 and His189 and zinc 2 by Asp124, Cys208 and His250. Indeed, zinc was found bound to the Zn1 site in the crystal structure of NDM-1 obtained in the presence of zinc chloride. All four monomers in the asymmetric unit contain zinc atoms bound to the Zn1 site (His120, His122 and His189), therefore confirming NDM-1 as a member of subclass B1 of MBLs[236,247] and showing that Zn1 is a higher affinity site, as predicted for other MBLs[248,249]. This zinc atom is shifted approximately 0.8 Å compared with the di-zinc NDM-1 structure and shows somewhat longer Zn-His distances (Figure 5.2)[236]. The zinc coordinating residues are provided by ASL2, ASL3, ASL4, and ASL5. ASL2 contributes residues coordinating both zinc ions. In apoNDM-1 structure conformations of some of these residues are very

similar to zinc-bound states (His120, Asp124, and His250), while others show somewhat different side chain orientations (His122, His189, and Cys208) (Figure 5.2). Cys208 exists in two orientations in apo-state, one is similar to the zinc bound state and the other is rotated about 45 and 90 degrees in chain A and B, respectively. It has been noticed that MBLs are sensitive to metal chelators and it was suggested that they could bind zinc with lower affinity[57,126,219,248,250]. The range of affinities for zinc reported for MBLs vary from micromolar to millimolar.

The NDM-1 active site is located on its surface and is fully accessible to solvent. In the apoNDM-1 structure, two water molecules are coordinated by zinc-binding side chains, including Asp124, His122, and His250. In MBLs, the metal ions may have a dual role in catalysis. One zinc ion activates a metal-bound water molecule to perform a nucleophilic attack on the β-lactam carbonyl. The second zinc ion binds and polarizes this carbonyl group. A negatively charged carboxyl group of a zinc-bound Asp residue is involved in the activation of the water molecule. During the reaction, a tetrahedral intermediate is formed, followed by the delivery of a proton from a general acid/base residue (possibly Asp or another water molecule) to the lactam nitrogen and the cleavage of the lactam bond. All required residues are present in NDM-1 and therefore this enzyme should follow the general MBL catalytic mechanism involving a hydrolytic water molecule activated by a metal ion. In the mZnNDM-1 Δ36NY structures, there are several water molecules near the zinc atom. Monomer C contains tightly coordinated water (H-bond distance 2.8 Å) that may correspond to the position of the catalytic water molecule involved in β-lactam hydrolysis. Conserved Asp223 was proposed to function

as the general acid/base during catalysis suggesting that conserved Thr190 (or Ser), which is centrally positioned on the loop overhanging the active site, may play an important role in substrate recognition and transition-state stabilization[249,251]. It is easy to envision this loop undergoing movements upon substrate binding. The structure of zinc-free NDM-1, along with the previously reported structures, provides important insight into the conformational changes associated with the metal binding properties of NDM-1.

Steady state kinetics

NDM-1 kinetic parameters obtained using NDM-1 Δ38 are summarized in Table 5.1. NDM-1 is an extended spectrum zinc dependent β-lactamase capable of hydrolyzing nearly all classes of β-lactams, impairing the ability to treat life-threatening infections with intravenously and orally available carbapenems. Carbapenem substrates appear to be the most specific class of β-lactams for NDM-1. However, the specificity constants for cephamycin and penem substrates deviate by less than an order of magnitude, indicating that the evolved promiscuity is related to the relaxed the substrate specificity of NDM-1. The observed lack of well-defined substrate specificity has previously been observed for the MBL NDM-1 homolog GIM-1[218,252]. The carbapenems; imipenem, biapenem and tebipenem have very similar kinetic constants likely due to their structural similarity. Tebipenem, although turned over less quickly (*kcat* = 0.39 s^{-1}), has relatively high specificity, with a nearly two fold tighter Michaelis complex (K_m=69 mM) relative to other carbapenems. The majority of the Michaelis constants falls between 50 μM and 150 μM, and includes penem, carbapenem and cephamycin classes of β-lactams.

β-lactam antibiotic	β-lactam Class	K_M (μM)	Error	% Error	Vmax (μM s^{-1})	Error	% Error	*kcat* (s^{-1})	kcat/K_M (s^{-1}/μM)
Biapenem	carbapenem	130	12	9	2.6E-03	5.8E-05	3	49.8	0.38
Imipenem	carbapenem	134	12	9	2.5E-03	7.8E-05	3	64.9	0.48
Tebipenem	carbapenem	69	7	10	2.8E-03	4.3E-05	3	39.0	0.57
Nitrocefin	cephalosporin	3	0.6	20	5.6E-03	2.2E-05	5	12.5	4.18
Cefoxitin	cephamycin	95	20	21	5.8E-03	3.4E-05	7	13.2	0.14
Faropenem	penem	99	16	16	4.5E-03	4.2E-05	8	14.7	0.15

Table 5.1. Steady state kinetic parameters of NDM-1 Δ38 with a selected set of β-lactam antibiotics.

Substrates that are most efficiently ($kcat/K_m$) turned over in general have extended hydrophobic characteristics that complement the linear and hydrophobic nature of the NDM-1 active site cavity. The primary hydrophobic arrangement is contributed by residues Leu65, Met67, Pro68, Val73, Gly69, Phe70, and Val73 of ASL1, which contour the flexible roof of the active site (Figures 5.3, 5.4). In addition, alkyl moieties of Leu209, Ile210, Lys211, Asp212, Lys214, Ala215, Lys216, and Asn220 side chains of ASL4 give the distal region and base of the active site a partially hydrophobic surface area, while simultaneously maintaining hydrogen bond capability. The degrees of freedom of the aforementioned residues serve to increase the flexibility of the active site, thereby increasing promiscuity, but may do so at the expense of Michaelis complex formation for most substrates.

In accordance with previous kinetic characterizations of metallo-β-lactamases GIM-1[218,252], IMP-1[253], VIM-2[254], and NDM-1[109], kinetic constants could not be calculated for the suicide inhibitor clavulanic acid or the monobactam aztreonam. Although not yet implemented, this observation signifies the potential of treating NDM-1 harboring pathogenic bacteria with aztreonam or other structurally similar monobactams in combination with a new NDM-1 inhibitor.

Mechanistic and drug discovery implications

It is likely that NDM-1 has evolved to have a more open and flexible active site, to be able to inactivate the highly decorated β-lactam antibiotics that have progressed over the years from relatively simple (penicillin) to larger and more complex compounds

with new added substituents. It has been suggested that evolution of MBLs has enabled these enzymes to hydrolyze many compounds that interfere with key bacterial pathways, and is linked to increased flexibility and improved catalysis[249,251,255].

The X-ray structures of NDM-1 presented herein provide a structural foundation for the corroboration of the proposed reaction mechanism of NDM-1 and drug design. It seems that there are three distinct states of the NDM-1: metal free, singly metalated and doubly metalated. All these states could be targeted for structure-based inhibitor design. Analysis of structures and previously reported kinetic and spectroscopic studies on MBL enzymes allows us to propose a refined mechanism of catalysis for this antibiotic resistant lactamase. NDM-1 would bind a zinc atom to the Zn1 site and a second zinc to the Zn2 site. The binding of the second zinc could be cooperative as proposed for some MBLs. This would organize the residue in the active site for productive catalysis. The key step in catalysis for NDM-1 is likely recognition of the ligand by side chains in the cavity adjacent to the Zn1 site. Only ligands conforming to the NDM-1 site would bind. Next, the β-lactam ring of the ligand coordinates to Zn1, expanding its coordination number from four to five and activating it for a nucleophilic attack. It is clear that the ASL1 plays a key role in positioning the β-lactam ring over the dimetalated site. Deprotonation of the metal-bound water molecule by Asp124 to form a nucleophilic hydroxide moiety is consistent with the postulated pKa of the zinc-bound water molecule. Once the zinc-bound hydroxide is formed, it can attack the activated carbonyl carbon of the substrate, forming a transition-state complex[249,251,256,257]. In the dimetalated site, the second metal ion likely coordinates the β-lactam oxygen in a bridging fashion of

the substrate. Asp124 may provide a proton to the penultimate amino nitrogen, similar to that observed for DapE[258], returning it to its ionized state thus facilitating product release. Here again the flexibility of ASL1 is important to release the product. Once the products are released, a water molecule bridging the two metal ions is replaced. Recent mechanistic studies of MBL showed that Zn2 is the only metal ion capable of stabilizing an anionic intermediate that accumulates during β-lactam hydrolysis, in which the C–N bond has already been cleaved. Conserved Asp124 would provide a proton to complete product release.

Kinetic studies with NDM-1 show that the K_m for biapenem and imipenem were 130 μM and 134 μM, respectively (Table 5.1), which are significantly above the minimum inhibitory concentrations (MICs) against most pathogenic microorganisms (< 2 μg/mL or 6 μM) including Klebsiella spp. and *E. coli* , and *Pseudomonas aeruginosa*[259,260], each of which has been found to harbor the NDM-1 gene[261]. Pharmacokinetic analysis demonstrates that human serum levels of biapenem were maintained at above the aforementioned MICs in young and elderly adults in a dose dependent manner[262]. Unlike other carbapenems, biapenem is stable to human renal dihydropeptidase-1 (DHP-1), eliminating the need to co-administer the DHP-1 inhibitor cilistatin[263]. These studies suggest that the orally available carbapenem, biapenem, could be of potential use to treat patients with NDM-11 linked bacterial infections because the MICs and human serum concentrations are far below the K_m of biapenem for NDM-1. Therefore, next generation β-lactams used to fight NDM-1 linked bacterial infection may be derivatives of carbapenems like biapenem. However, given the broad specificity and

likelihood of compensatory mutations, novel metallo-β-lactamase inhibitors will be required.

MATERIALS AND METHODS

Protein cloning, expression, and purification

The ORF NDM-1 gene from *Klebsiella pneumoniae* subsp. pneumoniae MGH 78578 was synthesized chemically and initially cloned into vector pUC57. The full length NDM-1 and several Nterminal deletion constructs were subsequently amplified with KOD DNA polymerase using conditions and reagents provided by Novagen, Madison, WI and cloned into the pMCSG7 according to the ligation-independent procedure[264,265] and transformed into the *E. coli* BL21(DE3)-Gold strain (Stratagene), which harbors an extra plasmid (pMgk) encoding one rare tRNA (corresponding to rare Arg codons, AGG and AGA). These constructs provided a system to produce a fusion protein containing an N-terminal His6-tag followed by a TEV protease cleavage site and a target protein (pMCSG7). To produce the protein, the bacterial culture was grown at 37°C, 200 rpm in enriched M9 medium[266] until it reached OD600 = 1.0. After air-cooling it down at 4uC for 60 min, NDM-1 expression was induced by 0.5 mM isopropyl-b-Dthiogalactoside (IPTG). The cells were incubated overnight at 18uC, harvested and resuspended in lysis buffer (500 mM NaCl, 5% (v/v) glycerol, 50 mM HEPES pH 8.0, 20 mM imidazole, and 10 mM β-mercaptoethanol). Cells were disrupted by lysozyme treatment (1 mg/ml) and sonication, and the insoluble cellular material was

removed by centrifugation. The native NDM-1 protein was purified from other contaminating proteins using Ni-NTA affinity chromatography and the AKTAxpress system (GE Health Systems) with the addition of 10 mM β-mercaptoethanol in all buffers as described previously. This was followed by the cleavage of the His6-tag using recombinant His6-tagged TEV protease and an additional step of Ni-NTA affinity chromatography was performed to remove the protease, uncut protein, and affinity tag. The pure protein was concentrated using Centricon (Millipore, Bedford, MA, USA) in 20 mM HEPES pH 8.0 buffer, 250 mM NaCl, and 2 mM dithiothreitol (DTT). Protein concentrations were determined from the absorbance at 280 nm using a molar absorption coefficient (28,500 M^{-1} cm^{-1}). The concentration of NDM-1 Δ38 and NDM-1 Δ36NY samples used for crystallization was ~40 mg/mL. Individual aliquots of purified NDM-1 Δ38 and NDM-1 Δ36NY were stored in -80°C until needed. The full-length protein expressed rather poorly at ~ 2 mg/L of culture and it could only be concentrated to 8 mg/mL. Truncation of the first 38 residues of NDM-1 yielded a much more stable protein construct (NDM-1 Δ38) with the expression yield of soluble protein ~100 mg/L culture that can be concentrated up to 150 mg/mL. Protein crystallization Native NDM-1 as well as several mutants, including NDM-1 Δ38 (the first 38 N-terminal residues deleted) and NDM-1 Δ36NY (the first 36 N-terminal residues deleted followed by Q36N and Q37Y mutations), were screened for crystallization conditions with the help of the Mosquito liquid dispenser (TTP Labtech, Cambridge, MA, USA) using the sitting-drop vapor-diffusion technique in 96-well CrystalQuick plates (Greiner Bio-one, Monroe, NC, USA). For each condition, 0.4 mL of protein (40 mg/mL) and 0.4 mL of

crystallization formulation were mixed; the mixture was equilibrated against 135 mL of the reservoir in the well. Some protein was prepared in the presence of 5 mM zinc acetate or 5 mM zinc acetate and 20 mM citrate. Several commercially available crystallization screens were used including: MCSG-1–4 (Microlytic Inc. MA, USA) and Index (Hampton Research, Aliso Viejo, CA, USA) at 16uC and 4uC. Microcrystals were obtained under several conditions. Crystals of the zinc-free form of NDM-1 Δ38 and NDM-1 Δ36NY in the presence of 5 mM zinc acetate were grown at 16°C by vapor diffusion in sitting drops containing 0.4 mL of precipitant solution and 0.4 mL of 40 mg/mL of NDM-1 Δ38 or NDM-1 Δ36NY with 5 mM zinc acetate. The crystals grew within five days and reached sizes of approximately 0.100 mm x 0.020 mm x 0.010 mm^3. The best crystals appeared at 16°C under the condition of 0.17 M ammonium sulfate, 25.5% (w/v) PEG4000 and 15% glycerol, which corresponds to condition G6 from the MCSG-3 screen. These crystals had dimensions of 100 x 25 x 10 $microns^3$ and diffracted to 1.9 Å using the 19-ID minibeam[267]. The crystals of NDM-1 Δ38 belonged to the primitive space group P21 with unit cell parameters a= 59.71 A °, b= 51.11 Å, c = 70.6 Å, β =106.96°. The NDM-1 Δ36NY crystals were also P21 with a similar unit cell dimension of a= 59.76 Å, b= 50.86 Å , c = 70.72 Å , b = 106.98°. The asymmetric unit contains two molecules with a Vm value of 2.1 $Å^3$/dalton (solvent content 41.5%). Data collection was carried out on the 19-ID beamline of the Structural Biology Center at the Advanced Photon Source according to the procedure described previously[268]. Data for the NDM-1 Δ38 and the NDM-1 Δ36NY crystals were collected to 2.0 Å and 2.35 Å at a wavelength of 0.9792 Å from the single crystals using a 20 micron mini-beam and were

processed using HKL3000[269]. The third crystal was obtained from NDM-1 Δ36NY co-crystallizing with 10 mM aztreonam in the condition containing 1.8 M ammonium citrate dibasic, and 0.1 M sodium acetate trihydrate pH 4.6. The I-centered orthorhombic crystal (I222) of approximately 0.2x0.1x0.07 mm, a broken piece from a big multiple congregate, diffracted beyond 2.0 Å, though they are multiple with cell dimensions of a =66.05 Å, b =83.27 Å, c = 105.4 Å. The data were collected using ~75 micron beam. Crystals of mZnNDM-1 Δ36NY were obtained in the presence of 10 mM ZnCl2 in the presence of 0.17 M ammonium sulfate, 25.5% (w/v) PEG 4000, 15% (v/v) glycerol and 20 mM citrate and belong to tetragonal space group $P4_32_12$, with unit cell dimensions of a= 97.94 Å, b =97.94 Å, c =187.55 Å. These crystals diffracted X-rays to 2.2 Å.

Size exclusion chromatography

The molecular weight of native NDM-1 protein in solution was determined by size-exclusion chromatography using a Superdex 200 GE Healthcare 16/60 column. The column was calibrated with aprotinin (6.5 kDa), carbonic anhydrase (29 kDa), conalbumin (75 kDa), catalase (232 kDa), and thyroglobulin (669 kDa).The separation was carried out at 22°C at a flow rate of 2.0 mL/min. The calibration curve of Kav versus log molecular weight was prepared using the equation Kav= (Ve-Vo/)/(Vt-Vo,), where Ve = elution volume for the protein, Vo = column void volume, and Vt = total bed volume. Size exclusion chromatography indicates a protein monomer.

Data collection

An X-ray diffraction data set extending to 2.0 Å resolution was collected at the Structural Biology Center 19-ID beamline with the 20 x 20 μm mini-beam at the Advanced Photon Source, Argonne National Laboratory using the program SBCcollect. The crystal was pre-cooled in liquid nitrogen and exposed for 3 sec. per 1.0° rotation of omega with the crystal to a detector distance of 280 mm at 100 K using 0.9792 Å X-rays. The complete data were recorded on an ADSC 315r CCD detector scanning 185° on omega until the crystal was severely decayed. The second crystal form of NDM-1 Δ36NY was prepared in the presence of 5 mM zinc acetate and diffracted beyond 2.35 Å and a data set was collected similarly at the same beamline. The third crystal form produced by co-crystallization with aztreonam diffracted beyond 2.0 Å, however, the data were good only to 2.30 Å, because the crystal was multiple and decaying during the data collection. The data were collected by the similar procedures. For the mZnNDM-1 Δ36NY crystal, the energy was set to 1.2825 Å to exploit anomalous signal from zinc atoms. All of the diffraction data were integrated and scaled with the HKL3000 suite[269]. The processing statistics are given in Appendix Table A4.

Structure solution and refinement

The structure of NDM-1 Δ38 was determined by molecular replacement with the native data using MOLREP[270] within the HKL3000 software suite and BALBES[271] (R-factor of 42.2%, correlation coefficient score of 0.634), as described previously. Coordinates of MBL (PDB id 2YZ3) from *P. aeruginosa,* which exhibits ~33% identity

with NDM-1 from *K. pneumoniae*, were used as a search model. Further extensive model building was performed manually in COOT[272], while crystallographic maximum likelihood refinement with TLS groups[273] for two protein chains were refined by PHENIX.refine [156]. The structure of the two protein chains each containing residues 45–270 was refined to final R and Rfree factors of 0.19 and 0.24, respectively. The final model is characterized by a 0.007 Å rmsd from ideal bond lengths. 97.8% of the residues occupy the most favored areas of the Ramachandran plot according to the MOLPROBITY validation results[274]. The 2.35 Å structure from the second crystal with zinc acetate was determined by molecular replacement using the first structure as a search model on HKL3000 and refined using COOT and PHENIX.refine. The final refined model of the two protein chains (residues of 44–270 and 45–270) converged to the R and Rfree values of 0.21 and 0.28, respectively. The two protein structures are very close in details (rmsd of 0.21 Å with 452 Ca atoms) except that the second structure contains an acetate molecule in the active site. The structure was refined to a final model after several rounds of COOT and PHENIX.refine steps. Similarly, the third structure obtained from the co-crystallization with aztreonam was also determined to 2.31 Å by molecular replacement using the same search model (3RKJ). The final refined structure includes one chain with residues 41–269 and has an Rwork of 20.6% and Rfree of 27.0% with a good stereochemistry. Although the antibiotic molecule was not present in the structure, there were subtle changes found in the structure. For the NDM-1 Δ36NY crystal obtained in the presence of zinc chloride (mZnNDM-1 Δ36NY), the data were collected near the zinc absorption peak energy (1.2825 Å). However, zinc

anomalous diffraction signal was weak and structure could not be solved. Instead, molecular replacement with the structure of chain A of 3Q6X as a search model yielded the structure using HKL3000. The structure contained a single zinc bound NDM-1 Δ36NY in all four monomers in the asymmetric unit. The subsequent number of cycles of refinement by PHENIX.refine and COOT finalized the structure with Rwork of 18.1% and Rfree of 23.6% with a good stereochemistry. The final refinement statistics for all three structures are presented in Appendix Table A4.

Steady state kinetics

Steady state kinetic parameters were calculated for NDM-1 Δ38 β-lactamase substrates by directly monitoring initial velocities as the appearance or disappearance of the respective β-lactam antibiotic chromophore over time; Nitrocefin (λ =486 nm, e=20,500 M^{-1} cm^{-1}), Imipenem (λ =298 nm, Δε=9,035 M^{-1} cm^{-1}), Tebipenem (λ=300 nm, Δε =6,850 M^{-1} cm^{-1}), Biapenem (λ=295 nm, Δε=7,020 M^{-1} cm^{-1}), Cefoxitin (l=262 nm, Δε =5,382 M^{-1} cm^{-1}), Faropenem (λ =306 nm, Δε =2,662 M^{-1} cm^{-1}). All experiments were performed in 10 mM HEPES pH=6.75, 250 mM NaCl, 100 mM $ZnCl_2$. The final concentration of NDM-1 was 10 nM. Reactions were performed in UV transparent Costar 96 well plates and monitored with the Thermo Scientific Multiskan Go plate reader. Initial velocities were fit to the Michaelis-Menten Equation using KaleidaGraph 4.0.

CHAPTER VI

NDM-1, THE ULTIMATE PROMISCUOUS ENZYME: SUBSTRATE RECOGNITION AND CATALYTIC MECHANISM*

OVERVIEW

The specter of a return to an era in which infectious disease looms as a significant threat to human health is not just hyperbole; there are serious concerns about the widespread overuse and misuse of antibiotics contributing to increased antibiotic resistance in pathogens. The recent discovery of a new enzyme, first identified in *Klebsiella pneumoniae* from a patient from New Delhi and denoted as NDM-1, represents an example of extreme promiscuity: It hydrolyzes and inactivates nearly all known β-lactam-based antibiotics with startling efficiency. NDM-1 can utilize different metal cofactors and seems to exploit an alternative mechanism based on the reaction conditions. Here we report the results of a combined experimental and theoretical study that examines the substrate, metal binding, and catalytic mechanism of the enzyme. We utilize structures obtained through X-ray crystallography, biochemical assays, and numerical simulation to construct a model of the enzyme catalytic pathway. The NDM-1

*Reprinted with permission from NDM-1, the ultimate promiscuous enzyme: substrate recognition and catalytic mechanism. Kim, Y., Cunningham, M. A., Mire, J., Tesar, C., Sacchettini, J., and Joachimiak, A., (2013). *The FASEB Journal, 27*, 1917, Copyright 2013 by the Federation of American Societies for Experimental Biology.

enzyme interacts with the substrate solely through zinc, or other metals, bound in the active site, explaining the observed lack of specificity against abroad range of β-lactam antibiotic agents. The zinc ions also serve to activate a water molecule that hydrolyzes the β-lactam ring through a proton shuttle.

INTRODUCTION

Bacterial resistance to antibiotic agents is now recognized as an ancient evolutionary adaptation and not solely provoked by modern therapeutic practice [275]. Nevertheless, the spread of pathogenic strains resistant to multiple drugs is a serious issue, and human activities strongly contribute to it, although the situation is not quite as desperate as depicted in the popular press[133]. Microorganisms must continuously cope with microbial warfare and have developed a wide range of mechanisms to achieve antibiotic resistance[276]. One of the most effective mechanisms employed by pathogens is the expression of enzymes known as β-lactamases that can hydrolyze the 4-membered β-lactam ring found in commonly used antibiotics like penams, cephalosporins, and carbapenems. These antimicrobials target bacterial cell wall synthesis. The β-lactamase enzymes are divided into 4 main classes (classes A–D) based on sequence homology[53]. Class B enzymes utilize 1 or 2 zinc ions to catalyze the hydrolysis; the other 3 classes rely on an active-site serine residue[53].

A recent addition to the list of class B enzymes is the New Delhi metallo-β-lactamase (NDM-1) from *Klebsiella pneumoniae* that has demonstrated an ability to

proficiently hydrolyze nearly all β-lactam antibiotics[107,277-279]. A number of X-ray crystal structures of the apo enzyme and the enzyme in complex with a variety of substrates and with varying occupation of the zinc binding sites have been reported[46-50]. In addition, mechanistic studies have been conducted in an attempt to understand how the enzyme achieves its catalytic capacity[51]. A general framework for the activity of metallo-β-lactamases has been laid out previously[127]. Briefly, it is presumed that the carbonyl carbon atom of the β-lactam ring is attacked by a hydroxide ion, forming an intermediate state that is stabilized by the zinc ions[280]. Ring cleavage requires subsequent protonation of the nitrogen atom. However, at issue are the specifics of mechanistic and energetic details defining how precisely the enzyme environment facilitates the reaction.

Theoretical calculations have been carried out for the monozinc enzyme, CphA, with results that generally agree with the experimental data for that system[45,129,281]. Recent calculations in the dinuclear zinc L1 enzyme from *Stenotrophomonas maltophilia* have also been reported and offer insights into the catalytic mechanism, but these calculations do not provide evidence for protonation of the nitrogen in the final state of the reaction and presume that an active site aspartic acid plays the key role of a general base in the reaction[128]. This is contrary to mutational studies of the CphA enzyme in which an aspartic acid to asparagine mutation resulted in a 100-fold reduction in catalytic efficiency but did not stop the reaction entirely, suggesting that the aspartic acid is important for zinc binding but does not serve as a general base[127,129].

Here, we report the results of a combined experimental/theoretical examination

of the NDM-1 enzyme designed to address a number of outstanding issues regarding substrate recognition and the hydrolytic pathway. The experimental data suggest a multistep process[51], but the available crystal structures represent either the initial step of the reaction, prior to substrate binding or the (relaxed) product state subsequent to the catalytic reaction. As a result, definition of the Michaelis complex and the reaction pathway remain contentious subjects. In addition, different distances between zinc ions observed in several crystal structures and solution measurements suggest a possibility for alternative mechanisms[46-51]. To resolve these issues, we have determined the crystal structure of NDM-1 with 2 zinc ions and hydrolyzed ampicillin at atomic resolution (1.05 Å, the highest resolution of an NDM-1 structure to date); the crystal structure with 2 manganese ions and hydrolyzed ampicillin at 1.50 Å resolution; the crystal structure with 2 cadmium ions and a mixture of hydrolyzed and unhydrolyzed ampicillin at 1.50 Å resolution; and the lower-resolution crystal structure with 2 cadmium ions and faropenem. The structure with ampicillin and cadmium corresponds to the Michaelis complex. We have utilized these structures as starting points for our numerical studies and employed molecular dynamics calculations to assess structural aspects of substrate binding. Subsequent hybrid quantum mechanics/molecular mechanics (QM/MM) calculations were performed to determine the energy surfaces along the putative reaction pathways. We have also determined the pH dependence and metal requirements of the NDM-1 catalyzed reaction.

RESULTS

Active site organization

The NDM-1 active site contains 2 zinc-binding sites. One notable discrepancy among the experimental crystal structures is the observed distance between the zinc ions, which ranges on average from 3.5 to 4.6 Å[46-51]. It was shown earlier that the zinc ion (Zn1 site) coordinated by 3 histidine residues is occupied before the second zinc ion (Zn2 site) coordinated by Asp124, Cys208, and His250. It appears that both zinc ions have the flexibility to move considerably within the active site[48]. All of the structures confirm electron density between the zinc ions that is interpreted variously as a water molecule or hydroxide ion. We have conducted a number of molecular dynamics simulations with and without substrates for typical times of 10–15 ns duration. In the simulations, the site between the zinc ions was populated with alternatively, a water molecule, a hydroxide ion, or a chloride ion. For the cases where the site was occupied by water, we observed the Zn-Zn distance to be 5.6 Å; for Cl, the distance is 4.6 Å; and for OH, the distance is 3.6 Å. Averaged over several nanoseconds of simulation time, the standard deviaions are in the range of 0.10–0.15 Å and are largely independent of the presence or absence of the substrate (imipenem). The shortened distances observed in our simulations with ions present between the two zinc ions reflect the strong electrostatic interactions between the positively charged zinc ions and the negatively charged hydroxide or chloride ion. In our atomic resolution 1.05-Å structure of the NDM-1 protein, depicted in Figure 6.1 (similar but higher resolution structure to PDB

3Q6X[46]), in which a hydrolyzed ampicillin substrate is present, the observed Zn-Zn distance is 4.6 Å, suggesting that the active site is partially occupied by a water molecule and partially by a hydroxide ion (electron density is consistent with both). In one of the NDM-1 structures published recently (PDB 3SPU), Zn-Zn distances are substantially shorter (3.8 Å) and consistent with the presence of a bridging hydroxide ion[47]. These crystals were obtained at a high pH. Interestingly, our atomic resolution structure with ampicillin was crystallized at a pH of 6.5, and the crystals leading to the 3SPU structure were obtained at a pH of 7.5. Similarly, EXAFS solution scattering data[51], suggesting a 3.38-Å spacing between the zinc ions, were obtained at a higher pH (pH 7.6). We suggest that the different experimentally observed zinc distances reflect the pH conditions of crystallization: occupation by a water molecule at low pH and a hydroxide ion at higher pH.

K. pneumoniae is a gram-negative bacterium, and it belongs to the Enterobacteriaceae family that can grow in a variety of environments in a pH range of 5 to 8. Its intracellular pH has not been measured, but we can expect it to be similar to other bacteria in this family. Intracellular pH for Escherichia coli is very well established using several methods, and its value (7.6 ± 0.1) is quite independent of the external medium pH[282,283]. The pH of the periplasm, where NDM-1 resides, is more variable, more closely reflecting the pH of the extracellular environment. Assuming a similar intracellular pH for *K. pneumoniae*, we anticipate that the active site of NDM-1 is populated partly by a water molecule and partly by a hydroxide ion. This finding is

consistent with the observation that the distance between zinc ions at a pH range of 6.5 to 7.5 varies between 3.9 and 3.6 Å, respectively.

Promiscuity of substrate recognition

The active site in NDM-1 is a narrow slot defined by the two mobile loops, ASL1 and ASL4[46]. At the bottom of the slot, 2 zinc ions are each coordinated by 3 protein side chains: His120, His122, and His189 for Zn1, and Asp124, Cys208, and His250 for Zn2, as depicted in Figure 6.1. The zinc ions held by the protein side chains appear to provide the essential capability to recognize β-lactam substrates and define what we term the catalytic core of the active site. The β-lactam substrates that are hydrolyzed by NDM-1 all possess carboxyl and carbonyl groups that are spaced by their similar, roughly planar core geometries. Oxygen atoms from these groups coordinate with the zinc ions to form the principal substrate-recognition unit of the enzyme. The distance between zinc atoms (4.1 Å; an average from available crystal structures) matches well with the distance range of the β-lactam carbonyl and carboxyl (3.45– 4.42 Å) oxygen atoms. Other potential substrates with a nonplanar core are selected against by the action of the slot narrowing. The various substitutions to the R1 and R2 moieties extend into larger, open, and solvent-filled spaces on the protein surface[46]. Crystal structures with ligands and modeling show that R1 and R2 generally do not interact with the protein directly, thus explaining the enzyme's capacity for hydrolyzing a broad range of substrates, all containing supported by the crystal structure of NDM-1 with ampicillin and 2 manganese ions (Δ30-amp-Mn).

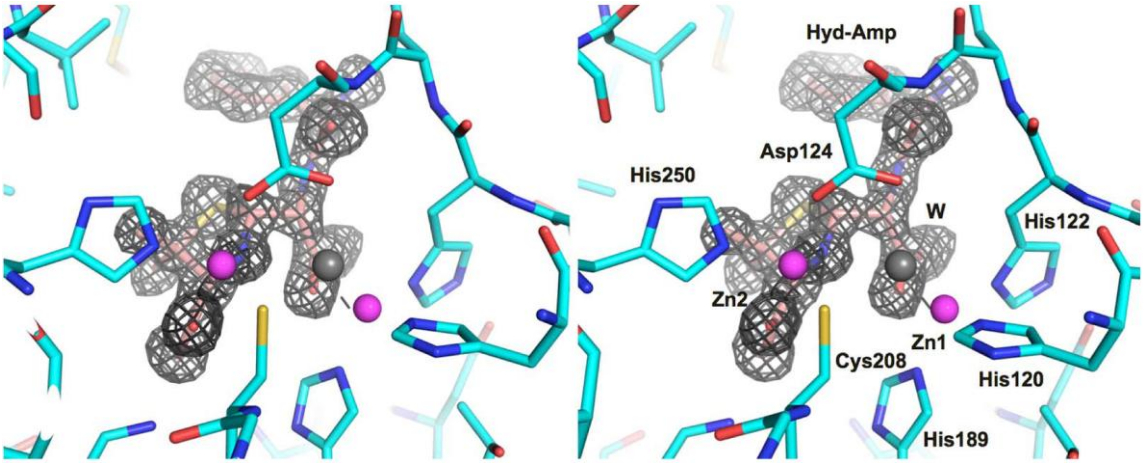

Figure 6.1. NDM-1 in complex with hydrolyzed ampicillin. Stereoview of the active site, with carbon atoms in the protein shown in cyan; those in the substrate are pink. Nitrogen atoms are blue, oxygen atoms are red, sulfur atoms are yellow, and zinc ions are magenta. An oriented water molecule (W) is gray. The *Fo*-*Fc* electron density around the substrate is contoured at 3σ. Dashed lines indicate key interactions between the protein and zinc ions.

This structure obtained at pH 7.5 shows a metal distance of 4.5 Å and a completely hydrolyzed ampicillin. Similarly, structures with ampicillin, faropenem, and 2 cadmium ions show partly disordered ligands with exception of the β-lactam core. Our data clearly suggests that NDM-1can substitute zinc with manganese, or cadmium, as was reported earlier[284], and bind substrates using different metals in the catalytic core.

In our molecular dynamics simulations with imipenem and ampicillin bound to NDM-1, we found persistent interactions only between the β-lactam carbonyl and carboxyl oxygen atoms of the substrate and the zinc ions (Figure 6.2). The binding cleft in NDM-1 is lined with nominally hydrophobic residues, so no specific hydrogen-bonding interactions occurred between the β-lactam core and the protein. The R1 and R2 substituents of imipenem and ampicillin extend into larger cavities and are primarily solvated by water. For imipenem, we observed a hydrogen bond formed between Asp124 and the hydroxyethyl group (R2) that can persist for hundreds of picoseconds, but no long-lived bonds were observed between the protein and the R1 moiety. No such interactions were observed in simulations with ampicillin, where the R2 moiety made sporadic interactions with the protein. R1 and R2 substituents are partly disordered in the crystal structures with unhydrolyzed β-lactams.

What we have also observed in our simulations, as illustrated in Figure 6.2 b, is that the cavity can widen due to the relative motion of the mobile ASL1 and ASL4.

a

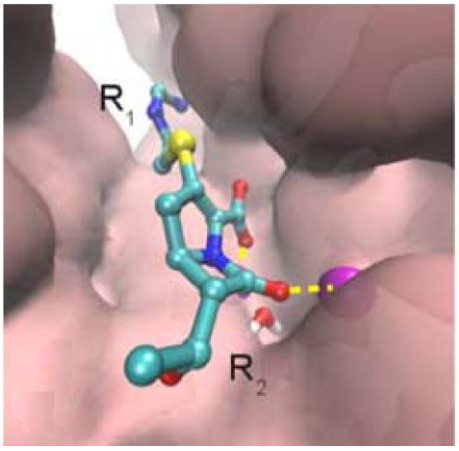

b

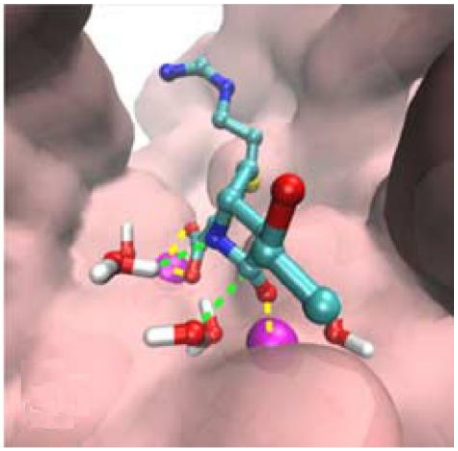

Figure 6.2. NDM-1 simulation active site. The protein is depicted as a surface and the (imipenem) substrate is colored as in Fig. 1, except for carbon atoms, which are cyan here. (a) Substrate recognition is provided by interactions between the zinc ions and the carboxyl and carbonyl oxygen atoms of the substrate (dashed yellow lines) and nonspecific, generally hydrophobic interactions with the protein. The oriented water molecule occupies a pocket between the zinc ions. (b) When the mobile loops move, a thin film of water surrounds the substrate, including 2 water molecules that serve as the nucleophile and as the source of the final proton required for cleavage (dashed green lines).

When this happens, although this does not necessarily always occur in the time scales accessible in our simulations, a monolayer of water molecules can intrude between the substrate and the protein. The hydrogen bonding network of the bulk water is disrupted within the monolayer, with hydrogen bonds forming preferentially with the ligand and not the (hydrophobic) protein residues. We believe that the motion of the active site loops provides a mechanical filter of sorts that selects substrates with a core geometry that is nearly planar.

Reaction pathways

Previous discussions of the enzyme mechanism have focused on the oriented water molecule (hydroxide ion) identified between the two zinc ions, where it is presumed that this molecule will serve as the nucleophile that initiates the hydrolytic reaction. We have investigated several possible reaction pathways by identifying conformations from the molecular dynamics simulations where molecules were aligned appropriately for an attack of the C7 carbon atom of the substrate to be productive. That is, we initiated the attacks from what would be described as near-attack conformations[285]. The QM/MM calculations were conducted by computing optimized structures along a putative reaction pathway, defined by placing constraints on key distances like that between the C7 carbon atom of the substrate and the O_w oxygen atom of the attacking water (hydroxide) and changing the constraints in a stepwise fashion. This initial guess for the reaction pathway was then optimized using a nudged elastic band method[286], in which no atoms were constrained, producing an estimate of the

potential energy surface along the path. Subsequent dynamics calculations on the MM partition allowed us to estimate the free energy along the pathway; given the computational requirements for such calculations, free energy calculations were only performed for the most favorable pathways. In our methodology, the estimate of the free energy is dominated by the quantum component, with the MM component providing corrections typically of the order of 20–30 kJ/mol. In our experience, the MM component will not lower a 200 kJ/mol barrier to a 100 kJ/mol barrier.

On analyzing all of the different reaction pathways, the subset of pathways studied in which the oriented water or hydroxide ion served as the nucleophile was energetically unfavorable. For the attack of a hydroxide ion, we observed a potential energy surface that rises monotonically to 170 kJ/mol at the intermediate state. Such a state would not be stable, so we have also considered attacks using an initial oriented water molecule and a pathway that utilized Asp124 as a general base; a concerted attack in which the N4 nitrogen atom was directly protonated by the attacking water molecule; and a pathway in which a bulk water molecule served as a base. In each of these scenarios, we found barriers of 200 kJ/mol or more, suggesting that the oriented water molecule is not the nucleophile. Previous experimental results in the CphA system, which is a class B2 β-lactamase, have excluded Asp124 as a base. It is possible that the mechanisms in the two enzymes differ, but we believe the experimental findings lend credence to our computational modeling results, at least in terms of excluding Asp124 as the general base.

We have identified conformations from the molecular dynamics simulations in

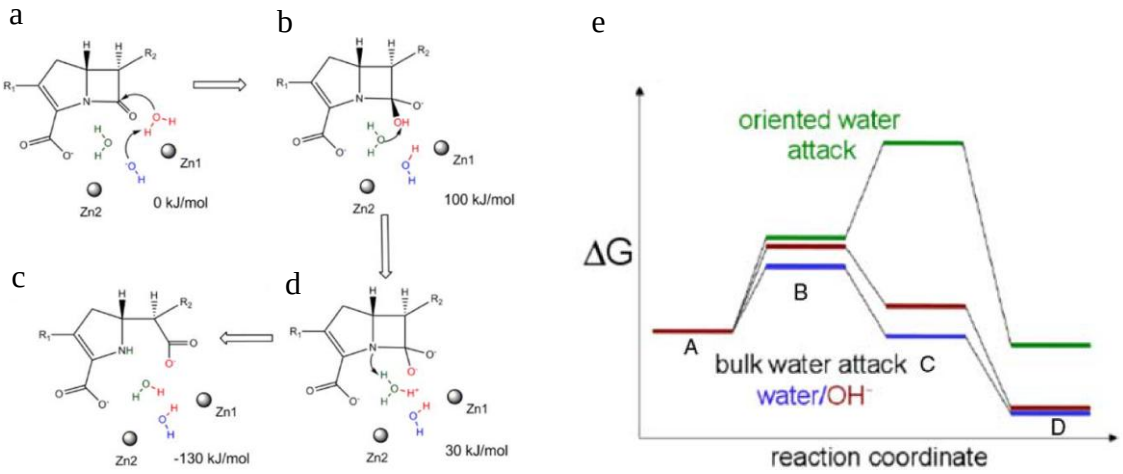

Figure 6.3. NDM-1 reaction mechanism. (a) The oriented hydroxide ion serves as a general base to accept a proton from a bulk water molecule. (b) A proton from the intermediate state is transferred to another bulk water molecule. (c) The proton is then shuttled to the N4 nitrogen of the substrate. (d) The nitrogen (N4)-carbon (C7) bond is cleaved in the final state. Energy values are estimates of the free energy from the QM/MM calculations. (e) Comparison of the pathway energetics with a bulk water as the nucleophile (red, blue) or the oriented water acting as the nucleophile (green). Reaction coordinates correspond to steps shown in panels (a–d).

which the substrate was solvated by bulk water. We have also examined pathways in which the oriented water or hydroxide ion served as a general base and the nucleophilic water originated from the bulk solvent. In Figure 6.3 a-d, we depict the proposed mechanism of action for a pathway in which a bulk water molecule transfers a proton to the oriented hydroxide ion and then attacks the carbonyl group of the substrate. Formation of the intermediate is the rate-limiting step of the reaction; subsequent proton translocations involving a second bulk water molecule result in protonation of the N4 nitrogen atom of the substrate and ring cleavage. Subsequent steps along the pathway are energetically downhill.

Finally, we have also studied the pathway possibility where a water molecule occupies the site between the zinc ions. In this case, the initial proton transfer to the oriented water results in protonation of the carboxyl group of the substrate. Subsequent proton translocations also result in cleavage of the N4-C7 bond. The observed barrier is ~80 kJ/mol. By comparison, in Figure 6.3 e, we compare the relative energetics along the pathways involving bulk water serving as the nucleophile and one of the cases in which the oriented water served as the nucleophile. We observed a relatively large barrier for the latter pathway, typical of all the pathways in which the oriented water or hydroxide ion served as the nucleophile. These results suggest that the most probable reaction mechanism involves a bulk water molecule serving as the nucleophile, and either the oriented water molecule or hydroxide ion, serving as the general base. Our proposed mechanism is consistent with an increased volume of the active site, high flexibility of NDM-1 and its chemical environment.

pH and metal dependence of NDM-1 activity

To gain further structural insights into the mechanism of binding and hydrolysis of β-lactam substrates by NDM-1, we sought to trap the Michaelis complex of NDM-1 with various β-lactam substrates. Several attempts were made by co-crystallization, as well as crystal soaking, but structures revealed only product bound in the active site when NDM-1 was liganded with zinc or manganese. To facilitate trapping of the Michaelis complex of NDM-1 with β-lactam substrates, we sought to identify conditions that would decrease the turnover number of NDM-1. We approached this from the perspective of pH and selection of divalent metal cation.

We have determined the turnover number of NDM-1 as a function of pH, and in the presence of varying concentrations of divalent cations zinc and cadmium. The results reveal a direct dependence of turnover number *kcat* on pH (Figure 6.4). As the pH is increased from 5.5 to 8.5, *kcat* increased 4-fold from 26 ± 2 to 101 ± 5 s^{-1}, respectively. The results are consistent with an increasing frequency of zinc-liganded hydroxide ion as the pH increased.

The dependence of *kcat* on divalent cation concentration showed that in the presence of 1–200 M zinc, the turnover number increased from 23 ± 3 to 110 ± 4 s^{-1}, with a plateau between 100 and 200 μM zinc. In the presence of 1–200 μM cadmium, *kcat* decreased from 6 ±1 to 1 ± 1 s^{-1}, with a plateau between 100 and 200 μM.

Although the activity of NDM-1 was severely attenuated when liganded with cadmium, a basal level of hydrolysis was maintained, which is consistent with partially hydrolyzed faropenem and ampicillin molecules in the active site of cadmium liganded

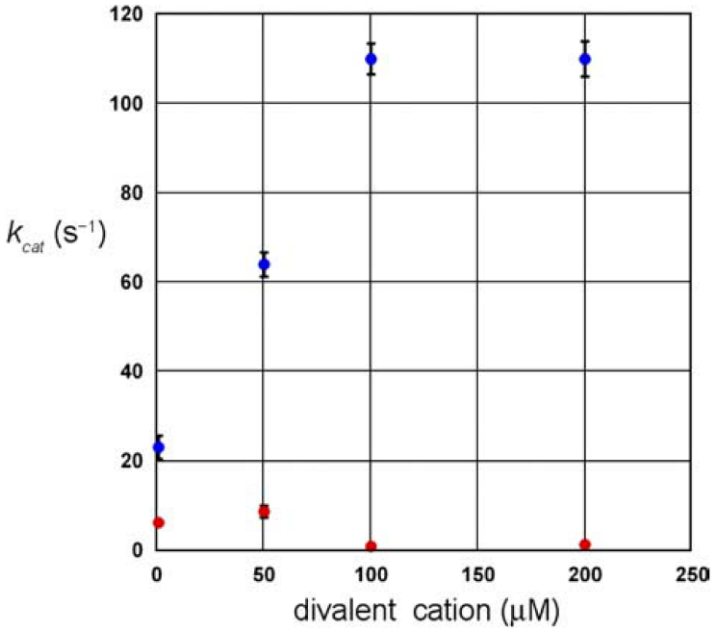

Figure 6.4. Dependence of NDM-1 turnover number on divalent cation concentration. The kinetic parameter (*kcat*) was determined for NDM-1 using ampicillin as a substrate and increasing concentrations of Zn^{2+} (blue circles) or Cd^{2+} (red circles). Error bars are depicted in black.

NDM-1 (Figure 6.5).

Structure of the Michaelis complex

As shown in Figure 6.4, cadmium ion is a very poor substituent for zinc, consistent with earlier reports that substituting cadmium for zinc inhibits enzyme activity[40]. We have obtained 2 crystal structures of the enzyme with cadmium: a high-resolution structure in complex with ampicillin (Δ30-amp-Cd) and a lower resolution structure in complex with faropenem (Δ30-far-Cd). Unlike the Δ30-amp-Zn structure that shows well-defined electron density for hydrolyzed ampicillin bound to the active site containing 2 Zn ions, only partial electron density (2Fo-Fc) for the ligand was observed in the presence of cadmium ions. In the case of the high-resolution Δ30-amp-Cd structure (Figure 6.6), Cd in the primary metal site (Cd1)[48] is split into 2 positions in both protein chains in the asymmetric unit, Cd1a and Cd1b, that are 1.01–1.18 Å apart and have 64–65 and 35–36% occupancies, respectively. Both metal ions are coordinated by the same set of interactions with active site residues. The second metal site (Cd2) maintains its usual position and shows two different distances between the two metal sites, 3.53–3.72 and 4.29–4.30 Å, respectively. The electron density for the ligand is somewhat different from both hydrolyzed ampicillin and unhydrolyzed ampicillin; while the 5-membered ring in the lactam moiety and its carboxyl group are well-defined, the 4-membered ring (unhydrolyzed) or carboxyl group (hydrolyzed) are partly disordered, and the phenyl peptide assumes a distinct conformation from that of a hydrolyzed ampicillin, albeit not well-defined (Figure 6.6 c). This electron density was interpreted as

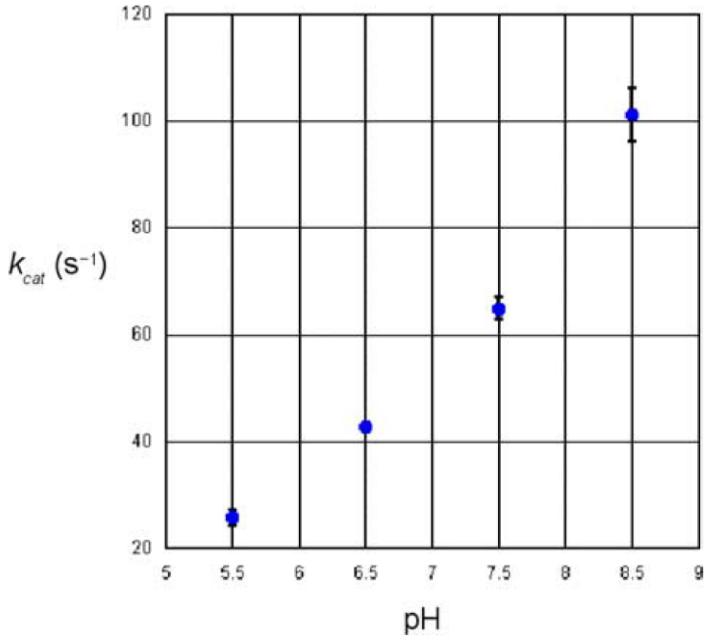

Figure 6.5. pH dependence of NDM-1 turnover number. The kinetic parameter, (*kcat*) was determined for NDM-1 using CENTA as a substrate. Error bars are depicted in black.

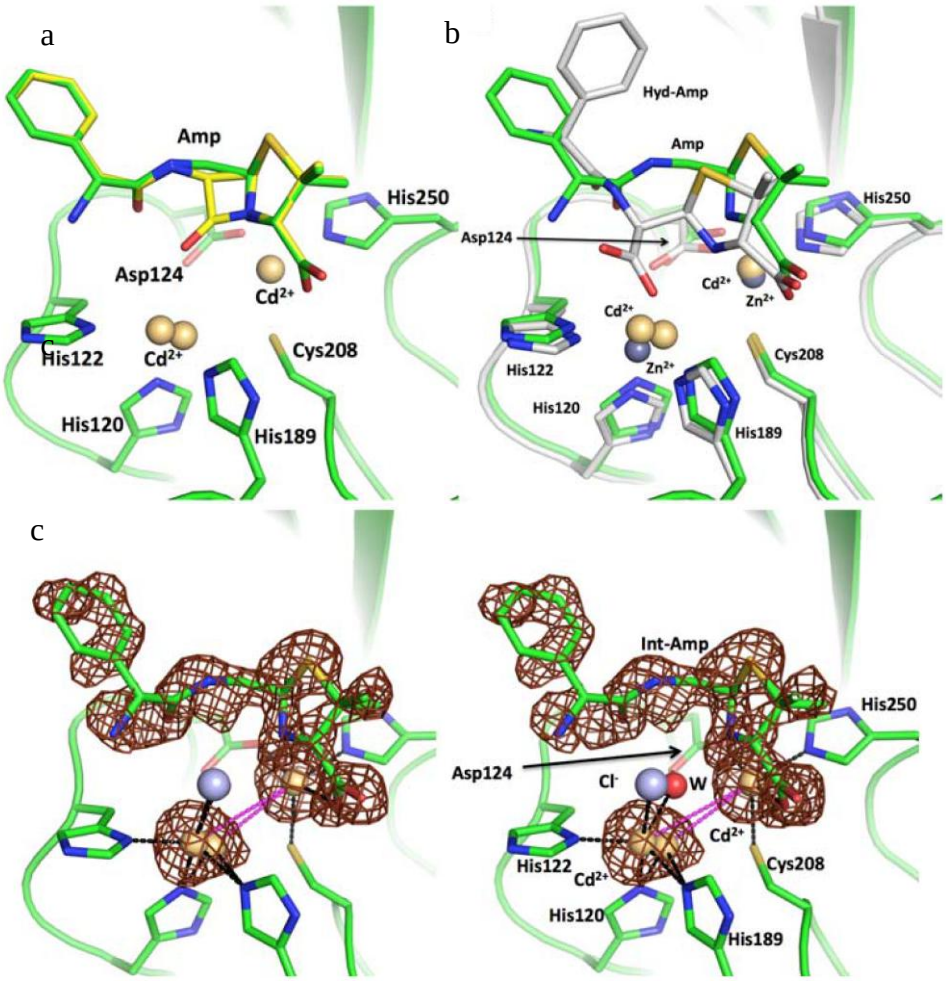

Figure 6.6. Structure of NDM-1 in complex with two cadmium ions and ampicillin. (a) The intermediate (int-amp) is superposed with the modeled unhydrolyzed ampicillin (yellow). (b) The hydrolyzed ampicillin (gray) from Δ30-amp-Zn is compared with the int-amp. Notice that the hydrolyzed ampicillin is rotated a few degrees (ccw) from the intamp. (c) The partially hydrolyzed ampicillin (green; intermediate) is fitted in the *F*o-*F*c electron density contoured at 2σ level. The split Cd^{2+} is also indicated.

being partially occupied by unhydrolyzed and hydrolyzed ampicillin. This crystal structure indicates that on hydrolysis, one part of the ligand is very well ordered, and the other part undergoes conformational changes. The 5-membered ring of the β-lactam and the R1 moiety of the phenyl peptide show an ensemble of unhydrolyzed and hydrolyzed intermediates and appear as disordered regions in the ligand. We also noted that the position of the ligand in the Δ30-amp-Cd structure is slightly different from that of the hydrolyzed ampicillin in the Δ30-amp-Zn structure (Figure 6.6 a,b). Perhaps the action of active site narrowing and widening by ASL1 and ASL4 as the catalytic reaction progresses forces the ligand (substrate, intermediate, or product) to move about, rotation of a few degrees counterclockwise in this case, for a higher catalytic efficiency.

In the lower-resolution Δ30-far-Cd structure, the density for the ligand is not as well defined as that of other structures of NDM1-hydrolized ampicillin complexes (3Q6X, 4H0D, 4HL2) and is only visible for the β-lactam moiety. Faropenem is smaller than ampicillin, but the electron density is different from what was predicted for hydrolyzed faropenem. We modeled the electron density as a mixture of hydrolyzed and unhydrolyzed faropenem; however, only a portion corresponding to the β-lactam moiety refined well, and it is difficult to resolve the two conformations. The metal-metal distance is significantly shortened (3.46 –3.48 Å); no well-ordered oriented water molecule is present between the cadmium ions, and the Asp124 carboxyl group coordinates both cadmium ions (2.80 –2.83 and 3.44 –3.82 Å). With this rearrangement, the active site appears to be in a conformation that is not quite optimal for binding β-lactam antibiotics (faropenem) and hydrolyzing it. We also note that the furyl group (R1)

of the substrate is poorly resolved in the structure, consistent with our observations that the R1 and R2 moieties of ampicillin were only partially ordered in the other NDM1-hydrolyzed ampicillin structures.

Using the cadmium-bound structures observed experimentally as a starting model we have conducted a number of molecular dynamics simulations. From these simulations, we have obtained a structure in which the active site is organized in a conformation like the proton shuttle-starting configuration that was described for our zinc containing structures. The potential energy along a proposed proton shuttle pathway computed through QM/MM yields a high barrier of 200 kJ/mol. The high-energy barrier is consistent with experimental observations that the enzyme efficiency is greatly reduced when zinc is substituted by cadmium. In the structure depicted in Figure 6.6, we interpret the density to indicate that the ampicillin is only partially hydrolyzed, suggesting that cadmium replacement does not completely disable the enzymatic activity of the protein and this is confirmed experimentally (Figure 6.4). These results show that the dimetal ion core is essential for ligand binding and that very specific framework of that core is needed for efficient substrate hydrolysis.

DISCUSSION

Metallo-β-lactamases represent a family of enzymes capable of evolving multiple catalytic activities and accepting a wide range of substrates[276]. Therefore, it is not very surprising that the NDM-1 represents an evolutionary step that can bind and hydrolyze a

broad range of β-lactam-based antibiotics. The enzyme shows a high flexibility of loops forming the active site and, with exception of the β-lactam moiety, does not seem to make extensive interactions with the substrates, which is a characteristic of promiscuous enzymes[287-289]. Recognition of the substrate is provided almost entirely by what we can call the catalytic core of the active site; the two zinc ions interact with the carboxyl and carbonyl oxygen atoms of the β-lactam. The presence of divalent metal cations seems to be essential for binding. The zinc ions can be replaced with other metals (Mn^{2+},Cd^{2+}) that provide an equivalent β-lactam binding framework, but not necessarily the same catalytic potential as Zn^{2+}. Modest substrate specificity is provided by the mechanical action of the mobile loops, ASL1 and ASL4, which select planar core ligand structures.

When the mostly hydrophobic trench widens, a single layer of water molecules is admitted into the space between the substrate and protein, and it is these water molecules that are apparently recruited to hydrolyze the β-lactam ring. As the protein surface is predominantly hydrophobic, the water molecules preferentially coordinate with the substrate and catalytic core. The dinuclear zinc catalytic core is coordinated by 6 side chains that form 2 catalytic triads. Interestingly, the distance between the metal ions can vary considerably (3.1– 4.6 Å) and this distance seems pH dependent. In addition, dizinc coordinates water or a hydroxide ion between the metal ions that we propose serves as the general base in the catalytic reaction. The presence of the zinc ions provides a pathway for shuttling protons among the water molecules that would not be present in bulk water, explaining the relative stability of the substrates in solution.

Our structures and calculations are consistent with two pathways; one, at lower pH, involves a zinc-coordinated water molecule, and the second, at higher pH, involves a zinc-coordinated hydroxide ion. In both of these mechanisms, a bulk water molecule serves as the nucleophile, and the zinc-coordinated molecule serves as the general base. Ring cleavage is achieved through a proton translocation process that utilizes another bulk water molecule. The suggested mechanism (Figure 6.3) is in some sense similar to that we have previously observed in the human aldose reductase system[290], where proton translocation was shown to be essential for catalysis. Our proposed mechanism is also in agreement with EXAFS data[51] that suggest a multistep reaction. The NDM-1 enzyme can be considered the ultimate example of enzyme promiscuity. It shows lack of specificity for substrate recognition, with exception of the β-lactam moiety, and can use multiple metal cofactors and switch catalytic mechanisms based on pH.

We believe that the cadmium structures represent the Michaelis complex for the reaction. A significant reorganization of the active site is observed in Figure 6.6, and the shorter Cd-Cd distance does not admit an oriented water molecule as was observed in the zinc liganded structures. We find the near-attack conformations from our simulations correspond closely with the observed crystal structures with cadmium. We believe that this lends credibility to the Michaelis complexes that we identified from our simulations in the zinc bound systems, where no crystal structures are available. Moreover, our simulations indicate that a proton shuttle pathway would encounter a high barrier when NDM-1 is liganded with Cd^{2+}, in agreement with our observation of partially hydrolyzed

ampicillin in the crystal structure, and the known much lower enzyme activities. From these results we would predict a significant isotopic effect for the reaction.

Development of inhibitors for the NDM-1 enzyme has proven challenging. A structure of NDM-1 in complex with L-captopril (IUPAC (2S)-1-[(2S)-2-methyl-3-sulfanylpropanoyl] pyrrolidine-2-carboxylic acid) has been reported recently[50]. In this structure, the sulfur atom binds between the two zinc ions, with the remainder of the molecule extending beyond the catalytic core of the active site. Our results suggest that other planar scaffolds that contain oxygen atoms to coordinate the zinc ions should also prove to be successful inhibitors.

MATERIALS AND METHODS

Protein cloning, expression, and purification

The Δ30 construct of the NDM-1 gene from *K. pneumoniae subsp. pneumoniae* MGH 78578 was cloned into the pMCSG7 vector using a modified LIC protocol as described by Kim et al[291]. This process generated an expression clone producing a fusion protein with an N-terminal His6 tag and a tobacco etch virus (TEV) protease recognition site. The expressed protein was purified using standard procedures on an ÄKTAxpress automated purification system (GE Healthcare Life Sciences, Piscataway, NY, USA) as described previously[292]. The concentration of the purified protein was determined utilizing an ND-1000 spectrophotometer system (NanoDrop Technologies, Wilmington, DE, USA). The fusion tag was then removed by adding recombinant TEV protease at a

ratio of ~1:75 (mg) and incubated for 48 h at 4°C. The cleaved protein was then separated using Ni-NTA affinity chromatography and the ÄKTAxpress system. The purified protein solution was dialyzed in a crystallization buffer [20 mM HEPES, pH 8.0; 250 mM NaCl; and 2 mM dithiothreitol (DTT)] and concentrated using an Amicon Ultra centrifugal filter device with a nominal molecular weight limit of 3000 (Millipore, Bedford, MA, USA).

Protein crystallization

The protein was crystallized using sitting-drop vapor diffusion at 16 and 4°C in 96-well CrystalQuick plates (Greiner Bio-One North America, Inc., Monroe, NC, USA). A 400-nl droplet of protein (40–80 mg/ml) was mixed with a 400-nl droplet of crystallization reagent and allowed to equilibrate over 135 µl of crystallization reagent. Nanopipetting was performed using the Mosquito nanoliter liquid handling system (TTP LabTech, Cambridge, MA, USA). Several commercially available crystallization screens were used, including MCSG-1–4 (Microlytic Inc. Burlington, MA, USA) and Index (Hampton Research, Aliso Viejo, CA, USA). The plates were then incubated at 16 and 4°C in a RoboIncubator automated plate storage system (Rigaku, The Woodlands, TX, USA). Automated crystal visualization was utilized in locating several crystals (CrystalTrak; Rigaku). The best crystals of the 30 construct protein preincubated with 80 mg/ml of ampicillin (Δ30-amp-Zn) appeared at 16°C under the conditions of 0.2 M ammonium sulfate, 0.1 M Bis-Tris (pH 5.5), and 25% PEG3350, which corresponds to condition A6 from the MCSG-1 screen. The 30 protein preincubated with 80

mg/ml of faropenem and mixed with 10 mM cadmium chloride (Δ30-far-Cd) was crystallized in the same conditions, except for an additional 5 mM $CdCl_2$. The 30, ampicillin, manganese (Δ30-amp-Mn) crystals were produced from the MCSG-1 screen condition H11, containing 0.2 M sodium chloride, 0.1 M HEPES (pH 7.5), and 25% (w/v) PEG3350, plus 5 mM $MnCl_2$. The co-crystals of Δ30, ampicillin, and cadmium (Δ30-amp-Cd) were obtained from the MCSG-1screen condition B11, containing 0.2 M lithium sulfate, 0.1 M Bis-Tris-HCl (pH 6.5), and 25% (w/v) PEG3350, plus 10 mM $CdCl_2$. These crystals were cryoprotected and flash-cooled in liquid nitrogen before they were analyzed in the synchrotron X-ray beam at the Structural Biology Center (SBC), sector 19-ID at the Advanced Photon Source (APS; Argonne National Laboratory). The proteins with ampicillin and zinc, manganese, or cadmium were crystallized in the same space group ($P2_12_12_1$) with similar cell dimensions of a = 39.1–39.2, b = 78.6 –79.2, c = 133.7–134.5 Å, although they were grown under two different conditions. However, Δ30-far-Cd crystallized in a different space group (C2) with cell dimensions of a = 145.63, b = 39.32, c = 75.37 Å and $\gamma = 99.96°$.

Data collection

All diffraction data were collected at 100 K at the 19-ID beamline of the SBC at the APS, using the ADSC Q315r detector. The high-resolution data to 1.05 Å resolution for the co-crystal of Δ30-amp-Zn were collected at 0.5166 Å with the detector distance of 200 mm from a rectangular crystal (0.1 x 0.06 x 0.03 mm) by exposing for 20 s/frame of 1.0° rotation on over 150° in 2 wedges (100 and 50°) from 2 different places of the

same crystal. For the Δ30-amp-Mn crystal, the data at 0.9793 to 1.5 Å were collected from a single protein crystal (0.10 x 0.04 x 0.05 mm). The crystal was exposed for 3 s/1.0° rotation of ω with a crystal-to-detector distance of 280 mm. The data were obtained by scanning 160° on ω. The Δ30-far-Cd and Δ30-amp-Cd data were collected similarly at 0.9793 Å by exposing a crystal for 3 s/1.0° rotation frame over 200° on ω up to 2.5 Å for Δ30-far-Cd and by exposing a crystal for 3 s/1.0° rotation frame over 170° on ω for Δ30-amp-Cd. The detailed data collection statistics are shown in Appendix Table A5.

Structure determination and refinement

All structures were determined by molecular replacement using HKL-3000 (23), and Molrep with the Protein Data Bank identification (PDB ID) 3Q6X structure as a search model. Iterative manual adjustment using Coot[293] and phenix.refine[156] refinement made the models converge to the final Rwork and Rfree values of 14.7 and 16.8%, respectively, for Δ30-amp-Mn; 20.4 and 25.1% for Δ30-far-Cd; 12.7 and 16.7% for Δ30-amp-Cd; and 13.3 and 15.7% for the 1.05 Å 30-amp-Zn (Appendix Table A5). In the Δ30-amp-Zn structure, 2 zinc ions were found in the active site, although no additional zinc was included during purification and crystallization. The presence of Zn, Mn, and Cd ions was confirmed by the residual anomalous difference electron density map, metal-metal distances, metal-N (or O) distances, and/or fluorescence emission spectra (Zn Kα1, 8.6 keV; Mn Kα1, 5.9 keV; Cd Kα1, 4.0 keV).

Validation and deposition

The stereochemistry of the structures was checked with PROCHECK [294] and a Ramachandran plot. The main-chain torsion angles for nearly all residues are in allowed regions: for Δ30-amp-Zn, 98.7% of all residues in favored region with 1 outlier; for Δ30-amp-Mn, 98.7% with 2 outliers; for Δ30-amp-Cd, 98.9% with 3 outliers; for Δ30-far-Cd, 97.6% with 3 outliers.

Molecular dynamics

Molecular dynamics simulations were performed with the code NAMD[295], developed by the Theoretical and Computational Biophysics Group at the Beckman Institute for Advanced Science and Technology (University of Illinois at Urbana-Champaign, Urbana-Champaign, IL, USA). The CHARMM 27 force field[296] parameters were used. Parameters for the ampicillin and imipenem substrates were developed using the standard methodology. Analysis of dynamics trajectories and preparation of figures was conducted with the program VMD[297]. Initial coordinates for protein atoms were obtained from the crystal structures. Missing atom coordinates (hydrogens) were defined with the PSFGEN module of VMD, which was also used to solvate the protein and neutralize the total charge of the simulation model. The solvation box was extended for 10 Å beyond the protein. With a 12-Å cutoff for electrostatic interactions, the box dimensions ensured a "diffuse" simulation model, in which no protein atoms interacted directly with protein atoms in the periodic images. Electrostatic interactions were computed using a smooth particle-mesh Ewald method[298], with a grid size of ~1-Å

spacing. Simulations began with a small amount of minimization (1000 steps) and then utilized typically 100,000 steps of NVT dynamics and 100,000 steps of NPT dynamics run with 1-fs time steps to equilibrate the system. Constant temperature was maintained by a Langevin method[299], and constant pressure conditions were enforced through a modified version of the Langevin piston[300]and Hoover[301,302] methods. Typical production runs were of 10 ns duration and were conducted using NPT dynamics with 2-fs time steps, recording coordinate information at 1-ps intervals. Simulations were conducted for the dimeric conformation of the protein, as observed in the crystal structure. There were ~50,000 atoms in the simulations, in a box of nominal dimensions, 65 x 68 x 102 Å.

QM/MM studies

To study energetics along the proposed reaction pathway, we performed QM/MM calculations with the program NWChem[303]. We utilized a nudged elastic band (NEB) method[286] implemented recently. Initial coordinates for reactant states were taken from snapshots of the dynamics trajectories in which the attacking water molecule was positioned in what we would describe as a near attack conformation[285]. The quantum partitions for all simulations included the side chains of residues His120, His122, Asp124, His189, Cys208, and His250. Also treated quantum mechanically were the penem moiety of the imipenem substrate (excluding the R1and R2 substituents), the zinc or cadmium ions, the attacking water, and additional waters that were coordinated to the zinc or cadmium ions. Atoms beyond 15 Å from the target carbon atom of the

substrate were frozen in place, and only atoms within that spherical region were allowed to move. The reactant state was defined by optimizing the original model using the density functional method B3LYP[304] and a 6–31 + + G** basis set for all atoms except zinc and cadmium and a 6–31G**(2s,2f) basis set for the zinc ions and a def2-tzvp basis set for the cadmium ions. The def2 basis set includes an effective core potential (ECP) for 28 electrons. An initial estimate of the reaction pathway was constructed by optimizing intermediate structures subject to constraints. For example, the distance between the water molecule oxygen atom and the substrate carbonyl carbon atom would be systematically reduced from its original value of ~3 Å to a final value of 1.4 Å. The product-state geometry was then obtained by removing all constraints and reoptimizing the geometry, starting from the last step along the pathway. The pathways produced utilized between 10 and 15 intermediate structures to represent the initial pathway guess. The initial pathways were subjected to further NEB optimizations to define an optimal QM pathway. Free energy calculations were then conducted for some pathways, using the (static) reference geometries of the QM partition atoms and allowing the MM partition atoms to move dynamically. Typical simulations utilized 30 ps of dynamics, and the free energy values reported represent the average values obtained by neglecting the initial (equilibration) 10 ps of the trajectories. Trajectories were examined visually for stability and s.d. of all results were < 2 kJ/mol.

Enzymatic studies

pH dependence of NDM-1 activity was assayed at 25°C in a reaction buffer

containing 50 mM Bis-Tris (pH 5.5, 6.5, 7.5) or 50 mM Tris (pH 8.5), 100 mM NaCl, and 50 μM $ZnCl_2$, varying concentrations of CENTA substrate (EMD Biosciences, San Diego, CA, USA), and 2 nM NDM-1. Steady-state hydrolysis of the β-lactam ring by NDM-1 was monitored by increase in max: 405 nm during the linear portion of the reaction initial velocity. The extinction coefficient of CENTA was experimentally determined (ε=1767 M^{-1} cm^{-1}). The rate of spontaneous hydrolysis of the β-lactam ring was determined in absence of enzyme at each pH and was subtracted from the initial velocities determined with NDM-1. Metal dependence of NDM-1 activity was assayed at 25°C using ampicillin as a substrate in reaction buffer containing 50 mM Tris (pH 6.5), 100 mM NaCl, and varying concentrations of $ZnCl_2$ and $CdCl_2$. Hydrolysis of the β-lactam ring by NDM-1 was monitored by decrease of the lactam chromophore max: 235 nm (ε = 900 M^{-1} cm^{-1}) during the linear portion of the reaction initial velocity. Kinetic parameters were determined by plotting the initial velocities against substrate concentration and curve fitting with the Michaelis-Menten equation using KaleidaGraph 4.0 (Synergy Software, Reading, PA, USA).

CHAPTER VII

CONCLUSION AND FUTURE DIRECTIONS

β-lactams have received a great deal attention with respect to their potential to be used for TB treatment[69,70,97,98,101,102,144]. Carbapenems are very effective β-lactam antibiotics because of their inhibitor activity against serine β-lactamases[99], which allows them to be used against otherwise β-lactam resistant bacteria. The primary mechanism of *Mtb* resistance β-lactam antibiotics is the extended spectrum β-lactamase BlaC[96,305]. Inhibition of BlaC by carbapenems and clavulanate is sufficient to re-sensitize *Mtb* to β-lactams[98]. However, these molecules are β-lactams that are hydrolyzed by BlaC. Unfortunately, the inhibitory activity is only transient[69,70]. Once they become hydrolyzed by BlaC, they are permanently inactivated, and can no longer function to inhibit their cell wall biosynthetic PBP targets or BlaC.

Ideally, a β-lactam could selectively inhibit the cell wall PBP targets and not bind to BlaC. However, BlaC is evolutionally related to the cell wall PBPs, so they can naturally bind similar molecules. Therefore, the similarity of BlaC to PBP targets precludes designing a target selective β-lactam. To identify target selective β-lactams, the antibacterial activities of β-lactam antibiotics on *Mtb* cells in presence and absence of active BlaC enzyme was compared to quantify the contribution of BlaC to *Mtb* resistance to these β-lactams. As expected, the antibiotic activities of carbapenems are less affected by the presence of BlaC than other β-lactams that are rapidly hydrolyzed by

BlaC. Interestingly, faropenem (a penem) was less affected by the presence of BlaC than the carbapenems. The structure activity relationship of BlaC with multiple β-lactams provided insight into faropenem's ability to evade BlaC structure activity relationship more than other β-lactams, and reveals desirable structural features for the future design of target selective β-lactams with reduced binding to BlaC.

Faropenem, biapenem, and tebipenem were biochemically and biophysically characterized with BlaC. Inhibition kinetics demonstrated that faropenem has less affinity for BlaC than structurally similar carbapenems: biapenem and tebipenem. Mass spectrometry demonstrated that faropenem formed a transient acyl-intermediate complex with BlaC, as did biapenem, tebipenem, and other carbapenems[98,144]. This result is unique because the BlaC-faropenem complex was less stable than biapenem and tebipenem. These results showed that faropenem's ability to evade BlaC more than other β-lactams is due to having a weaker affinity for the enzyme. The acyl-intermediate crystal structures of BlaC with faropenem, biapenem, and tebipenem elucidated the intermolecular interactions that are responsible for binding to BlaC and for the stability of the acyl-intermediates. The defining feature that likely distinguishes tighter binding carbapenems, biapenem and tebipenem, from faropenem is hydrophobic interaction with the side chain of Ile105 that borders the active site upon binding. Biapenem and tebipenem have R2 methyl groups that mediate this contact. The R2 methyl group is absent in faropenem, preventing hydrophobic interaction between faropenem and Ile105, which decreases the affinity of faropenem for the BlaC active site. This ultimately yields a measurable decrease in β-lactamase mediated resistance of *Mtb* to faropenem relative

to other β-lactams. This feature can be exploited in future efforts to rationally design selectivity into novel β-lactams to evade BlaC mediated resistance while maintaining potent activity against *Mtb*. The importance of the hydrophobic patch created by Ile105 in ligand binding to BlaC is further demonstrated by the structure activity relationship between BlaC and boronic acid inhibitors.

In addition to using structure-based design to improve the activities of β-lactams for use against tuberculosis, BlaC inhibitors are of particular interest. The FDA approved β-lactamase inhibitor clavulanic acid potentiates the activities of β-lactams by inhibiting BlaC[69,98]. However, clavulanic acid is inactivated by BlaC and the β-lactamase activity is eventually restored[70]. More stable inhibitors of BlaC are a topic of current investigation[70]. In addition, the low micromolar affinity of clavulanic acid for BlaC is modest compared to recently designed boronic acids for class C β-lactamase AmpC, which have reached subnanomolar binding constants and are effective *in vivo*[81-84]. Designing a more potent and stable BlaC inhibitor may improve β-lactam activity against *Mtb*.

Benzoxaboroles are a relatively new class of β-lactamase inhibitor that have demonstrated activity against class A and class C β-lactamases[85] including TEM-1, CMY-2-, KPC-2, and AmpC P99. They function by forming reversible covalent bonds with the active site serine[81-84], and are stable to β-lactamase hydrolysis unlike β-lactam-based inhibitors. Only enzymatic data has been reported for optimization of the benzoxaborole scaffold as β-lactamase inhibitors; therefore, structural data for benzoxaboroles is of great interest for rational design. To gain insight into the binding

and inhibition of benzoxaboroles with BlaC, a boronic acid inhibitor library from Anacor Pharmaceuticals was enzymatically screened, which revealed that the benzoxaborole scaffold also inhibits BlaC. To identify structural features of the BlaC active site that can be exploited for inhibitor design, we generated a structure activity relationship with derivative benzoxaboroles and BlaC. Co-crystal structures of BlaC with derivative benzoxaborole inhibitors provided insight into the inhibition of β-lactamases by benzoxaboroles by revealing key intermolecular interactions that govern binding to the active site. The structure activity relationship enabled us to visualize how specific modifications to the benzoxaborole scaffold either increased or decreased the potency of BlaC inhibition, and provided a platform for the design of improved BlaC inhibitors.

Three locations on the benzoxaborole scaffold were chemically modified to probe for BlaC inhibition. A carboxymethyl group at the 3' position was determined to be indispensable for tight binding and inhibition. Electrostatic surface potential maps of BlaC generated from the co-crystal structures show that the carboxylate binds in a positively charged region of the active site (next to the oxyanion hole), which is the same location that the carboxylate group of substrate β-lactams binds[98,144]. In this manner, the 3' carboxylate seems to mimic β-lactam substrates. The 4' position of the benzoxaborole tolerated small and large modifications without drastically affecting the binding or inhibition of BlaC because the 4' position mostly faces open solvent. However, the general trend of the enzymatic data shows that more hydrophobic modifications at this position increase potency. Examination of the crystal structures showed that the nearby hydrophobic side chain of Ile105 is responsible for the

preference for hydrophobic groups. This observation lends credence to the previous observation that substrates biapenem and tebipenem bind tighter to BlaC than faropenem by hydrophobically interacting with Ile 105 upon binding. Substitutions made to the benzoxaborole 6' position reached into the distal cavity of the BlaC active site bordered by the substrate specificity loop. Each of the 6' modifications interacted with the backbone amide nitrogen of Ile105 either directly or through a solvent bridge, which further confirms the importance of Ile105 in ligand recognition by BlaC. The other contacts made by 6' derivative benzoxaboroles were hydrogen bonds with the side chain of Asp240.

From this investigation, it seems that the best place to probe for additional potent modifications to the benzoxaborole scaffold resides with the 6' position, which is proximal to the BlaC substrate specificity loop in crystal structures. Importantly, hydrogen bonding donors and acceptors stem from the side chains of residues in the substrate specificity loop (Asn170, Glu166). Asn170 and Glu166 are conserved because of their role in binding β-lactam substrates like amoxicillin and their essential role in catalysis. Theoretically, these residues, especially Glu166, will be less tolerant to mutations because they would decrease activity of BlaC. Therefore, a logical strategy for inhibitor design would be to make additional interactions with Glu166. The effectiveness of this strategy is exemplified by the interruption of catalysis by carbapenems[69,99,144]. Although, the inhibitors characterized in this investigation did not bind directly to these residues, the crystal structures illustrate the potential for modifications at the 6' benzoxaborole position that would facilitate hydrogen bonding to the substrate

specificity loop, and increase potency for BlaC inhibition. In addition, further characterization of the inhibitory activity of benzoxaboroles with modifications at the 5' and 7' positions remain to be investigated.

According to the W.H.O., rapid spreading of drug resistant tuberculosis infections across the globe particularly in resource limited environments in South Africa, India, and southeast Asia demands the development of newer and more rapid diagnostic strategies to reduce transmission and decrease mortality. One of the main hurdles to detecting tuberculosis is the slow growth rate of the pathogen, which prevents rapid detection because of the long time required to culture the bacilli. Furthermore, the conventional methods of detection including smear microscopy, skin tests and chest x-rays are not sensitive or conclusive enough to diagnose tuberculosis infection[105,106,188]. Newer nucleic acid-based and fluorescence based techniques are improving the sensitivity and specificity of detection[170,181,306]. Amplification of signal is ideal for detecting very small concentrations of pathogen, which offers a distinct advantage for the early detection of tuberculosis. The fact that BlaC is a constitutively expressed and secreted enzyme facilitates detection of the *Mtb in vitro* and *in vivo* through the use of β-lactam fluorogenic probes[103,181] .

The challenge that is posed by using β-lactam-based probes is the possibility for false positives due to normal flora or other pathogens that infect the respiratory tract and secrete β-lactamases. This challenge can be met by increasing the specificity of β-lactam probes for BlaC relative to other similar class A β-lactamases. The TEM family of β-lactamases is the most prevalent plasmid encoded family of β-lactamases found in the

clinic[57], and the active site is nearly identical to BlaC[97]. Therefore, TEM-1 was selected as a model enzyme for comparison of probe specificity relative to BlaC. The cephalosporin β-lactam was selected for probe design because of its ability to release a fluorescent leaving group upon hydrolysis by β-lactamase. The cephalosporin scaffold was modified at the side chain of the 7' amino group (R1) or at the 7' position of the β-lactam ring. BlaC is known for its large active site relative to other class A β-lactamases[97]. In order to see if extension of the R1 side chain would confer specificity of the probes for BlaC relative to TEM, modifications made to the R1 position increased in size from methyl to benzyl and then to the extended side chain of cefoperazone[103]. This resulted in probes that were hydrolyzed by both β-lactamases and exhibited slightly more selectivity for the TEM-1 enzyme because of increased turnover relative to BlaC. However, selectivity of the probes for BlaC was generated by modification of the 7' position of the β-lactam ring with methoxy and ethoxy groups. BlaC and TEM were able to hydrolyze the 7'-methoxy modified probe. Addition of the larger ethoxy group decreased turnover for BlaC by 100 fold, but abolished turnover by TEM-1. The 7'-methoxy probe (CDC-OMe) exhibited over 3 orders of magnitude selectivity for BlaC ($kcat$/Km = 2.1×10^4 s^{-1} M^{-1}) over TEM-1 ($kcat/K_m$ = 16 s^{-1} M^{-1}). These observations show that increasing the size of the modification at the 7'-postion of the β-lactam ring is sufficient to generate selectivity of fluorogenic probes for BlaC over the very similar TEM-1 enzyme[103].

To identify the structural basis behind the observed selectivity of CDC-OMe for BlaC over TEM-1, acyl-intermediate crystal structures of BlaC were solved with the

selective probe CDC-OMe and the non-selective probe CDC-1[103]. The crystal structures showed probes bound in the same orientation as substrates, forming conserved interactions with substrate recognition residues. Superimposition of these structures with the TEM-1 crystal structure showed that the main structural difference between the BlaC active site and the TEM-1 active site was the flexible nature of the BlaC substrate specificity loop relative to TEM-1[97,186]. BlaC and TEM-1 share 3 conserved salt bridges that serve to stabilize the conformation of the substrate specificity loops for catalysis. The R164 side chain increases the rigidity of the TEM-1 substrate specificity loop relative to BlaC by making 3 additional salt bridges. This residue is A164 in BlaC, which increases the flexibility of BlaC substrate specificity loop allowing it to expand the active site and facilitate Glu166 to adopt a catalytically competent conformation for reaction completion. The structural basis for decreased turnover of 7'-methoxy substituted fluorogenic probes by BlaC and TEM-1 was revealed by the acyl-intermediate crystal structure of BlaC with CDC-OMe. The structure showed that the 7'-methoxy group was positioned directly in the path of catalytic base Glu166, preventing hydrolytic water coordination for hydrolysis. This observation supports the hypothesis that the flexibility of BlaC substrate specificity loop relative to TEM-1 facilitates selectivity for BlaC by allowing Glu166 to sample more conformations for reaction completion[103].

The selectivity of CDC-OMe was further demonstrated with whole *E. coli* cells expressing either TEM-1 or BlaC. Further optimization of the fluorescent leaving group led to an additional >10 fold increase in specificity for BlaC, resulting in greater than

four orders of magnitude selectivity for BlaC over TEM *in vitro*[103]. The sensitivity and specificity of the final probe was also demonstrated with raw unprocessed human sputum that contained *Mtb* var. *bovis* BCG or other β-lactamase producing bacteria including *E. coli*, *P. aeruginosa*, *M. smegmatis*, and *S. aureus*. The final probe was able to detect down to 10 mycobacteria in 200 μL of human sputum. Furthermore, there are still positions of the β-lactam probe scaffold that have yet to be chemically explored, which offers possibility for design of even more specific and selective biosensors for a rapid and cost effective method for early tuberculosis detection[103].

The recent discovery and rapid dissemination of the New Delhi Metallo-β-lactamase (NDM-1) foreshadows a future where β-lactam antibiotics are no longer effective against pathogenic bacteria[107,133,194,277]. The NDM-1 gene isolated from a patient carrying *K. pneumonia* was characterized by susceptibility testing with β-lactam antibiotics. NDM-1 carrying *E. coli* and *K. pneumonia* displayed extended spectrum resistance to β-lactam antibiotics including several cephalosporins and carbapenems. In order to understand the contribution of NDM-1 to the observed extended spectrum antibiotic resistance due to NDM-1, the truncated NDM-1 enzyme lacking the N-terminal signal peptide was over-expressed in non-pathogenic *E. coli* and purified to homogeneity[108,279]. Biochemical characterization of purified NDM-1 *in vitro* revealed that NDM-1 is a potent MBL enzyme with a very broad and non-specific substrate profile. Furthermore, it has the ability to non-discriminately bind and hydrolyze cephalosporin, cephamycin, and carbapenem and penem classes of β-lactams[108,279].

To identify the mechanism of NDM-1 promiscuity in substrate recognition and hydrolysis, the crystal structure of NDM-1 was solved in apo, monometalated [108] and dimetalated forms. About the same time, several other investigators published the structure of NDM-1 with slightly different N-terminal truncations in dimetalated forms, and with the hydrolyzed β-lactam substrate ampicillin[46,47,49]. Comparison of the apo, monometalated, dimetalated NDM-1 revealed the structural plasticity of five active site loops, and the preserved fold in absence or presence of cofactors[108]. The two zinc co-factors are coordinated via two catalytic triads (His, His, His / His, Asp, Cys); the triad residues are donated from five flexible active site loops. The HHH triad is the higher affinity site, which is evident by its presence in the three monometalated NDM-1 structures[108] and consistency with other structurally characterized MBLs[126]. Binding of the second zinc co-factor orders the second catalytic HDC triad by pulling the residues into closer proximity, and stabilizes the active site in a catalytically competent conformation for substrate recognition and hydrolysis[108,236]. The most important structural feature of NDM-1 that contributes to promiscuous substrate recognition and hydrolysis is the enlarged active site formed by the five flexible active site loops. The enlarged active site is partially due to insertions in the active site loops, and substitution of the large hydrophobic residues in other MBL active sites with alanines in NDM-1. These features allow for decreased rigidity of the active site loops and increased volume of the NDM-1 active site, facilitating the acceptance of structurally diverse substrates[108]. The crystal structures of NDM-1 with hydrolyzed substrates showed that the substrate R groups extended into the open cavities of the active site, and the oxygen atoms of the β-

lactam carbonyl and carboxylate moieties were recognized by the zinc co-factors[47,52,236]. Active site loop 1 has the most conformational variability, and is flexed outward to expand the active site cavity when liganded[46,48,52]. The hydrophobic surface area formed by active site loop 1 is hypothesized to non-specifically recognize substrates for hydrolysis[46,50,52].

The MBL mechanism is generally accepted to function through assisted catalysis from zinc co-factor(s) that activate an ordered solvent molecule for nucleophilic attack of the lactam, and the specific details of the reaction mechanism have been the subject of investigation[45,127]. The catalytic base is important to note. It has been suggested that the conserved aspartate in the second zinc binding site serves as the catalytic base, but mutational studies confirmed that this residue is not absolutely essential for catalysis[128,129]. Spectroscopic studies of the NDM-1 reaction show three reactions species that were hypothesized to represent substrate, ring-opened intermediate, and product[51]. Protonation of the ring-opened lactam nitrogen is required for product formation, but the exact origin of the proton is still at question. In addition, no data suggests whether or not the ordered solvent molecule coordinated by the zinc co-factor(s) is a water molecule or hydroxide ion.

To gain insight into the pH dependence of the reaction mechanism of NDM-1, the activity of NDM-1 at pH ranging from 5.5-8.5 was examined. NDM-1 was approximately 5-fold more catalytically active at higher pH[52]. The ability of NDM-1 to function in acidic and basic environments suggests that the zinc-ordered catalytic solvent molecule is a hydroxide ion at high pH and a water molecule at low pH. Molecular

dynamics simulations predicted that the NDM-1 zinc-zinc distance is theoretically 5.6 Å, when an ordered water molecule is bound and 3.6 Å when an ordered hydroxide ion is bound[52]. Consistent with the biochemical and computational data, examination of the available structural data for NDM-1 showed that the variation in the distance between the zinc co-factors was pH dependent[46,47,49,50,52,108]. In general, greater zinc-zinc distances were observed in low pH conditions, consistent with an ordered water molecule, and shorter zinc-zinc distances at higher pH, consistent with an ordered hydroxide. In the high resolution (1.05 Å) crystal structure of NDM-1 solved at pH 6.5, the zinc-zinc distance was 4.6 Å, suggesting partial occupancy by a hydroxide ion and water molecule[52]. In another study, data collected at pH 7.6 suggested a 3.38 Å zinc-zinc distance, consistent with an ordered hydroxide. In summary, these observations suggested that the NDM-1 reaction mechanism can proceed with a zinc ordered water or hydroxide, in a pH dependent manner[52].

Metal dependence studies showed that NDM-1 was almost completely inactivated when the zinc co-factor was replaced by cadmium, which enabled structure determination of NDM-1 with unhydrolyzed and partially hydrolyzed ampicillin. Zinc liganded structures of NDM-1 with ampicillin only yielded hydrolyzed product[52]. To gain further insight into the NDM-1 reaction mechanism, computational studies were conducted using the aforementioned substrate-liganded NDM-1 structures as starting points[52]. The simulations estimated the energy along the reaction coordinate of NDM-1 reaction using the previously proposed model that uses active site aspartate as the general base, and investigated other potential mechanisms where the coordinated solvent

(water or hydroxide) serves as the catalytic base. These simulations revealed that the most energetically favorable NDM-1 reaction mechanism used the zinc ordered solvent molecule (hydroxide at high pH, or water at low pH) as the catalytic base to activate a water molecule from bulk solvent for attack of the β-lactam ring. Subsequent to ring opening, the lactam nitrogen is protonated by translocation through a bulk solvent mediated proton shuttle[52]. Cumulatively, the biochemical, biophysical, and computational data support that NDM-1 is a promiscuous MBL due to its expanded active site cavity that enables it to indiscriminately bind structurally diverse substrates through recognition of the β-lactam core by zinc co-factors and hydrolyze them with a pH-dependent proton shuttle based mechanism.

From the BlaC studies, we see that single interactions or active site features are able to distinguish rapidly and poorly hydrolyzed β-lactam substrates, increase the affinity of β-lactamase inhibitors, or enhance the selectivity of β-lactam based fluorogenic probes, while the majority of the interactions involved in ligand recognition remain the same. This implies that resistance to inhibitors, expanded enzymatic activity, or loss of probe selectivity can easily arise from single point mutations, and that future design efforts should target interactions with residues that will be less likely to tolerate mutations.

On the other hand, NDM-1 retains promiscuous enzymatic activity primarily through recognition of the core of β-lactam substrates, and a lack of specific interactions that confer substrate specificity. The mechanistic details of the NDM-1 reaction described in this record of study will aid in the future design of specific NDM-1

inhibitors. Inhibitors will likely be non-specifically recognized by the catalytic zinc co-factors as are many existing MBL inhibitors[61]. Additional specificity and potency will have to be rationally designed by making additional interactions with the hydrophobic pocket formed by active site loop 1, or other hydrogen bonding residues that extend along the active site cavity of NDM-1. These inhibitor structure activity relationship studies are underway.

REFERENCES

(1) Fleming, A. *Br. J. Exp. Pathol.* **1929**, *10*, 226.

(2) Diggins, F. W. *Br. J. Biomed. Sci* .**1999**, *56*, 83.

(3) Abraham, E., Chain, E., Fletcher, C. M., Gardner, A. D., Keatley, N. G., Jennings, M. A. and Florey, H. W. *The Lancet* **1941**, *238*, 177

(4) Khardori, N. *Med. Clin. N. Am.* **2006**, *90*, 1049.

(5) Elander, R. P. *Appl. Microbiol. Biotechnol.* **2003**, *61*, 385.

(6) Strominger, J., Willoughby, E., Kamiryo, T., Blumberg, P. and Yocum, R. *Ann. NY. Acad. Sci.* **1974**, *235*, 210.

(7) Blumberg, P. M., Strominger, J. L. *Bacteriol. Rev*. **1974**, *38*, 291.

(8) Tomasz, A. *Ann. Rev. Microbiol.* **1979**, *33*, 113.

(9) Gardner, A. D. *Nature* **1940**, *146*, 837.

(10) Park, J. T., Strominger, J. L. *Science* **1957**, *125*, 99.

(11) Strominger, J. L., Park, J. T., Thompson, R. E. *J. Biol. Chem.* **1959**, *234*, 3263.

(12) Spratt, B. G. *Proc. Natl. Acad. Sci.* **1975**, *72*, 2999.

(13) Wise, E. M., Park, J. T. *Proc. Natl. Acad. Sci.* **1965**, *54*, 75.

(14) Tipper, D. J., Strominger, J. L. *Proc. Natl. Acad. Sci.* **1965**, *54*, 1133.

(15) Izaki, K., Matsuhashi, M., Srtominger, J. L. *Proc. Natl. Acad. Sci.* **1966**, *55*, 656.

(16) Jamin, M., Wilkin, J. M., Frère, J. M. *Essays Biochem.* **1995**, *29*, 1.

(17) Holten, K., Onusko, E. M. *Am. Fam. Physician* **2000**, *62*, 611.

(18) Chain, E., Florey, H. W., Adelaide, M. B., Gardner, A. D., Heatley, N. G., Jennings, M. A., Orr-Ewing, J., Sanders, A. G. *The Lancet* **1940**, *236*, 226.

(19) Hobby, G. L. *Science* **1944**, *100*, 500.

(20) Silhavy, T. J., Kahne, D., Walker, S. *Cold Spring Harb. Perspect. Biol.* **2010**, *2*, a000414.

(21) Chatterjee, D. *Curr. Opin. Chem. Biol.* **1997**, *1*, 579.

(22) Waxman, D. J., Strominger, J. L. *Annu. Rev. Biochem.* **1983**, *52*, 825.

(23) Casal, M., Rodriguez, F., Benavente, M., Luna, M. *Eur. J. Clin. Microbiol.* **1986**, *5*, 453.

(24) Giamarellou, H. *Am. J. Med.* **1986**, *80*, 126.

(25) Mainardi, J. L., Legrand, R., Arthur, M., Schoot, B., van Heijenoort, J., Gutmann, L. *J. Biol. Chem.* **2000**, *275*, 16490.

(26) Wietzerbin, J., Das, B. C., Petit, J. F., Lederer, E.; Leyh-Bouille, M., Ghuysen, J. M. *Biochemistry-Us* **1974**, *13*, 3471.

(27) Flores, A. R.; Parsons, L. M.; Pavelka, M. S., Jr. *J. Bacteriol.* **2005**, *187*, 1892.

(28) Lavollay, M., Arthur, M., Fourgeaud, M., Dubost, L., Marie, A., Veziris, N., Blanot, D., Gutmann, L., Mainardi, J. L. *J.Bacteriol.* **2008**, *190*, 4360.

(29) Ghuysen, J. M. *Ann. Rev. Microbiol.* **1991**, *45*, 37.

(30) Massova, I., Mobashery, S. *Antimicrob. Agents Chemother.* **1998**, *42*, 1.

(31) Medeiros, A. A. *Clin. Infect. Dis.* **1997**, *24*, S19.

(32) Ambler, R. P. *Phil. Trans. R. Soc. Lond.* **1980**, *B 289*, 321.

(33) Bush, K., Jacoby, G. A., Medeiros, A. A. *Antimicrob. Agents Chemother.* **1995**, *39*, 1211.

(34) Bush, K., Jacoby, G. A. *Antimicrob. Agents Chemother.* **2010**, *54*, 969.

(35) Jacoby, G. A. *Antimicrob. Agents Chemother.* **2006**, *50*, 1123.

(36) Lamotte-Brasseur, J., Knox, J., Kelly, J. A., Charlier, P., Fonzé, E., Dideberg, O., Frére, J. M. *Biotechnol. Genet. Eng. Rev.* **1994**, *12*, 189.

(37) Page, M., Badarau, A. *Bioinorganic Chemistry and Applications* **2008**, *576297*, 1.

(38) Bebrone, C. *Biochem. Pharmacol.* **2007**, *74*, 1686.

(39) Bulychev, A., Massova, I., Miyashita, K., Mobashery, S. *J. Amer. Chem. Soc.* **1997**, *119*, 7619.

(40) Golemi, D., Maveyraud, L., Vakulenko, S., Samama, J. P., Mobashery, S. *Proc. Natl. Acad. Sci.* **2001**, *98*, 14280.

(41) Adachi, H., Ohta, T., Matsuzawa, H. *J. Biol. Chem.* **1991**, *266*, 3186.

(42) Escobar, W. A., Tan, A. K., Fink, A. L. *Biochemistry* **1991**, *30*, 10783.

(43) Strynadka, N. C., Adachi, H., Jensen, S. E., Johns, K., Sielecki, A., Betzel, C., Sutoh, K., James, M. *Nature* **1992**, *359*.

(44) Golemi, D., Maveyraud, L., Vakulenko, S., Tranier, S., Ishiwata, A., Kotra, L. P., Samama, J., Mobashery, S. *J. Am. Chem. Soc.* **2000**, *122*, 6132.

(45) Simona, F., Magistrato, A., Dal Peraro, M., Cavalli, A., Vila, A. J., and Carloni, P. *J. Biol. Chem.* **2009**, *284*, 28164.

(46) Zhang, H.-M., and Hao, Q. *FASEB J.* **2011**, *25*, 2574.

(47) King, D., and Strynadka, N. *Prot. Sci.* **2011**, *20*, 1484.

(48) Kim, Y., Tesar, C., Mire, J., Jedrzejczak, R., Binkowski, A., Babnigg, G., Sacchettini, J., and Joachimiak, A. *PLoS ONE* **2011**, *6*, e24621.

(49) Green, V. L., Verma, A., Owens, R. J., Phillips, S. E. V., and Carr, S. B. *Acta Crystallogr.* **2011**, *F67*, 1160.

(50) King, D. T., Worrall, L. J., Gruninger, R., and Strynadka, N. C. J. *J. Am. Chem. Soc.* **2012**, *134*, 11362.

(51) Yang, H., Aitha, M., Hetrick, A. M., Richmond, T. K., Tierney, D. L., and Crowder, M. W. *Biochemistry* **2012**, *51*, 3839.

(52) Kim, Y., Cunningham, M.A., Mire, J. , Tesar, C., Sacchettini, J.C., Joachimiak, A. *FASEB J.* **2013**, *12*, 224014.

(53) Bush, K., Jacoby, G. A. *Antimicrob. Agents Chemother.* **2010**, *54*, 969.

(54) Petrosino, J., Cantu, C. III and Palzkill, T. *Trends Microbiol.* **1998**, *6*, 323.

(55) Watanabe, T., Fukasawa, T. *J. Bacteriol.* **1961**, *81*, 669.

(56) Giamarellou, H., Zissis, N., Tagari, G., and Bouzos, J. *Antimicrob. Agents Chemother.* **1984**, *25*, 534.

(57) Bush, K., Jacoby, G. A. *Antimicrob. Agents Chemother.* **2010**, *54*, 969.

(58) Watanabe, T. *Bacteriol. Rev.* **1963**, *27*, 87.

(59) Jain, A., Dixit, P. *J Biosci* **2008**, *33*, 605.

(60) Migliori, G. M., Richardson, M., Sotgiu, G., Lange, C. *Clin. Chest. Med.* **2009**, *30*, 637.

(61) Drawz, S. M., Bonomo, R.A *Clin. Microbiol. Rev.* **2010**, *23*, 160.

(62) Reading, C., Cole, M. *Antimicrob. Agents Chemother.* **1977**, *11*, 852.

(63) English, A. R., Retsema, J. A., Girard, A. E., Lynch, J. E., Barth, W. E. *Antimicrob. Agents. Chemother.* **1978**, *14*, 414.

(64) Fisher, J., Belasco, J. G., Charnas, R. L., Khosla, S., Knowles, J. R. *Philos. Trans. R. Soc. Lond. B Biol. Sci.* **1980**, *289*, 309.

(65) Brown, R. P., Aplin, R. T., Schofield, C. J. *Biochemistry* **1996**, *35*, 12421.

(66) Chen, C. C., Herzberg, O. *J. Mol. Biol.* **1992**, *224*, 1103.

(67) Padayatti, P. S., Helfand, M. S., Totir, M. A, Carey, M. P, Hujer, A. M, Carey, P. R.,Bonomo, R. A., van den Akker, F. *Biochemistry* **2004**, *43*, 843.

(68) Padayatti, P. S., Helfand, M. S., Totir, M. A, Carey, M. P, Carey, P. R., Bonomo, R. A., van den Akker, F. *J. Biol. Chem.* **2005**, *280*, 34900.

(69) Hugonnet, J. E. a. B., J. S. *Biochemistry* **2007**, *46*, 11998.

(70) Xu, H., Hazra, S., Blanchard, J. S. *Biochemistry* **2012**, *51*, 4551.

(71) Philipp, M., Bender, M. L. *Proc. Natl. Acad. Sci.* **1971**, *68*, 478.

(72) Koehlcr, K. A., Lienhardf, G. E. *Biochemistry* **1971**, *10*, 2477.

(73) Matthews, D. A., Alden, R. A., Birktoft, J., Freer, S. T., Kraut, J. *J. Biol. Chem.* **1975**, *250*, 7120.

(74) Kettner, C. A., Shenvi, A. B. *J. Biol. Chem.* **1984**, *259*, 15106.

(75) Adams, J., Behnke, M., Chen, S., Cruickshank, A., Dick, L. R., Grenier, L., Klunder, J. M., Ma, Y. T., Plamondon, L., Stein, R. L. *Bioorg. Med. Chem. Lett.* **1998**, *8*, 333.

(76) Lindquist, R. N., Terry, C. *Arch. Biochem. Biophys.* **1974**, *160*, 135.

(77) Bone, R., Shenvi, A. B., Kettner, C. A., Agard, D. A. *Biochemistry* **1987**, *26*, 7609.

(78) Kiener, P. A., Waley, S. G. *Biochem. J.* **1978**, *169*, 197.

(79) Beesley, T., Gascoyne, N., Knott-Hunziker, V., Petursson, S., Waley, S. G., Jaurin, B., Grundstrom, T *Biochem. J.* **1983**, *209*, 229.

(80) Strynadka, N. C., Martin, R., Jensen, S. E., Gold, M., Jones, J. B. *Nat. Struct. Biol.* **1996**, *3*, 688.

(81) Weston, S. G., Blazquez, J., Baquero, F. Shoichet, B. K. *J. Med. Chem.* **1998**, *41*, 4577.

(82) Morandi, S., Morandi, F., Caselli, E., Shoichet, B. K., Prati, F. *Bioorg. Med. Chem.* **2008**, *16*, 1195.

(83) Tondi, D., Calò, S., Shoichet, B. K., Costi, M. P. *Bioorg.Med. Chem. Lett.* **2010**, *20*, 3416.

(84) Eidama, O., Romagnolib, C., Dalmassoc, G., Bareliera, S., Casellib, E., Bonnet, R. Shoichet, B. K., Prati, F. *Proc. Natl. Acad. Sci.* **2012**, *109*, 17448.

(85) Xia, Y., Cao, K., Zhou, Y., Alley, M. K., Rock, F., Mohan, M., Meewan, M., Baker, S. J., Lux, S., Ding, C. Z., Jia, G., Kully, M., Plattner, J. B. *Bioorg. Med. Chem. Lett.* **2011**, *21*, 2533.

(86) Wyrembak, P., Babaoglu, K., Pelto, R. B., Shoichet, B. K., Pratt, R. F *J. Am. Chem. Soc.* **2007**, *129*, 9548.

(87) Pelto, R. B., Pratt, R. F. *Biochemistry* **2008**, *47*, 12037.

(88) Bonnefoy, A., Dupuis-Hamelin, C., Steier V., Delachaume, C., Seys, C., Stachyra, T., Fairley, M., Guitton, M., Lampilas, M. *J. Antimicrob. Chemother.* **2004**, *54*, 410.

(89) Stachyra, T., Pechereau, M., Bruneau, J., Miossec, C., Frere, J. M., Black, M. T. In *49th ICAAC* San Francisco, 2009.

(90) Stachyra, T., Pechereau, Petrella, S., Ziental-Gulusm, N., Sougakoff, W., Claudon, M., Black, M. T., Levasseur, P., Girard, A., Miossec, C. In *47th ICAAC* Chicago, IL, 2007.

(91) Docquier, J. D., Stachyra, T., Benvenuti, M., Rossolini, G. M., Mangani,S., Pechereau, M. C., Bruneau, J. M., Claudon, M., Barbosa, F., Miossec, C., Black, M. T. In *49th ICAAC* San Francisco, 2009.

(92) Levasseur, P., Girard, A., Lavallade, L., Miossec, C., Shales, D., Black, M. T., Pace, J., Coleman, K. In *49th ICAAC* San Francisco, 2009.

(93) Weiss, W. J., Pulse, M. E., Endimiani, A., Hujer, K. M., Hujer, A. M., Bonomo, R. A. In *49th ICAAC* San Francisco, 2009.

(94) *WHO/HTM/TB/2012.6* **2012** http://www.who.int/tb/publications/global_report/en/index.html.

(95) Ioerger, T. R., Feng, Y., Chen, X., Dobos, K. M., Victor, T. C., Streicher, E. M., Warren, R. M., Gey van Pittius, N. C., Van Helden, P. D., Sacchettini, J. C. *BMC Genomics* **2010**, *11*, 670.

(96) Flores, A. R., Parsons, L. M. and Pavelka, M. S. Jr. *Microbiology* **2005**, *151*, 521.

(97) Wang, F., Cassidy, C. and Sacchettini, J. C. *Antimicrob. Agents Chemother*. **2006**, *50*, 2762.

(98) Hugonnet, J. E., Tremblay, L.W., Boshoff, H. I., Barry, C. E. II, Blanchard, J. S. *Science* **2009**, *323*, 1215.

(99) Queenan, A. M., Shang, W., Flamm, R., Bush, K. *Antimicrob. Agents Chemother.* **2010**, *54*, 565.

(100) Tremblay, L. W., Fan, F. and Blanchard, J. S. *Biochemistry* **2010**, *49*, 3766.

(101) England, K., Boshoff, H., Arora, K., Weiner, D., Dayao, E., Schimel, D.,Via, L. E., Barry, C. E. *Antimicrob. Agents Chemother.* **2012**, *56*, 3384.

(102) Tremblay, L. W., Hugonnet, J. E., and Blanchard, J. S. *Biochemistry* **2008**, *47*, 5312.

(103) Xie, H., Mire, J., Kong, Y., Chang, M., Hassounah, H. A., Thornton, C., Sacchettini, J. C., Cirillo, J. D. and Rao, J. *Nat. Chem.* **2012**, *4*, 802.

(104) Chaturvedi, N., Cockcroft, A. *Occup. Med.* **1992**, *42*, 179.

(105) Pouchot, J., Grasland, A., Collet, C., Coste, J., Esdaile, J., Vinceneux, P. *Ann. Intern. Med.* **1997**, *126*, 210.

(106) Kumar, N., Bhargava, S. K., Agrawal, C. S., George, K., Karki, P., Baral, D. *J. Nepal. Med. Assoc.* **2005** *44*, 138.

(107) Walsh, T. R., Weeks, J., Livermore, D. M., and Toleman, M. A. *Lancet Infect. Dis.* **2011**, *11*, 334.

(108) Kim, Y., Tesar, C., Mire, J., Jedrzejczak, R., Binkowski, A., Babnigg, G., Sacchettini, J., Joachimiak, A. *PLoS One* **2011**, *6*, e24621.

(109) Yong, D., Toleman, M. A., Giske. C. G., Cho, H. S., Sundman, K., Lee, K., Walsh, T. R. *Antimicrob. Agents Chemother.* **2009**, *53*, 5046.

(110) Nordmann, P., Couard, J. P., Sansot, D., Poirel, L. *Clin. Infect. Dis.* **2012**, *54*, 150.

(111) Kumarasamy, K., Kalyanasundaram, A. *J. Antimicrob. Chemother.* **2012**, *67*, 243.

(112) Bogaerts, P., Rezende de Castro, R., Roisin, S., Deplano, A., Huang, T. D., Hallin, M., Denis, O., Glupczynski, Y. *J. Antimicrob. Chemother.* **2012**, *67*, 1552.

(113) Ho, P. L., Li, Z., Lai, E. L., Chiu, S. S., Cheng, V. C. *J. Antimicrob. Chemother.* **2012,** *67*, 1553.

(114) Pasteran, F., Albornoz, E., Faccone, D., Gomez, S., Valenzuela, C., Morales, M., Estrada, P., Valenzuela, L., Matheu, J., Guerriero, L., Arbizu, E., Calderon, Y., Ramon-Pardo, P., Corso, A. *J Antimicrob. Chemother.* **2012,** *67*, 1795.

(115) Brink, A. J., Coetzee, J., Clay, C. G., Sithole, S., Richards, G. A., Poirel, L., Nordmann, P. *J. Clin Microbiol.* **2012**, *50*, 525.

(116) Jamal, W., Rotimi, V. O., Albert, M. J., Khodakhast, F., Udo, E. E., Poirel, L. *Int. J. Antimicrob. Agents* **2012**, *39*, 183.

(117) Wilson, M. E.; Chen, L. H. *Curr. Infect. Dis. Rep.* **2012,** *14*, 213.

(118) Boulanger, A.; Naas, T.; Fortineau, N.; Figueiredo, S.; Nordmann, P. *Antimicrob. Agents Chemother.* **2012**, *56*, 2214.

(119) Khan, A. U., Nordmann, P. *J. Med. Microbiol.* **2012**, *61*, 454.

(120) Poirel, L.; Lascols, C.; Bernabeu, S.; Nordmann, P. *Antimicrob. Agents Chemother.* **2012**, *56*, 598.

(121) Poirel, L., Ozdamar, M., Ocampo-Sosa, A. A., Turkoglu, S., Ozer, U. G., Nordmann, P. *Antimicrob. Agents Chemother.* **2012**, *56*, 2784.

(122) Mazzariol, A., Bosnjak, Z., Ballarini, P., Budimir, A., Bedenic, B., Kalenic, S., Cornaglia, G. *Emerg. Infect. Dis.* **2012**, *18*, 532.

(123) Ghazawi, A., Sonnevend, A., Bonnin, R. A., Poirel, L., Nordmann, P., Hashmey, R., Rizvi, T. A., M, B. H., Pal, T. *Clin. Microbiol. Infect.* **2012**, *18*, E34.

(124) Nordmann, P.; Boulanger, A. E.; Poirel, L. *Antimicrob. Agents Chemother.* **2012**, *56*, 2184.

(125) Kim, M. N.; Yong, D.; An, D.; Chung, H. S.; Woo, J. H.; Lee, K.; Chong, Y. *J. Clin. Microbiol.* **2012**, *50*, 1433.

(126) Bebrone, C. *Biochem. Pharmacol.* **2007**, *74*, 1686.

(127) Page, M. I., and Badarau, A. *Bioinorg. Chem. Appl.* **2008**, *2008*.

(128) Xu, D., Guo, H., and Cui, Q. *J. Am. Chem. Soc.* **2007**, *129*, 10814.

(129) Bebrone, C., Anne, C., Kerff, F., Garau, G., De Vriendt, K., Lantin, R., Devreese, B., Van Beeumen, J., Dideberg, O., Frère, J. M., and Galleni, M. *Biochem. J.* **2008**, *414*, 151.

(130) Georgopapadakou, N. H. *Antimicrob. Agents Chemother.* **1993**, *37*, 2045.

(131) Magnet, S., Arbeloa, A., Mainardi, J. L., Hugonnet, J. E., Fourgeaud, M., Dubost, L., Marie, A., Delfosse, V., Mayer, C., Rice, L. B., Arthur, M. *J. Biol. Chem.* **2007**, *282*, 13151.

(132) Udwadia, Z., Amale, R. A., Ajbani, K. K., Rodrigues, C. *Clin. Infect. Dis.* **2012**, *54*, 579.

(133) Livermore, D. M. *J. Antimicrob. Chemother.* **2009**, *64*.

(134) Kasik, J., Weber, M., Winberg, E., Barclay, W. *Am. Rev. Respir. Dis.* **1966**, *94*, 260.

(135) Kasik, J., Weber, M., Freehill, P. *Am. Rev. Respir. Dis.* **1967**, *95*, 12.

(136) Maveyraud, L., Mourey, L., Kotra, L., Pedelacq, J. D., Guillet, V., Mobashery, S., Samama, J. P. *J. Am. Chem. Soc.* **1998**, *120*, 9748.

(137) Nukaga, M., Bethel, C. R., Thomson, J. M., Hujer, A. M., Distler, A., Anderson, V. E., Knox, J. R., Bonomo, R. A. *J. Am. Chem. Soc.* **2008**, *130*, 12656.

(138) Neu, H. C. *Ann. Intern. Med.* **1982**, *97*, 408.

(139) Faraci, W. S. a. P., R. F. *Biochemistry* **1985**, *24*, 903.

(140) Shimamura, T., Ibuka, A., Fushinobu, S., Wakagi, T., Ishiguro, M., Ishii, Y., Matsuzawa, H. *J. Biol. Chem.* **2002**, *277*, 46601.

(141) Delmas, J., Leyssene, D., Dubois, D., Birck, C., Vazeille, E., Robin, F., Bonnet, R. *J. Mol. Biol.* **2010**, *400*, 108.

(142) Bonnet, R., Recule, C., Baraduc, R., Chanal, C., Sirot, D., De Champs, C., Sirot, J. *J Antimicrob. Chemother.* **2003**, *52*, 29.

(143) Cole, S. T., Brosch, R., Parkhill, J., Garnier, T., Churcher, C., Harris, D., Gordon, S. V., Eiglmeier, K., Gas, S., Barry, C. E., Tekaia, F., Badcock, K., Basham, D., Brown, D., Chillingworth, T., Connor, R., Davies, R., Devlin, K, Feltwell, T., Gentles, S., Hamlin, N., Holroyd, S., Hornsby, T., Jagels, K., Krogh, A.,

McLean, J., Moule, S., Murphy, L., Oliver, K., Osborne, J., Quail, M., Rajandream, M., Rogers, J., Rutter, S., Seeger, K., Skelton, J., Squares, R., Squares, S., Sulston, J. E., Taylor, K., Whitehead, S., Barrell, B. G. *Nature* **1998**, *393*, 537.

(144) Tremblay, L. W., Fan, F., Blanchard, J. S. *Biochemistry* **2010**, *49*, 3766.

(145) Schurek, K. N., Wiebe, R., Karlowsky, J. A., Rubinstein, E., Hoban, D. J., Zhanel, G. G. *Expert Rev. Anti. Infect. Ther.* **2007**, *5*, 185.

(146) Gettig, J. P., Crank C. W., Philbrick, A. H. *Ann. Pharmacother.* **2008**, *42*, 80.

(147) Kato, K., Shirasaka, Y., Kuraoka, E., Kikuchi, A., Iguchi, M., Suzuki, H., Shibasaki, S., Kurosawa, T., Tamai, I. *Mol. Pharm.* **2010**, *7*, 1747.

(148) Erdemli, S. B., Gupta, R., Bishai, W. R., Lamichhane, G., Amzel, M., Bianchet, M. *Structure* **2012**, *20*, 2103.

(149) Triboule, S., Mainardi, J. L., Veckerlé, C., Dubée, V., Guekam-Moumi, A., Gutmann, Rice, L., Hugonnet, J. E. *J. Biol. Chem.* **2011**, *286*, 22777.

(150) Kim, H. S., Kim, J., Im, H., Yoon, J. Y., An, D. R., Yoon, H. J., Kim, J. Y., Min, H. K., Kim, S. J., Lee, J. Y., Hanb, B. W., Suh, S. W. *Acta Crystallogr. D Biol Crystallogr.* **2012**, *D69*, 420.

(151) McPherson, A. *Preparation and Analysis of Protein Crystals*; Waverly, 1982.

(152) Minor, W., Cymborowski, M., Otwinowski, Z., and Chruszcz, M. *Acta Crystallogr.* **2006**, *D62*, 859.

(153) McCoy, A. J., Grosse-Kunstleve, R. W., Adams, P. D., Winn, M. D., Storoni, L. C. and Read, R. J. *J. Appl. Crystallogr.* **2007**, *40*, 658.

(154) Bailey, S. *Acta Crystallogr. D Biol. Crystallogr.* **1994**, *50*, 760.

(155) Emsley, P., Lohkamp, B., Scott,W. G. and Cowtan, K. *Acta Crystallogr. D Biol. Crystallogr.* **2010**, *66*, 486.

(156) Adams, P. D., Afonine, P. V., Bunkóczi, G., Chen, V. B., Davis, I. W., Echols, N., Headd, J. J., Hung, L. W., Kapral, G. J., Grosse-Kunstleve, R.W., McCoy, A. J., Moriarty, N. W., Oeffner, R., Read, R. J., Richardson, D. C., Richardson, J. S., Terwilliger, T. C. and Zwart, P. H. *Acta Crystallogr. D Biol. Crystallogr.* **2010**, *66*, 213.

(157) Cheng, Y. a. P., W. H. *Biochemical Pharmacology* **1973**, *22*, 3099.

(158) Sambandamurthy, V. K., Wang, X., Chen, B., Russell, R. G., Derrick, S., Collins, F. M., Morris, S. L., Jacobs, W. R. Jr *Nature Medicine* **2002**, *8*, 1171.

(159) Franzblau, S. G., Witzig, R. S., McLaughlin, J. C., Torres, P., Madico, G., Hernandez, A., Degnan, M. T., Cook, M. B., Quenzer, V. K., Ferguson, R. M. and Gilman, R. H. *J. Clin. Microbiol.* **1998**, *36*, 362.

(160) Holtz, T. H., Cegielski, J. P. *Eur. Respir. J.* **2007**, *30*, 396.

(161) Migliori, G. B., Loddenkemper, R., Blasi, F., Raviglione, M. C. *Eur. Respir. J.* **2007**, *29*, 423.

(162) Chiang, C. Y., Centris, R., Battista, Migliori, G. B. *Respirology* **2010**, *15*, 413.

(163) Adamczyk-Wozniak, A., Cyranski, M. K., b, Zubrowska, A., Sporzynski, A. *Journal of Organometallic Chemistry* **2009**, *694*, 3533.

(164) Voskuil, M. I., Visconti, K. C., Schoolnik, G. K. *Tuberculosis (Edinb)* **2004**, *84*, 218.

(165) Talaat, A. M., Lyons, R., Howard, S. T., Johnston, S. A. *Proc. Natl. Acad. Sci.* **2004**, *101*, 4602.

(166) Gupta, R., Lavollay, M., Mainardi, J. L., Arthur, M., Bishai, W. R., Lamichhane, G. *Nat. Med*. **2010**, *16*, 466.

(167) Dye, C., Bassili, A., Bierrenbach, A. L., Broekmans, J. F., Chadha, V. K., Glaziou, P., Gopi, P. G., Hosseini, M., Kim, S. J., Manissero, D., Onozaki, I., Rieder, H. L., Scheele, S., van Leth, F., van der Werf, M., Williams, B. G. *Lancet Infect. Dis.* **2008**, *8*, 233.

(168) Dinnes, J., Deeks, J., Kunst, H., Gibson, A., Cummins, E., Waugh, N., Drobniewski, F., Lalvani, A. *Health Technol. Assess.* **2007**, *11*, 1.

(169) Ling, D. I., Flores, L. L., Riley, L. W. and Pai, M. *PLoS One* **2003**, *3*, e1536.

(170) Greco, S., Girardi, E., Navarra, A. and Saltini, C. *Thorax* **2006**, *61*, 783.

(171) Boehme, C., Nabeta, P., Hillemann, D., Nicol, M., Shenai, S., Krapp, F., Allen, J., Tahirli, R., Blakemore, R., Rustomjee, R., Milovic, A., Jones, M., O'Brien, S., Persing, D., Ruesch-Gerdes, S., Gotuzzo, E., Rodrigues, C., Alland, D., and Perkins, M. *N. Engl. J. Med.* **2010**, *363*, 1005.

(172) Hughes, R., Wonderling, D., Li, B. and Higgins, B. *Respir. Med.* **2012**, *106*, 300.

(173) Boyd, D. B. a. L., W. H. *J. Med. Chem.* **1979**, *22*, 778.

(174) Faraci, W. S. a. P., R. F. *J. Am. Chem. Soc.* **1984**, *106*, 1489.

(175) Pratt, R. F. a. F., W. S. *J. Am. Chem. Soc.* **1986**, *108*, 5328.

(176) Zlokarnik, G., Negulescu, P. A., Knapp, T. E., Mere, L., Burres, N., Feng, L., Whitney, M., Roemer, K., Tsien, R. Y. *Science* **1998**, *279*, 84.

(177) Gao, W., Xing, B., Tsien, R. Y. and Rao, J. *J. Am. Chem. Soc.* **2003**, *125*, 11146.

(178) Xing, B., Khanamiryan, A. and Rao, J. *J. Am. Chem. Soc.* **2005**, *127*, 4158.

(179) Yao, H., So, M. K. and Rao, J. *Angew. Chem. Int. Ed.* **2007**, *46*, 7031.

(180) Rukavishnikov, A., Gee, K. R., Johnson, I. and Corry, S. *Anal. Biochem.* **2011**, *419*, 9.

(181) Kong, Y., Yao, H., Ren, H., Subbian, S., Cirillo, S. L., Sacchettini, J. C., Rao, J., Cirillo, J. D. *Proc. Natl. Acad. Sci. U S A* **2010**, *107*, 12239.

(182) Banerjee, S., Pieper, U., Kapadia, G., Pannell, L. K. and Herzberg, O. *Biochemistry* **1998**, *37*, 3286.

(183) Knox, J. R. *Antimicrob. Agents Chemother.* **1995**, *39*, 2593.

(184) Albrecht, H. A., Beskid, G., Chan, K. K., Christenson, J. G., Cleeland, R., Deitcher, K. H., Georgopapadakou, N. H., Keith, D. D., Pruess, D. L., Sepinwall, J., Specian, A. Jr., Then, R. L., Weigele, M., West, K., Yang, R. *J. Med. Chem.* **1990**, *33*, 77.

(185) Baldwin, J. E., Urban, F. J., Cooper, R. D. G. and Jose, F. L. *J. Am. Chem. Soc.* **1973**, *95*, 2401.

(186) Minasov, G., Wang, X. J. and Shoichet, B. K. *J. Am. Chem. Soc.* **2002**, *124*, 5333.

(187) Urano, Y., Kamiya, M., Kanda, K., Ueno, T., Hirose, K., and Nagano, T. *J. Am. Chem. Soc.* **2005**, *127*, 4888.

(188) McNerney, R. a. D., P. *Nature Rev. Microbiol.* **2011**, *9*, 204.

(189) Backus, K. M., Boshoff, H.I., Barry, C.S., Boutureira, O., Patel, M. K., D'Hooge, F., Lee, S. S., Via, L. E., Tahlan, K., Barry, C. E. 3rd, Davis, B. G. *Nat. Chem. Biol.* **2011**, *7*.

(190) Kwon, H. H., Tomioka, H. and Saito, H. *Tuber. Lung. Dis.* **1995**, *76*, 141.

(191) Majiduddin, F. K., Materon, I. C. and Palzkill, T. G. *Int. J. Med. Microbiol.* **2002**, *292*, 127.

(192) Mitchell, R. S., Kumar, V., Robbins, S. L., Abbas, A. K. and Fausto, N. *Robbins Basic Pathology*; Saunders/Elsevier 2007.

(193) Minor, W., Cymborowski, M., Otwinowski, Z. and Chruszcz, M. *Acta Crystallogr. D Biol. Crystallogr.* **2006**, *62*, 859.

(194) Moellering, J. R. C. *N Engl J Med* **2010**, *363*, 2377.

(195) Cornaglia, G., Giamarellou, H., Rossolini, G.M. *Lancet Infect. Dis.* **2011**, *11*, 381.

(196) Llarrull, L. I., Testero, S.A., Fisher, J.F., Mobashery S. *Curr. Opin. Microbiol.* **2010**, *13*, 551.

(197) Nathwani, D., Davey, P.G., Marwick, C.A. *Clin. Evid.* **2010**, *(Online)*, 2010.

(198) Gillespie, S. H., Singh, K. *Recent Pat. Antiinfect. Drug Discov.* **2011**, *6*, 77.

(199) Feldman, C., Anderson, R. *Drugs* **2011**, *71*, 131.

(200) Sarma, J. B., Bhattacharya, P.K., Kalita, D., Rajbangshi, M. *Indian Journal of Medical Microbiology* **2011**, *29*, 22.

(201) Chen, Y., Zhou, Z., Jiang, Y., Yu, Y. *J. Antimicrob. Chemother.* **2011**, *66*, 1255.

(202) Yamamoto, T., Takano, T., Iwao, Y., Hishinuma, A. *Journal of Infection and chemotherapy* **2011**, *17*, 435.

(203) Prevention, C. f. D. C. a. *Morb. Mortal. Wkly. Rep.* **2010**, *59*, 750.

(204) Marra, A. *Future Microbiology* **2011**, *6*, 137.

(205) Mulvey, M. R. *Emerging Infectious Diseases* **2011**, *17*, 1.

(206) Kumarasamy, K., Toleman, M., Walsh, T., Bagaria, J., Butt, F., Balakrishnan, R., Chaudhary, U., Doumith, M., Giske, C., Irfan, S., Krishnan, P., Kumar, A., Maharjan, S., Mushtaq, S., Noorie, T., Paterson, D., Pearson, A., Perry, C., Pike, R., Rao, B., Ray, U., Sarma, J., Sharma, M., Sheridan, E., Thirunarayan, M., Turton, J., Upadhyay, S., Warner, M., Welfare, W., Livermore, D., Woodford, N. *Lancet Infect. Dis.* **2010**, *10*, 597.

(207) Walsh, T. R. *Int. J. Antimicrob. Agents* **2010**, *36*, S8.

(208) Harada, S., Ishii, Y., Yamaguchi, K. *The Korean Journal of Laboratory Medicine* **2008**, *28*, 401.

(209) Tamilselvi, A., Mugesh, G. *J. Biol. Inorg. Chem.* **2008**, *13*, 1039.

(210) Jin, W., Arakawa, Y., Yasuzawa, H., Taki, T., Hashiguchi, R., Mitsutani, K., Shoga, A., Yamaguchi, Y., Kurosaki, H., Shibata, N., Ohta, M., Goto, M. *Biol. Pharm. Bull.* **2004**, *27*, 851.

(211) Siemann, S., Clarke, A.J., Viswanatha, T., Dmitrienko, G.I. *Biochemistry* **2003**, *42*, 1673.

(212) Walsh, T. R., Weeks, J., Livermore, D.M., Toleman, M. *Lancet Infect. Dis.* **2011**, *11*, 355.

(213) Bush, K. *Curr. Opin. Microbiol.* **2010**, *13*, 558.

(214) Carfi, A., Pares, S., Duée, E., Galleni, M., Duez, C., Frère, J.M., and Dideberg, O. *The EMBO Journal* **1995**, *14*, 4914.

(215) Rasmussen, B. A., Yang, Y., Jacobus, N., Bush, K. *Antimicrob. Agents Chemother.* **1994**, *38*, 2116.

(216) García-Saez, I., Hopkins, J., Papamicael, C., Franceschini, N., Amicosante, G., Rossolini, G. M., Galleni, M., Frère, J. M. , Dideberg, O. *J. Biol. Chem.* **2003**, *278*, 23868.

(217) Queenan, A. M., Bush, K. *Clinical Microbiology Reviews* **2007**, *20*, 440.

(218) Jean, S. S., Hsueh, P. R. *Int. J. Antimicrob. Agents* **2011**, *37*, 291.

(219) Bebrone, C., Delbrück, H., Kupper, M. B., Schlömer, P., Willmann, C., Frère, J. M., Fischer, R., Galleni, M., Hoffmann, K. M. *Antimicrob. Agents Chemother.* **2009**, *53*, 4464.

(220) Walsh, T. R., Neville, W. A., Haran, M. H., Tolson, D., Payne, D. J., Bateson, J. H., MacGowan, A. P., Bennett, P. M. *Antimicrob. Agents Chemother.* **1998**, *42*, 436.

(221) Saavedra, M., Peixe, L., Sousa, J., Henriques, I., Alves, A., and Correia, A. *Antimicrob. Agents Chemother.* **2003**, *47*, 2330.

(222) McManus-Munoz, S., Crowder, M. W. *Biochemistry* **1999**, *38*, 1547.

(223) Ullah, J. H., Walsh, T. R., Taylor, I.A., Emery, D.C., Verma, C.S., Gamblin, S.J., Spencer, J. *J. Mol. Biol.* **1998**, *284*, 125.

(224) Mercuri, P. S., García-Sáez, I., De Vriendt, K., Thamm, I., Devreese, B., Van Beeumen, J., Dideberg, O., Rossolini. G. M., Frère, J. M., Galleni, M. *J. Biol. Chem.* **2004**, *279*, 33630.

(225) Morán-Barrio, J., González, J. M., Lisa M. N., Costello, A. L., Peraro, M. D., Carloni, P., Bennett, B., Tierney, D.L., Limansky, A. S., Viale, A. M., Vila, A. J. *J. Biol. Chem.* **2007**, *282*, 18286.

(226) Lisa M. N., H., L., Vila, A. J. *J. Biol. Chem.* **2010**, *285*, 4570.

(227) Docquier, J. D., Pantanella, F., Giuliani, F., Thaller, M. C., Amicosante, G., Galleni, M., Frère, J. M., Bush, K., Rossolini, G. M. *Antimicrob. Agents Chemother.* **2002**, *46*, 1823.

(228) Rossolini, G. M., Condemi, M. A, Pantanella, F., Docquier, J. D., Amicosante, G., Thaller, M. C. *Antimicrob. Agents Chemother.* **2001**, *45*, 837.

(229) Ho, P., Lo, W., Yeung, M. K., Lin, C., Chow, K., Ang, I., Tong, A., Bao, J., Lok, S., Lo, J. *PLoS One* **2011**, *6*, e17989.

(230) Kall, L., Krogh, A., Sonnhammer, E. L. L. *J. Mol. Biol.* **2004**, *338*, 1027.

(231) Yu, N. Y., Laird, M. R., Spencer, C., Brinkman, F. S. L *Nucleic Acids Res.* **2011**, *39*, D241.

(232) Jaroszewski, L., Rychlewski, L., Li, Z., Li, W., Godzik, A. *Nucleic Acids Res.* **2005**, *33*, W284.

(233) Concha, N. O., Janson, C. A., Rowling, P., Pearson, S., Cheever, C. A., Clarke, B. P., Lewis, C., Galleni, M., Frere, J. M., Payne, D. J., Bateson, J. H., Abdel-Meguid, S. S. *Biochemistry* **2000**, *39*, 4288.

(234) Garcia-Saez, I., Docquier, J., Rossolini, G. M., Dideberg, O. *J. Mol. Biol.* **2008**, *375*, 604.

(235) Lassaux, P., Traoré, D. A., Loisel, E., Favier, A., Docquier, J. D., Sohier, J. S., Laurent, C., Bebrone, C., Frère, J. M., Ferrer, J. L., Galleni, M. *Antimicrob. Agents and Chemother.* **2010**, *55*, 1248.

(236) Zhang, H., Hao, Q. *FASEB J* **2011**, *25*, 2574.

(237) Holm, L., Rosenstrom, P. *Nucleic Acids Res.* **2010**, *38*, W545.

(238) Li, W., Godzik, A. *Bioinformatics* **2006**, *22*, 1658.

(239) Laskowski, R. A., Watson, J. D., Thornton, J. M. *Nucleic Acids Res* **2005**, *33*, W89.

(240) Concha, N. O., Rasmussen, B. A., Bush, K., Herzberg, O. *Structure* **1996**, *4*, 823.

(241) García-Saez, I., Mercuri, P. S., Papamicael, C., Kahn, R., Frère, J. M., Galleni, M., Rossolini, G. M., Dideberg, O. *J. Mol. Biol.* **2003**, *325*, 651.

(242) Garau, G., Bebrone, C., Anne, C., Galleni, M., Frère, J.M., Dideberg, O. *J. Mol. Biol.* **2005**, *345*, 785.

(243) Yamaguchi, Y., Jin, W., Matsunaga, K., Ikemizu, S., Yamagata, Y., Wachino, J., Shibata, N., Arakawa, Y., Kurosaki, H. *J. Med. Chem.* **2007**, *50*, 6647.

(244) Fitzgerald, P. M., Wu, J. K., Toney, J. H. *Biochemistry* **1998**, *37*.

(245) Dundas, J., Ouyang, Z., Tseng, J., Binkowski, A., Turpaz, Y., Liang, J. *Nucleic Acids Res.* **2006**, *34*, W116.

(246) Zheng, B., Tan, S., Gao, J., Han, H., Liu, J., Lu, G., Liu, D., Yi, Y., Zhu, B., Gao, G.F. *Protein Cell* **2011**, *2*, 250.

(247) Guo, Y., Wang, J., Niu, G., Shui, W., Sun, Y., Zhou, H., Zhang, Y., Yang, C., Lou, Z., Rao, Z. *Protein Cell* **2011**, *2*, 384.

(248) Jacquin, O., Balbeur, D., Damblon, C., Marchot, P., De Pauw, E., Roberts, G. C., Frère, J. M., Matagne, A. *J. Mol. Biol.* **2009**, *392*, 1278.

(249) Page, M. I., Badarau, A. *Bioinorg. Chem. Appl.* **2008**, 576297.

(250) Fabiane, S. M., Sohi, M. K., Wan, T., Payne, D. J., Bateson, J. H., Mitchell, T., Sutton, B. J. *Biochemistry* **1998**, *37*, 12404.

(251) Crowder, M. W., Spencer, J., Vila, A. J. *Acc. Chem. Res.* **2006**, *39*, 721.

(252) Castanheira, M., Toleman, M. A., Jones, R. N., Schmidt, F. J., Walsh, T. R. *Antimicrob. Agents Chemother.* **2004**, *48*, 4654.

(253) Laraki, N., Franceschini, N., Rossolini, G.M., Santucci, P., Meunier, C., de Pauw, E., Amicosante, G., Frère, J. M., Galleni, M. *Antimicrob. Agents Chemother.* **1999**, *43*, 902.

(254) Docquier, J. D. *J. Antimicrob. Chemother.* **2003**, *51*, 257.

(255) Tomatis, P. E., Fabiane, S. M., Simona, F., Carloni, P., Sutton, B. J., Vila, A. J. *Proc. Natl. Acad. Sci.* **2008**, *105*, 20605.

(256) Oelschlaeger, P., Schmid, R. D., Pleiss, J. *Protein Engineering Design and Selection* **2003**, *16*, 341.

(257) Xu, D., Guo, H., Cui, Q. *J. Am. Chem. Soc.* **2007**, *129*, 10814.

(258) Nocek, B. P., Gillner, D. M., Fan, Y., Holz, R. C., Joachimiak, A. *J. Mol. Biol.* **2010**, *397*, 617.

(259) Malanoski, G. J., Collins, L., Wennersten, C., Moellering, R. C. Jr., Eliopoulos, G.M. *Antimicrob. Agents Chemother.* **1993**, *37*, 2009.

(260) Clarke, A. M., Zemcov, S. J. *Eur. J. Clin. Microbiol. Infect. Dis.* **1993**, *12*, 377.

(261) Peirano, G., Schreckenberger, P. C., Pitout, J. D. *Antimicrob. Agents Chemother.* **2011**, *55*, 2986.

(262) Kozawa, O., Uematsu, T., Matsuno, H., Niwa, M., Takiguchi, Y., Matsumoto, S., Minamoto, M., Niida, Y., Yokokawa, M., Nagashima, S.,and Kanamaru, M. *Antimicrob. Agents Chemother.* **1998**, *42*, 1433.

(263) Mori, M., Hikida, M., Nishihara, T., Nasu, T., Mitsuhashi, S. *J. Antimicrob. Chemother.* **1996**, *37*, 1034.

(264) Aslanidis, C., de Jong, P. J. *Nucleic Acids Res.* **1990**, *18*, 6069.

(265) Eschenfeldt, W. H., Lucy, S., Millard, C. S., Joachimiak, A., Mark, I. D. *Methods Mol. Biol.* **2009**, *498*, 105.

(266) Donnelly, M. I., Zhou, M., Millard, C.S., Clancy, S., Stols, L., Eschenfeldt, W. H., Collart, F. R., Joachimiak, A. *Protein Expr. Purif.* **2006**, *47*, 446.

(267) Alkire, R. W., Molitsky, M., Rotella, F. J., Lazarski, K., Joachimiak, A. *Nuclear Instruments and Methods in Physics Research A* **2011**, *649*, 112.

(268) Rosenbaum, G., Alkire, R. W., Evans, G., Rotella, F. J., Lazarski, K., Zhang, R. G., Ginell, S. L., Duke, N., Naday, I., Lazarz, J., Molitsky, M. J., Keefe, L.,

Gonczy, J., Rock, L., Sanishvili, R., Walsh, M. A., Westbrook, E., Joachimiak, A. *J. Synchrotron Radiat.* **2006**, *13*, 30.

(269) Minor, W., Cymborowski, M., Otwinowski, Z., Chruszcz, M. *Acta Crystallogr. D Biol. Crystallogr.* **2006**, *62*, 859.

(270) Vagin, A., Teplyakov, A. *Acta Crystallogr. D Biol. Crystallogr.* **2010**, *66*, 22.

(271) Long, F., Vagin, A. A., Young, P., Murshudov, G. N. *Acta Crystallogr. D Biol. Crystallogr.* **2008**, *64*, 125.

(272) Emsley, P., Cowtan, K. *Acta Crystallogr D Biol Crystallogr* **2004**, *60*, 2126.

(273) Winn, M. D., Isupov, M. N., Murshudov, G. N. *Acta Crystallogr. D Bio.l. Crystallogr.* **2001**, *57*, 122.

(274) Chen, V. B., Arendall, W. B. 3rd, Headd, J. J, Keedy, D. A., Immormino, R. M., Kapral, G. J., Murray, L. W., Richardson, J. S., Richardson, D. C. *Acta Crystallogr. D Biol. Crystallogr.* **2010**, *66*, 12.

(275) D'Costa, V. M., King, C. E., Kalan, L., Morar, M., Sung, W. W., Schwarz, C., Froese, D., Zazula, G., Calmels, F., Debruyne, R., Golding, G. B., Poinar, H. N., and Wright, G. D. *Nature* **2011**, *477*, 457.

(276) Fisher, J. F., Meroueh, S. O., and Mobashery, S. *Chem. Rev.* **2005**, *195*, 395.

(277) Kumarasamy, K. K., Toleman, M. A., Walsh, T. R., Bagaria, J., Butt, F., Balakrishnan, R., Chaudhary, U., Doumith, M., Giske, C. G., Irfan, S., Krishnan, P., Kumar, A. V., Maharjan, S., Mushtaq, S., Noorie, T., Paterson, D. L., Pearson, A., Perry, C., Pike, R., Rao, B., Ray, U., Sarma, J. B., Sharma, M., Sheridan, E., Thirunarayan, M. A., Turton, J., Upadhyay, S., Warner, M.,

Welfare, W., Livermore, D. M., and Woodford, N. *Lancet Infect. Dis.* **2010**, *10*, 597.

(278) Mollering, R. C. *N. Engl. J. Med.* **2010**, *363*, 2377.

(279) Thomas, P. W., Zheng, M., Wu, S., Guo, H., Liu, D., Xu, D., Fast, W. *Biochemistry* **2011**, *50*, 10102.

(280) Park, H., Brothers, E. N., and Merz, K. M., Jr. *J. Am. Chem. Soc.* **2005**, *127*, 4232.

(281) Tamiselvi, A., and Mugesh, G. *Biol. Inorg. Chem.* **2008**, *13*, 1039.

(282) Riondet, C., Cachon, R., Waché, Y., Alcaraz, G., and Diviès, C. *Biotech. Tech.* **1997**, *11*, 735.

(283) Wilks, J. C., and Slonczewski, J. L. *J. Bacteriol.* **2007**, *189*, 5601.

(284) Badaru, A., and Page, M. I. *Biochemistry* **2006**, *45*, 10654.

(285) Bruice, T. C., and Benkovic, S. J. *Biochemistry* **2000**, *39*, 6267.

(286) Valiev, M., Yang, J., Adams, J. A., Taylor, S. S., and Weare, J. H. *J. Phys. Chem.* **2007**, *B111*, 13455.

(287) Khersonsky, O., and Tawfik, D. S. *Annu. Rev. Biochem.* **2010**, *79*, 471.

(288) Carbonell, P., Lecointre, G., and Faulon, J.-L. *J. Biol. Chem.* **2011**, *286*, 43994.

(289) Nam, H., Lewis, N. E., Lerman, J. A., Lee, D.-H., Chang, R. L., Kim, D., and Palsson, B. O. *Science* **2012**, *337*, 1104.

(290) Blakeley, M. P., Ruiz, F., Cachau, R., Hazemann, I., Meilleur, F., Mitschler, A., Ginell, S., Afonine, P., Ventura, O. N., Cousido-Siah, A., Haertlein, M.,

Joachimiak, A., Myles, D., and Podjarny, A. *Proc. Natl. Acad. Sci. U. S. A.* **2008**, *105*, 1844.

(291) Kim, Y., Dementieva, I., Zhou, M., Wu, R., Lezondra, L., Quartey, P., Joachimiak, G., Korolev, O., Li, H., and Joachimiak, A. *J. Struct. Funct. Genomics* **2004**, *5*, 111.

(292) Walsh, M., Dementieva, I., Evans, G., Sanishvili, R., and Joachimiak, A. *Acta Crystallogr.* **1999**, *D55*, 1168.

(293) Emsley, P., and Cowtan, K. *Acta Crystallogr* **2004**, *D60*, 2126.

(294) Laskowski, R. A., MacArthur, M. W., Moss, D. S., and Thornton, J. M. *J. Appl. Cryst.* **1993**, *26*, 283.

(295) Phillips, J. C., Braun, R., Wang, W., Gumbart, J., Tajkhorshid, E., Villa, E., Chipot, C., Skeel, R. D., Kalé, L., and Schulten, K. *J. Comput. Chem.* **2005**, *26*, 1781.

(296) MacKerell, A. D., Jr., Bashford, D., Bellott, M., Dunbrack, R. L., Jr., Evanseck, J. D., Field, M. J., Fischer, S., Gao, J., Guo, H., Ha, S., Joseph-McCarthy, D., Kuchnir, L., Kuczera, K., Lau, F. T. K., Mattos, C., Michnick, S., Ngo, T., Nguyen, D. T., Prodhom, B., Reiher, W. E., III, Roux, B., Schlenkrich, M., Smith, J. C., Stote, R., Straub, J., Watanabe, M., Wiórkiewicz-Kuczera, J., Yin, D., and Karplus, M. *J. Phys. Chem.* **1998**, *B102*, 3586.

(297) Humphrey, W., Dalke, A., and Schulten, K. *J. Mol. Graphics* **1996**, *14*, 33.

(298) Essmann, U., Perera, L., Berkowitz, M. L., Darden, T., Lee, H., and Pedersen, L. G. *J. Chem. Phys.* **1995**, *103*, 8577.

(299) Brünger, A., Brooks, C. B., and Karplus, M. *Chem. Phys. Lett.* **1984**, *105*, 495.

(300) Feller, S. E., Zhang, Y., Pastor, R. W., and Brooks, B. R. *J. Chem. Phys.* **1995**, *103*, 4613.

(301) Hoover, W. G. *Phys. Rev.* **1985**, *A31*, 1695.

(302) Hoover, W. G. *Phys. Rev.* **1986**, *A34*, 2499.

(303) Kendall, R. A., Apra`, E., Bernholdt, D. E., Bylaska, E. J., Dupuis, M., Fann, G. I., Harrison, R. J., Ju, J., Nichols, J. A., Nieplocha, J., Straatsma, T. P., Windus, T. L., and Wong, A. T. *Comput. Phys. Comm.* **2000**, *128*, 260.

(304) Becke, A. D. *Phys. Rev.* **1988**, *A38*, 3098.

(305) Flores, A. R., Parsons, L. M., and Pavelka, M.S. Jr. *J. Bacteriol.* **2005**, *187*, 1892.

(306) Zelmer, A., Carroll, P., Andreu, N., Hagens, K., Mahlo, J., Redinger, N., Robertson, B. D., Wiles, S., Ward, T. H., Parish, T., Ripoll, J., Bancroft, G., Schaible, U. E. *J. Antimicrob. Chemother.* **2012**, *67*, 1948.

APPENDIX

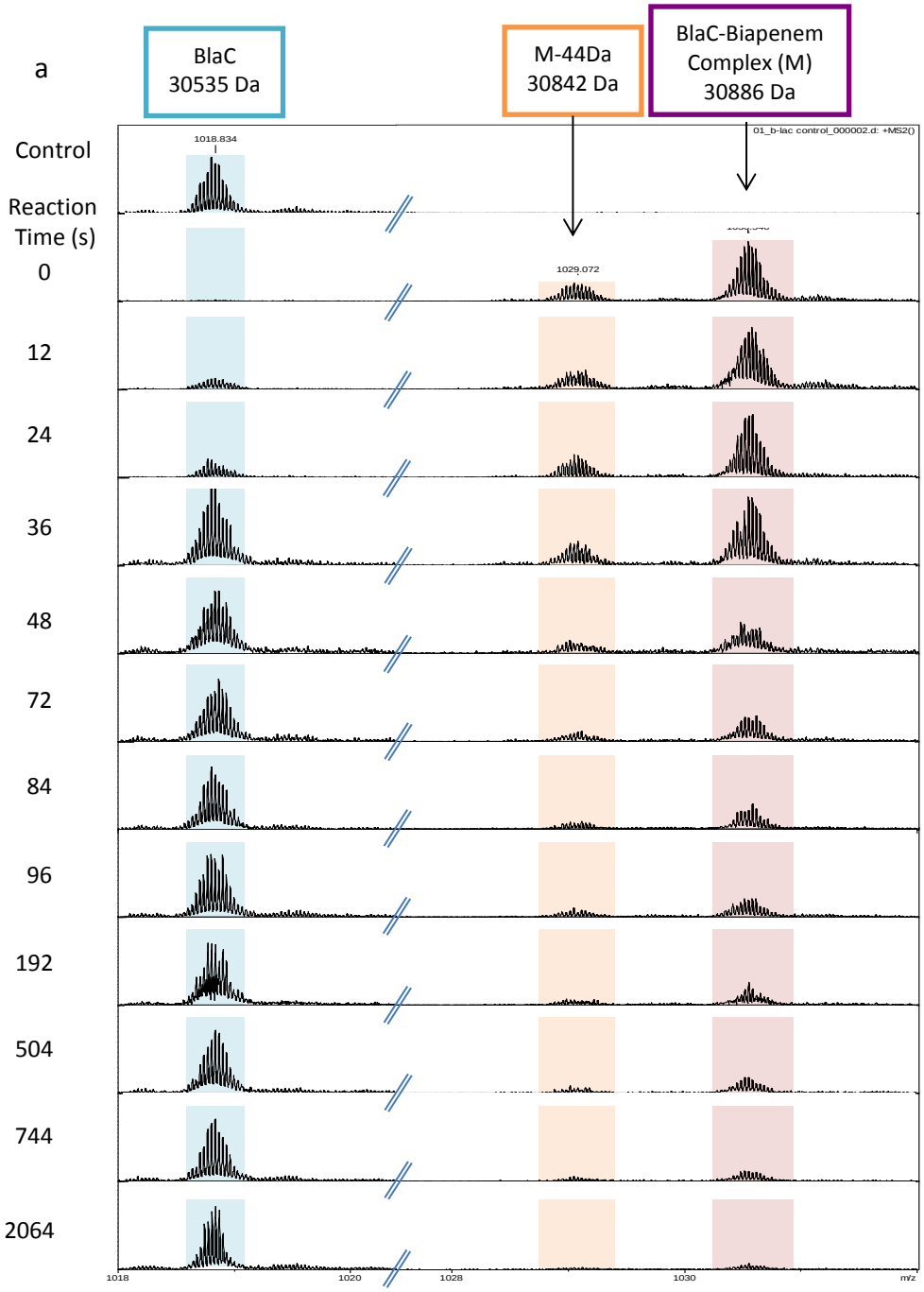
a
BlaC
30535 Da
M-44Da
30842 Da
BlaC-Biapenem
Complex (M)
30886 Da
Control
Reaction
Time (s)
0
12
24
36
48
72
84
96
192
504
744
2064
1018.834
1029.072
01_b-lac control_000002.d: +MS2()
1018
1020
1028
1030
m/z

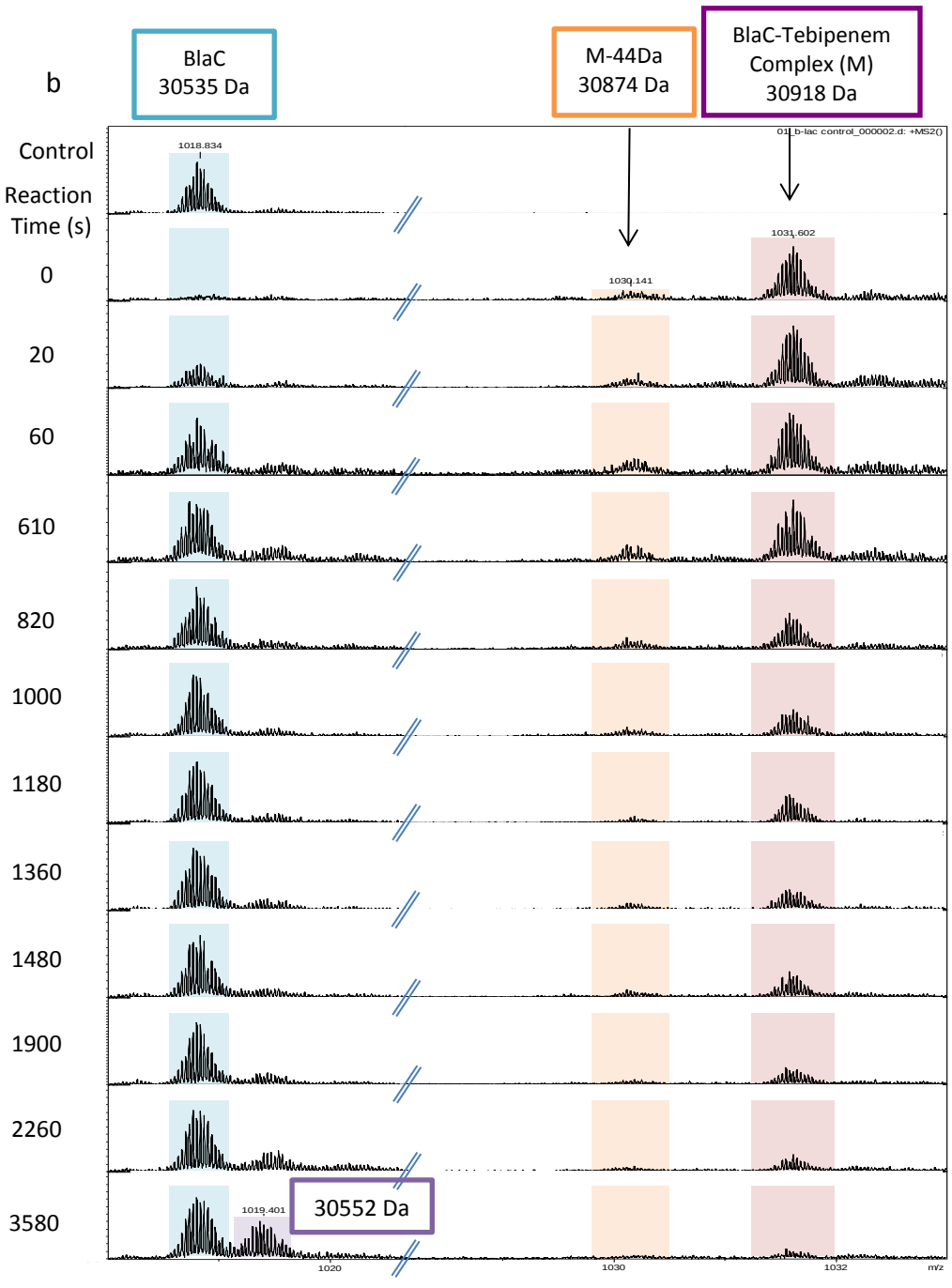
b
BlaC
30535 Da
M-44Da
30874 Da
BlaC-Tebipenem
Complex (M)
30918 Da
Control
Reaction
Time (s)
0
20
60
610
820
1000
1180
1360
1480
1900
2260
3580
1018.834
1030.141
1031.602
1019.401
30552 Da
1020
1030
1032
m/z

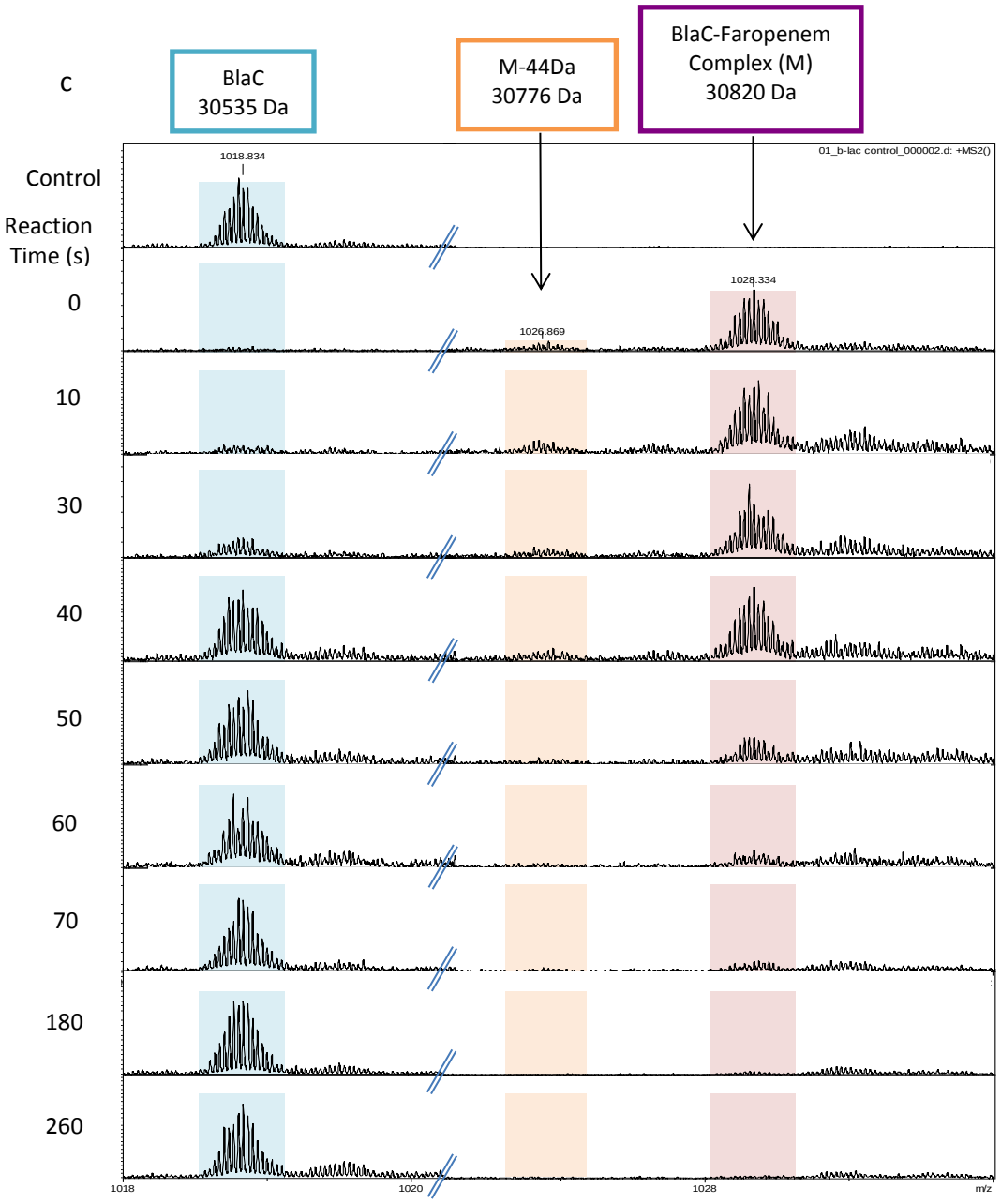

Figure A1. Raw FTICR-MS time course spectra of the BlaC reaction with (a) biapenem, (b) tebipenem, and (c) faropenem. Reaction species are labeled according to their respective mass (Da) and colored (blue) free enzyme, (purple) acyl-intermediate (M), and (orange) M – 44 Da. (left) Time of reaction quenching in seconds.

	E166A Amoxicillin	E166A Cefoperazone	E166A Cefotaxime
Data collection			
Space group	P21	P21	P21
Cell dimensions			
a, *b*, *c* (Å)	79.6, 96.7, 109.8	78.3, 95.6, 108. 7	78.8, 96.2, 107.1
α, β, γ (°)	90.0, 107.5, 90.0	90.0, 107.2, 90.0	90.0, 106.3, 90.0
Resolution (Å)	47-2.85 (2.93-2.85)*	47-2.25 (2.25-2.28) *	45-2.30 (2.34-2.29)*
R_{merge}	0.20 (0.87)	0.09 (0.55)	0.11 (0.63)
$I / \sigma I$	12.0 (2.1)	20.0 (2.2)	13.0 (2.0)
Completeness (%)	99 (99)	99 (99)	98 (81)
Redundancy	5.1 (5.1)	3.6 (3.6)	3.6 (3.5)
Wavelength (Å)	0.91990	0.97929	0.91959
Refinement			
Resolution (Å)	47.26 - 2.85	47 - 2.19	45 - 2.29
No. reflections	36,965	71,884	67,526
$R_{work/}$ R_{free}	.21/.24	.21/.22	.21/.24
No. atoms	7864	8026	7948
Protein	7784	7667	7730
Adduct	50	74	52
PO_4	30	40	45
Water	0	245	121
B-factors			
Protein	60.49	39.07	38.06
Adduct	62.37	53.90	60.86
PO_4	110.2	82.24	67.90
Water	n/a	48.91	39.69
R.m.s deviations			
Bond lengths (Å)	0.017	0.026	0.006
Bond angles (°)	1.662	1.521	0.818

Table A1. Crystallographic data collection and refinement statistics of BlaC-acyl-intermediate complexes.

	E166A Faropenem	WT Biapenem	WT Tebipenem
Data collection			
Space group	P21	P21	P21
Cell dimensions			
a, *b*, *c* (Å)	78.5, 97.0, 110.0	78.5, 97.0, 110.0	78.5, 96.3, 110.2
α, β, γ (°)	90.0, 108.7, 90.0	90.0, 108.7, 90.0	90.0, 108.3, 90.0
Resolution (Å)	47-2.10 (2.15-2.11)*	37-1.72 (1.75-1.72)*	47-2.04(2.09-2.05)*
R_{merge}	0.13 (0.84)	0.06 (0.71)	0.07 (0.51)
I / σI	16.1 (2.3)	20.9 (2.1)	24.14 (2.6)
Completeness (%)	98 (74)	100 (99)	98 (86)
Redundancy	5.1 (4.5)	2.5 (2.5)	3.6 (2.7)
Wavelength (Å)	0.91990	0.97926	0.97740
Refinement			
Resolution (Å)	47-2.10	37-1.72	47-2.04
No. reflections	89,625	157,565	97,020
R_{work}/ R_{free}	.17/.20	.17/.18	.17/.21
No. atoms	8380	8823	8622
Protein	7874	7912	7906
Adduct	38	48	50
PO_4	40	40	30
Water	428	823	636
B-factors			
Protein	29.65	24.08	29.88
Adduct	53.62	53.89	49.77
PO_4	64.14	41.36	52.76
Water	38.32	41.43	44.44
R.m.s deviations			
Bond lengths (Å)	0.015	0.008	0.015
Bond angles (°)	1.494	1.303	1.617

Table A1 continued. Crystallographic data collection and refinement statistics of BlaC-acyl-intermediate complexes.

a b

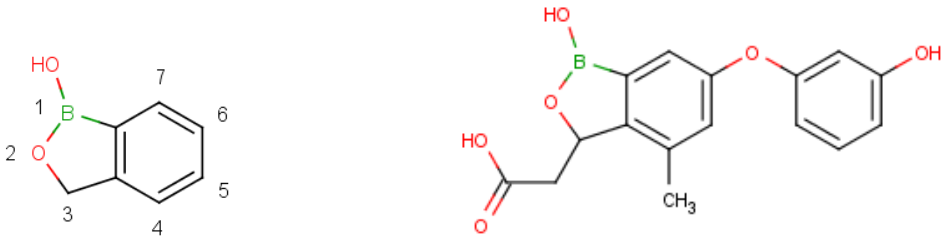

Figure A2. Benzoxaborole scaffold (a) and lead inhibitor AN4715 (b).

	BlaC AN4715	BlaC AN4845	BlaC AN4967
Data collection			
Space group	P21	P21	P21
Cell dimensions			
a, *b*, *c* (Å)	78.9, 96.8, 110.9	78.5, 96.7, 109.6	78.3, 96.2, 110.1
α, β, γ (°)	90.0, 108.2, 90.0	90.0, 107.9, 90.0	90.0, 108.4, 90.0
Resolution (Å)	47-2.4 (2.44-2.40)	47-2.23 (2.26-2.23)	47-2.34(2.37-2.34)
R_{merge}	0.15 (0.61)	0.14 (0.86)	0.18 (0.97)
$I / \sigma I$	13.8 (2.0)	15.2 (2.3)	10.6 (2.4)
Completeness (%)	99 (88)	97 (43)	99 (90)
Redundancy	7.0 (5.3)	5.9 (5.8)	5.5 (5.7)
Wavelength (Å)	0.95380	0.97947	0.97947
Refinement			
Resolution (Å)	47-2.40	37-1.72	47-2.34
No. reflections	61,695	73,601	61,269
R_{work}/ R_{free}	0.16/0.20	0.16/0.19	0.18/0.22
No. atoms	8427	8378	8351
Protein	7961	7952	7972
Adduct	46	58	54
PO_4	40	40	35
Water	380	328	290
B-factors			
Protein	24.82	35.86	34.40
Adduct	37.70	64.18	50.43
PO_4	49.72	61.62	63.16
Water	28.65	38.57	36.30
R.m.s deviations			
Bond lengths (Å)	0.007	0.007	0.008
Bond angles (°)	1.193	1.133	1.163

Table A2. BlaC-benzoxaborole crystallographic data collection and refinement statistics.

	BlaC CDC-1	BlaC CDC-3
Data collection		
Space group	P21	P21
Cell dimensions		
a, *b*, *c* (Å)	79.40, 97.46, 110.96	78.5, 97.0, 110.0
α, β, γ (°)	90.0, 108.37, 90.0	90.0, 107.69, 90.0
Resolution (Å)	50-2.60 (2.60-2.64) [a]	50-2.80 (2.80-2.85) [a]
R_{merge}	0.15 (0.72)	0.12 (0.80)
$I / \sigma I$	12.0 (2.1)	11.7 (1.2)
Completeness (%)	99 (98)	99.1 (99.9)
Redundancy	4.0 (3.9)	4.1 (4.1)
Wavelength (Å)	0.97929	0.91943
Refinement		
Resolution (Å)	47.26 - 2.57	47.16 - 2.77
No. reflections	49,807	38,850
$R_{work/}$ R_{free}	0.22/0.25	0.24/0.25
No. atoms	8124	7409
Protein	7928 [b]	7285 [b]
Adduct	46	96
PO_4	35	15
Water	114	13
B-factors		
Protein	49.19	72.59
Adduct	90.41	93.64
PO_4	77.61	103.98
Water	43.17	66.12
R.m.s deviations		
Bond lengths (Å)	0.010	0.011
Bond angles (°)	1.176	1.297

Table A3. BlaC-fluorogenic probe crystallographic data collection and refinement statistics. [a] Values in parentheses are for highest-resolution shell. Each dataset was collected from a single crystal. [b] Due to the difference in the disorder of the substrate specificity loop and resolution, the protein atom number in both structures is different.

Data collection statistics	NDM-1 Δ38 (39–270)	NDM-1 Δ36NY (37–270)	NDM-1 Δ36NY (37–270)	mZnNDM-1 Δ36NY (37–270)
Space group	$P2_1$	$P2_1$	I222	$P4_32_12$
Unit cell (Å)	$a = 59.71$ $b = 51.11$ $c = 70.68$ $\beta = 106.96$	$a = 59.76$ $b = 50.86$ $c = 70.72$ $\beta = 106.98$	$a = 66.05$ $b = 83.27$ $c = 10.5.4$	$a = 97.94$ $b = 97.94$ $c = 187.55$
Wavelength (Å)	0.9793	0.9793	0.9792	1.2825
Highest Resolution bin (Å)	2.03-2.00	2.39-2.35	2.34-2.30	2.31-2.27
Number of observed reflections	26835 (1377)[b]	16892 (709)[b]	12326(528)[b]	42642 (2066)[b]
R_{merge} (%)[a]	15.3 (55.7)[b]	14.4 (44.8)[b]	9.1(33.4)[b]	10.4 (57.0)[b]
Completeness (%)	95.0 (96.8)[b]	97.6 (80.9)[b]	95.5(84.3)[b]	99.1 (98.1)[b]
$I/\sigma I$	6.3 (2.5)[b]	5.9 (2.1)[b]	11.9(3.5)[b]	6.3 (2.0)[b]
Phasing and Refinement	**MR**	**MR**	**MR**	**MR**
Search model	Chain A of 2YZ3	Chain A of 3RKJ	Chain A of 3RKJ	Chain A of 3Q6X
Phasing resolution range (Å)	38.4-2.00	40.7-2.35	36.9-2.31	38.4-2.27
Refinement resolution range (Å)	38.4-2.00	40.7-2.35	36.9-2.31	38.4-2.27
R_{cryst} (%)	19.2	20.8	20.3	18.3
R_{free} (%)	24.3	28.3	26.0	23.6
Number of protein residues	464	464	237	928
Solvent molecules	262	170	61	324
Bond lengths (Å)	0.007	0.017	0.012	0.011
Bond angles (deg)	1.19	1.61	1.52	1.33
B-factors (Å^2)	30.1	30.6	50.6	32.6
Protein main chain	25.83	28.62	46.60	30.08
Protein side chain	31.04	30.31	52.92	33.51
Solvent (Water)	38.49	34.58	47.28	37.46
Wilson B-factor (Å^2)	25.89	24.97	36.45	30.32
Ramachandran Plot (%)[c]				
Preferred	97.4	98.0	97.8	99.5
Generously allowed	2.6	2.0	2.2	0.4
Disallowed	0	0	0	0.1
PDB ID	3RKJ	3RKK	3SBL	3SFP

Table A4. Summary of the NDM-1 crystallographic data. a Rmerge = $\Sigma hkl \Sigma i \mid Ii - < I > \mid / \Sigma hkl \Sigma i \mid < I > \mid$, where *Ii* is the intensity for the *i*th measurement of an equivalent reflection with indices h, k, and l. b Numbers in parentheses are values for the highest-resolution bin. c Refined using PHENIX.

Statistic	Δ30-amp-Zn	Δ30-amp-Mn	Δ30-amp-Cd	Δ30-far-Cd
Data collection				
Space group	$P2_12_12_1$	$P2_12_12_1$	$P2_12_12_1$	C2
Cell dimensions				
a, *b*, *c* (Å)	39.19, 79.17, 134.47	39.10, 78.61, 133.71	38.99, 78.70, 134.38	145.63, 39.32, 75.37
β (deg)				99.96
Resolution (Å)	1.05	1.50	1.50	2.0
Reflections (*n*)	185,255 (5746)	67,113 (3259)	66,056 (3509)	28,649 (1438)
R_{sym} or R_{merge}	0.089 (0.871)	0.085 (0.664)	0.096 (0.782)	0.103 (0.629)
$I/\sigma I$	6.4 (2.3)	9.3 (2.7)	9.8 (2.1)	8.7 (2.3)
Completeness (%)	94.9 (88.9)	100 (100)	98.2 (93.5)	99.5 (100)
Redundancy	5.5 (5.7)	7.8 (6.9)	6.2 (4.1)	3.9 (3.5)
Refinement				
Resolution (Å)	1.05	1.50	1.50	2.00
No. reflections	184,744	67,022	65,844	28,604
R_{work}/R_{free}	0.133/0.157	0.147/0.168	0.137/0.149	0.204/0.251
Residues (*n*)				
Protein	485	482	478	469
Ligand/ion	12	12	10	10
Water	612	469	469	136
B factors	11.9	21.9	18.9	45.2
Protein	10.3	20.5	14.8	45.1
Ligand/ion	14.3	27.5	22.9	60.1
Water	21.7	32.5	30.7	39.0
R.m.s. deviations				
Bond lengths (Å)	0.017	0.006	0.011	0.009
Bond angles (deg)	1.808	1.157	1.581	1.739
Me-Me distances	4.60/4.60	4.48/4.48	3.72/4.30, 3.53/4.29	3.48/3.46
pH	5.5	7.5	6.5	5.5
PDB ID	4HL2	4H0D	4HL1	4HKY

Table A5. NDM-1 Data collection, phasing, and refinement statistics. Values in parentheses are for highest-resolution shell.